Dynamics and control of slugging in oil production

Florent Di Meglio

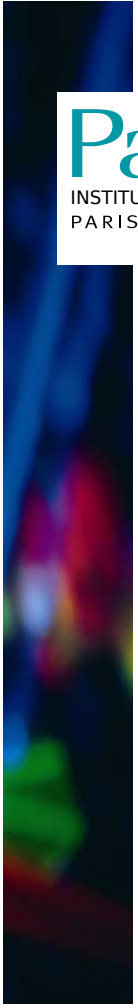

ParisTech
INSTITUT DES SCIENCES ET TECHNOLOGIES
PARIS INSTITUTE OF TECHNOLOGY

MINES ParisTech

École doctorale n°432 : SMI - Sciences des Métiers de l'Ingénieur

Doctorat ParisTech

T H È S E

pour obtenir le grade de docteur délivré par

l'École nationale supérieure des mines de Paris

Spécialité « Mathématiques et Automatique »

présentée et soutenue publiquement par

Florent DI MEGLIO

le 04 juillet 2011

Production de pétrole : étude dynamique et contrôle des écoulements à bouchons

Directeur de thèse : **Nicolas PETIT**

Jury

M. Denis DOCHAIN, Professeur, CESAME, Université Catholique de Louvain	Président
M. Sigurd SKOGESTAD, Professor, Department of Chemical Engineering, NTNU	Rapporteur
Mme Karine BEAUCHARD, Chargée de recherche HDR CNRS, CMLA, ENS Cachan	Examinatrice
M. Glenn-Ole KAASA, Ingénieur de recherche, Dept. Intelligent Drilling, Statoil	Examinateur
M. Vidar ALSTAD, Ingénieur de recherche, YARA	Examinateur
M. Nicolas PETIT, Professeur, Centre Automatique et Systèmes, MINES ParisTech	Examinateur

MINES ParisTech
Centre Automatique et Systèmes, Unité Mathématiques et Systèmes
60 boulevard Saint-Michel, 75006 Paris

T H È S E

ParisTech
INSTITUT DES SCIENCES ET TECHNOLOGIES
PARIS INSTITUTE OF TECHNOLOGY

MINES ParisTech

ParisTech Doctorate

THESIS

to obtain the

Doctor's degree from the Ecole nationale supérieure des Mines de Paris

Speciality « Mathematics and Control »

defended in public by

Florent DI MEGLIO

July, 4th, 2011

Dynamics and control of slugging in oil production

Advisor : **Nicolas PETIT**

THÈSE

Committee

M. Denis DOCHAIN, Professor, CESAME, Université Catholique de Louvain	Chair
M. Sigurd SKOGESTAD, Professor, Department of Chemical Engineering, NTNU	Referee
Mme Karine BEAUCHARD, Chargée de recherche HDR CNRS, CMLA, ENS Cachan	Examiner
M. Glenn-Ole KAASA, Principal Researcher, Dept. Intelligent Drilling, Statoil	Examiner
M. Vidar ALSTAD, Principal Researcher, YARA	Examiner
M. Nicolas PETIT, Professor, Centre Automatique et Systèmes, MINES ParisTech	Examiner

MINES ParisTech
Centre Automatique et Systèmes, Unité Mathématiques et Systèmes
60 boulevard Saint-Michel, 75006 Paris

Florent Di Meglio

Centre Automatique et Systèmes, Unité Mathématiques et Systèmes, MINES Paris-Tech, 60 bd St Michel 75272 Paris Cedex 06, France.

Statoil ASA, Norway

E-mail: florent.di_meglio@mines-paristech.fr

Key words. - Slugging,Mutliphase flow,Oil,Gas,Modelling,Partial Differential Equations,Control,Observers,Nonlinear
Mots clés. - Ecoulements à bouchons,Ecoulements polyphasiques, Pétrole,Gaz,Modélisation,Equations aux Dérivees Partielles,Contrôle,Observateurs,Nonlineaires

August 17, 2011

Je sais très bien *que je suis fou mais je m'en fous.*
FDM

Remerciements

Because of the large number of Norwegian people I want to thank, half of this page will be in English, the rest will be in French. I wish I could say the following directly in Norwegian, but my vocabulary is limited despite my several stays in Porsgrunn. First and foremost, I would like to thank Professor Skogestad for accepting to review this manuscript. His knowledge of the field and remarks have helped me improve it a lot. I especially thank him for traveling from Trondheim to Paris for my defense. I give very special thanks to Vidar Alstad and Glenn-Ole Kaasa who have been successively my supervisors, colleagues and friends in Porsgrunn. They have managed to provide me with a combination of freedom and constant help that I would never have had elsewhere, or with anyone else. I thank my colleagues in Porsgrunn, among which Robert Aasheim, Kjetil Fjalestad, Lene Amundsen, and Linn Bergfløt, and the whole Statoil organization for their support, their help, and the way I was welcomed to Norway.

Mes premiers remerciements francophiles vont au Professeur Denis Dochain, pour m'avoir fait l'honneur d'être le président du jury, et pour ses remarques toujours constructives, qui serviront longtemps ma carri‘ere débutante de chercheur. Je remercie également Karine Beauchard pour sa disponibilit'e constante et son aide précieuse, et pour sa présence à ma soutenance.

Je tiens à remercier l'ensemble du Centre Automatique et Systèmes, qui constitue un environnement de travail exceptionnel, en particulier grce à chacun des professeurs qui m'y ont fait découvrir et aimer le métier de chercheur. Je remercie également mes camarades de thèse Eric, Pierre-Jean et Caroline.

Les mots me manquent pour exprimer la reconnaissance et l'admiration que j'éprouve envers mon directeur de recherche, Nicolas Petit. Travailler avec vous est un plaisir véritable, que j'espère avoir l'occasion d'exercer pendant de nombreuses années encore (au moins jusqu'à l'obtention de votre légion d'honneur).

Je dédie cette thèse à ma famille, en particulier ma mère Véronique, mes trois frères Romain, Lucas et Raphaël et ma soeur Sara. Leur soutien inconditionnel m'a toujours porté, et me portera toujours. Je remercie également mes amis Delphine, Fred, Lionel, Nicolas, Paul, Laurent, Nathalie sur qui je peux toujours compter.

Enfin, je veux remercier Marine, qui m'a supporté et soutenu pendant ces trois ans, de me laisser partager sa vie.

Dynamics and control of slugging in oil production

Aux miens.

Resume

Le slugging (ou écoulement à bouchons) est un régime d'écoulement polyphasique indésirable apparaissant sur les systèmes de production de pétrole. Dans ce manuscrit, nous étudions la dynamique de ce phénomène intermittent dans le but de le supprimer par actionnement automatique de la vanne de sortie. Nous proposons des solutions de contrôle applicables dans une vaste gamme de situations industrielles. Après une analyse quantitative des propriétés physiques du slugging, nous proposons un modèle à paramètres distribués d'écoulement diphasique (gaz-liquide) reproduisant ce phénomène. Le modèle prend la forme d'un système hyperbolique de lois de conservation, pour lequel nous proposons un schéma de résolution numérique. De plus, nous procédons à une analyse de stabilité via la construction d'une fonction de Lyapunov de contrôle stricte pour le problème aux deux bouts avec condition initiale. Ensuite, nous présentons un modèle de dimension finie capable de reproduire les oscillations de pression et de débit qui caractérisent le slugging. Après une analyse des propriétés dynamiques de ce système, nous décrivons comment calibrer les paramètres du modèle afin que son comportement corresponde à celui d'un système donné. Enfin, nous proposons des lois de contrôle sous la forme de boucles de rétroaction, basées sur l'analyse du modèle réduit, dans deux situations industrielles disctinctes : selon qu'un capteur de pression de fond est disponible ou non. Les performances de ces solutions sont comparées avec les méthodes correspondant à l'état de l'art dans chaque situation. La conclusion de cette étude est qu'il n'est pas systématiquement nécessaire de disposer d'un capteur de pression de fond pour stabiliser l'écoulement. Quand un tel capteur est disponible, la loi de contrôle que nous proposons possède de meilleures propriétés de stabilisation que les méthodes communément utilisées dans l'industrie, ce qui, lors du passage à l'échelle, devrait se traduire par une augmentation de la production de pétrole.

Abstract

Slugging is an undesirable multiphase flow regime occurring on oil production facilities. This manuscript studies the dynamics of this intermittent phenomenon in view of suppressing it by feedback actuation of the outlet valve. We propose control

solutions applicable in a broad range of industrial settings. After a quantitative description of the physical characteristics of slugging, we propose a model for two-phase (gas-liquid) flow with distributed parameters reproducing the phenomenon. The model takes the form of a hyperbolic system of transport equations, for which we propose a numerical solving scheme. Besides, we proceed to a stability analysis by constructing a strict Lyapunov function for the mixed initial-boundary value problem. Then, we present a reduced-order model which reproduces the pressure and flow rate oscillations of slugging. After a dynamical analysis of this model, we describe how to calibrate its parameters so that its behavior corresponds to that of a given slugging system. Finally, we propose feedback control laws, based on the analysis of the reduced-order model, in two distinct industrial setups: whether a bottom pressure sensor is available or not. The performances of these solutions are compared with the state-of-the art methods in each situation. The conclusion is that a bottom pressure sensor is not systematically required to stabilize the flow. When one is available, the control law we propose yields better stabilization properties than the solution commonly used in the industry, which should improve the oil recovery process.

Contents

Introduction

Introduction

Ce mansucrit est consacré à l'étude du phénomène de slugging (ou écoulements à bouchons) dans les systèmes de production de pétrole. Le slugging est un régime d'écoulement polyphasique indésirable, car il provoque un abaissement du niveau moyen de production sur les systèmes concernés. La méthode la plus répandue pour supprimer cet écoulement intermittent (des poches de gaz sont intercalées entre des "bouchons" de liquide) consiste à "étouffer" le puit, c'est-à-dire à fermer partiellement la vanne de sortie, ce qui stabilise le débit[1]*. Malheureusement, cette solution a pour effet d'augmenter la pression dans le conduit et par conséquent, elle diminue aussi le niveau moyen de production. L'objet de cette thèse est de proposer des solutions de commande en boucle fermée visant à supprimer le slugging et se traduisant, lors du passage à l'échelle industrielle, par une augmentation de la production.*

De telles solutions boucle fermée ont été développées et implémentées depuis le milieu des années 1990 (voir notamment [12]). Toutefois, leurs performances ne sont pas toujours satisfaisantes, pour des raisons qui seront détaillées dans les chapitres à venir. Afin de les améliorer, il est possible de prendre appui sur des modèles physiques, qui mettent en lumière les mécanismes importants du slugging, afin d'élaborer des lois de contrôle. C'est l'approche que nous adoptons dans ce manuscrit.

Les modèles reproduisant le phénomène de slugging peuvent être séparés en deux classes de systèmes dynamiques. Les modèles basés sur des Equations aux Dérivées Partielles (EDP), prennent en compte la nature distribuée du problème. De tels modèles, comme celui intégré dans le logiciel de simulation d'écoulement polyphasique OLGA^{TM}*, sont principalement utilisés pour la simulation. A l'inverse, les modèles basés sur des systèmes d'Equations Différentielles Ordinaires (EDO) reproduisent les grandes tendances du phénomène, en considérant, plutôt que des quantités infinitésimales, des masses agrégées de gaz et de liquide. L'analyse mathématique de ces modèles est plus aisée que pour les modèles d'EDP, et se révèle un outil pratique pour l'élaboration d'observateurs et de contrôleurs. Dans ce manuscrit, nous considérons ces deux approches.*

[1] et permet, en particulier, de supprimer les larges oscillations de pression associées au slugging qui sont dangereuses pour les installations.

Dans le Chapitre 1, nous décrivons le phénomène de slugging, et les enjeux industriels qui y sont associés. En particulier, nous étudions les mécanismes qui conduisent à la diminution de la production. Nous proposons ensuite un modèle d'EDP pour le slugging, dit à dérive de flux *[18]. Le modèle peut se mettre sous la forme d'un système hyperbolique d'équations de transport nonlinéaires, qui forme, avec les conditions aux frontières, un problème bien posé. Après linéarisation du modèle, nous établissons des conditions suffisantes pour la stabilité asymptotique de l'équilibre, en utilisant un résultat récent de la littérature [3]. Enfin, le calcul numérique des solutions des équations mettent en évidence la capacité du modèle à reproduire le phénomène du slugging. Nous proposons un schéma de résolution adapté à la structure lent-rapide des équations de transport.*

Dans le Chapitre 2, nous présentons un modèle EDO pour le slugging élaboré spécifiquement en vue de la synthèse d'un contrôleur. Dans la lignée de contributions récentes [48, 52], le modèle que nous proposons suggère la possible existence d'une irrégularité dans le conduit d'écoulement, bloquant le flux de gaz à cet endroit, et à l'origine de l'instabilité. Des simulations numériques illustrent la capacité du modèle à reproduire le comportement observé sur des puits de pétrole, au prix d'un effort de calibration: une procédure permettant de choisir les "bonnes" (dans un sens qui sera détaillé) valeurs des paramètres du modèle est proposée.

Le Chapitre 3 est consacré à l'élaboration de lois de contrôle dans deux situations distinctes. Nous considérons séparemment le cas où aucune mesure de la pression de fond n'est disponible (Scenario 1), et le cas où une mesure fiable existe (Scenario 2). Dans le Scenario 1, nous proposons d'étudier un observateur basé sur le modèle du Chapitre 2 pour reconstruire les variables d'état non mesurées. Les estimations sont ensuite utilisées dans un algorithme de stabilisation sur un écoulement d'installations expérimentales reproduisant le phémonème de slugging (le Test-rig Staoil, situé à Porsgrunn, en Norvège). Nous discutons les limitations inhérentes à ce scenario, et à l'utilisation de la seule mesure de pression en tête de l'écoulement: la présence de zéros instables dans la fonction de transfert du système impose des restrictions sur les performance et la robustesse des lois de contrôle considérées. Dans le Scenario 2, le rôle d'une variable d'état particulière, la masse de liquide contenue dans le conduit, est mis en évidence à travers l'étude d'une loi de contrôle théorique. L'utilisation de cette variable dans un simple contrôleur PI (facilement implémentable) s'avère, à la lumière d'expériences rapportées dans le manuscrit, améliorer les performances des contrôleurs généralement utilisés dans l'industrie pétrolière.

Les deux scénarios considérés couvrent un large champ d'applications. Les conclusions de cette étudent soulignent qu'une commande en boucle fermée permet de stabiliser les écoulements à bouchons dans des zones d'intért pour la production.

This report studies the slugging phenomenon arising on oil wells and flowline risers. This intermittent two-phase flow regime (elongated bubble of gas being separated by slugs of liquid) must be avoided since it is detrimental to the production. A common

way to prevent slugging is to "choke" the system by closing the outlet valve. Unfortunately, this open-loop strategy increases the pressure in the pipe, and, consequently, also reduces the level of production. The main objective of this report is to provide closed-loop solutions which would result, when applied to large-scale slugging systems, into an increase of production by means of stabilization of the flow.

Such closed-loop solutions have been investigated and implemented since the mid-1990s [12]. Yet, they have failed to produce satisfying results, for several reasons that will be reviewed in this manuscript. A possible way of improvement is to use physical models that provide insight into the mechanisms of the phenomenon, and to infer control laws from them. This is the approach we follow here.

Models reproducing the slugging behavior are classically divided into two categories of dynamical systems. First, models based on Partial Differential Equations (PDE) take into account the distributed nature of the phenomenon. Such models, as incorporated to the commercial software OLGA$^{\text{TM}}$, are mainly used for simulation purposes. Conversely, models based on Ordinary Differential Equations (ODE) catch the main features of the phenomenon by considering lumped masses of gas and liquid as states rather than infinitesimal quantities. They are easier to analyze mathematically than PDE-based models, and reveal a handy tool to design control laws and observers. In this manuscript, both approaches are considered.

In Chapter 1, we describe the slugging phenomenon and the industrial challenges it raises. In particular, we focus on the mechanisms that lead to a decrease of production. Then, we propose a PDE model for slugging, following the drift-flux approach. The model is formulated as a nonlinear hyperbolic system of transport equations, which is convenient to prove the well-posedness of the mixed initial-boundary value problem. Besides, after linearizing the equations, it is possible to study the stability of the equilibrium by constructing a strict control Lyapunov function, following recent results from the literature (see [3], in particular). Eventually, a proposed numerical scheme allows to numerically compute a solution to the equations: the model reproduces the main features of the slugging phenomenon. We conclude the chapter by recalling the state-of-the-art on feedback control of slugging. The shortcomings of existing solutions suggest the need for control laws designed specifically for this phenomenon.

In Chapter 2, we describe a three-states ODE model elaborated in view of control design. Following similar models from the literature [48, 52], the model stresses the possible existence of an irregularity at a certain location in the considered pipe, affecting the flow of gas there, at the birth of the instability. Numerical simulations show that the model is able to reproduce the behavior of real observed wells and flowline risers, at the cost of a calibration effort on the parameters. Indeed, a proposed tuning procedure allows to match the dynamical properties of the model with that of a given slugging system.

In Chapter 3, we propose feedback control solutions to the slugging problem in two distinct industrial situations. We consider separately the case when no pressure sensor located at the bottom of the pipe is available (Scenario 1) and the case when

a reliable one is available (Scenario 2). In the first scenario, a proposed observer algorithm is used to estimate the three states of the model described in Chapter 2 from a topside pressure measurement only. The estimates are then used, during reported experiments, in a feedback control law to stabilize the flow on a mid-scale multiphase flow loop located in Porsgrunn, Norway. The limitations inherent to the unavailability of a bottom pressure sensor are discussed, as well as the performances of the proposed control solution. In Scenario 2, the study of the model reveals, through the design of a theoretical nonlinear control law, the particular role of a specific variable: the mass of liquid contained in the pipe, or, equivalently, the pressure difference between the bottom and top of the pipe. The study suggests an easily implementable control law, in the form of a PI controller applied to the pressure drop over the pipe. This solution, which only requires the use of both the bottom and topside pressure measurements, has better stabilizing properties than the commonly used PI controller applied to the bottom pressure, as illustrated by experiments on the multiphase flow loop.

The two considered scenarios cover a vast range of applications. The conclusions of this study underline that closed-loop control strategies can be used to stabilize slugging flows in cases of practical interest for oil production.

Notations and acronyms

Two classes of models are considered throughout the manuscript. We review here the notations.

Notations common to both models

Symbol	Quantity	Unit
L	Length of the pipe	m
θ	Inclination of the pipe	rad
g	Gravity constant	$m.s^{-2}$
T	Temperature inside the pipe	K
ρ_l	Liquid density	$kg.m^{-3}$
C_{out}	Outlet valve constant	[-]

PDE model

Symbol	Quantity	Unit
R_g	Specific gas constant	$J.kg^{-1}.K^{-1}$
α_g	Gas volume fraction	[-]
α_l	Liquid volume fraction	[-]
ρ_g	Gas density	$kg.m^{-3}$
ρ_m	Mixture density	$kg.m^{-3}$
v_g	Gas velocity	$m.s^{-1}$
v_l	Liquid velocity	$m.s^{-1}$
v_∞	Slip velocity	$m.s^{-1}$
F_g^W	Friction of the gas against the wall	$kg.m^{-2}.s^{-2}$
F_l^W	Friction of the liquid against the wall	$kg.m^{-2}.s^{-2}$
Φ_g	Gas mass flow rate per unit surface	$kg.s^{-1}.m^{-2}$
Φ_l	Liquid mass flow rate per unit surface	$kg.s^{-1}.m^{-2}$
PI	Productivity index	$m^{-1}.s$
Z	Outlet valve opening	[-]
P_r	Reservoir pressure	Pa
P_s	Separator pressure	Pa
bar	Conversion factor	Pa

ODE model

Symbol	Quantity	Unit
R	Ideal gas constant	$J.mol^{-1}.K^{-1}$
M	Molar mass of the gas	$kg.mol^{-1}$
A	Cross-section area	m^2
C_g	Virtual valve constant	m.s
V_{eb}	Volume of the elongated bubble	m^3
V_r	Volume of the riser	m^3
$m_{g,eb}$	Mass of gas in the elongated bubble	kg
$m_{g,r}$	Mass of gas in the riser	kg
$m_{l,r}$	Mass of liquid in the riser concerned by the dynamics	kg
$m_{l,still}$	Still mass of liquid	kg
p_{eb}	Pressure in the elongated bubble	Pa
$p_{r,b}$	Pressure at the base of the riser	Pa
$p_{r,t}$	Pressure at the top of the riser	Pa
p_s	Separator pressure	Pa
$w_{g,in}$	Gas mass inflow rate	$kg.s^{-1}$
$w_{l,in}$	Liquid mass inflow rate	$kg.s^{-1}$
$w_{g,out}$	Gas mass outflow rate	$kg.s^{-1}$
$w_{l,out}$	Liquid mass outflow rate	$kg.s^{-1}$
w_g	Mass flow rate of gas through the virtual valve	$kg.s^{-1}$
ϵ	Fraction of gas flowing directly into the riser	[-]
u	Opening of the virtual valve	[-]
GLR	Gas-liquid mass ratio	[-]

Chapter 1

Problem description and modelling

Description du problème et modélisation

Ce premier chapitre est consacré à la description du phénomène de slugging. Après une brève présentation du procédé de production de pétrole, et la définition des systèmes à l'étude dans la Section 1.1, nous présentons dans la Section 1.2 les caractéristiques de ce régime d'écoulement polyphasique intermittent. En particulier, nous nous attarderons sur l'impact du slugging sur le niveau production moyen. Afin d'illustrer cette description, nous proposons dans la Section 1.3 un modèle dynamique d'écoulement diphasique reproduisant le phénomène de slugging. Le modèle consiste en un système d'EDP de transport nonlinéaires. Une analyse de stabilité, ainsi qu'un schéma numérique de résolution des équations sont présentés. Enfin, nous décrivons dans la Section 1.4 l'état de l'art en matière de contrôle du slugging

This first chapter deals with the description of the slugging phenomenon. In Section 1.1, we briefly describe the process of the oil production and present the systems that will be considered throughout the manuscript. Then, in Section 1.2, we present the characteristics of this intermittent multiphase flow regime. The impact of slugging on the level of oil production will receive particular attention. To illustrate this description, we propose in Section 1.3 a dynamical model for two-phase flow able to reproduce the slugging phenomenon. A stability analysis of this system of nonlinear transport PDE is presented, along with a numerical scheme for the computation of the solution of the equations. Eventually, in Section 1.4, we recall the state-of-the-art in control of slugging in the oil industry.

1.1 Oil production

1.1.1 Description of the process and facilities [43]

Oil reservoirs Crude oil is a naturally occurring mixture of hydrocarbons and other organic compounds. It is found in large geological traps, referred to as reservoirs, which, for the most part, also contain natural gas. The reservoirs, which are located underground, are usually detected by seismic reflection surveys. The ground surface above such an accumulation is called an oil field. An oil field is called offshore when located under the sea, and onshore when it is located on the land.

The drilling process In order to produce oil from a reservoir, several wells are drilled through the ground. The drilling techniques have largely evolved, and continue to do so, to reach always deeper and thinner reservoirs. Whereas the first (onshore) wells only ran tens of meters deep, they can now run several thousand meters deep under the seabed, which can itself be one or two kilometers under the sea level. Recent technology advances emphasize the importance of well positioning (directional drilling) and pressure management (MPD, see e.g. [34]).

Offshore fields A schematic view of an offshore field is depicted on Figure 1.1. Oil, gas, and often water enter the wells from the underground reservoirs at high pressure, between a few hundred bars to a thousand. This multiphase mixture naturally flows upwards to the wellhead, located at the seabed. There, the production from several wells is gathered, and is conveyed through a flowline. The flowline lies at the seabed along thousands of meters before rising to the surface facilities. Although some recent fields feature undersea separators (such as the Tordis field, in the North Sea), the process of separating the oil, water and gas usually occurs at the surface.

The separation process Separation is the first step of oil and gas processing, which usually ends with the refining of the oil to produce gasoline, or the production of other derived compounds (e.g., plastic). The separation process aims at separating the gas, oil and water phases, and solid impurities from one another; conditioning the gas and treating crude oil to capture gas vapors [43]. A simple three-phase separator is schematically depicted on Figure 1.2. The levels of water and oil are kept constants by low-level controllers (usually Proportional-Integrator, or PI) using the outlet valves of the liquids as actuators. The pressure inside the separator is also kept constant using the outlet valve of the gas.

1.1.2 Systems of interest: wells and flowline risers

The framework of our study is limited to specific sub-systems of this complex setup. Indeed, we will now focus on the systems where the so-called slugging phenomenon (described in details in the next sections) occurs, namely wells and flowline risers.

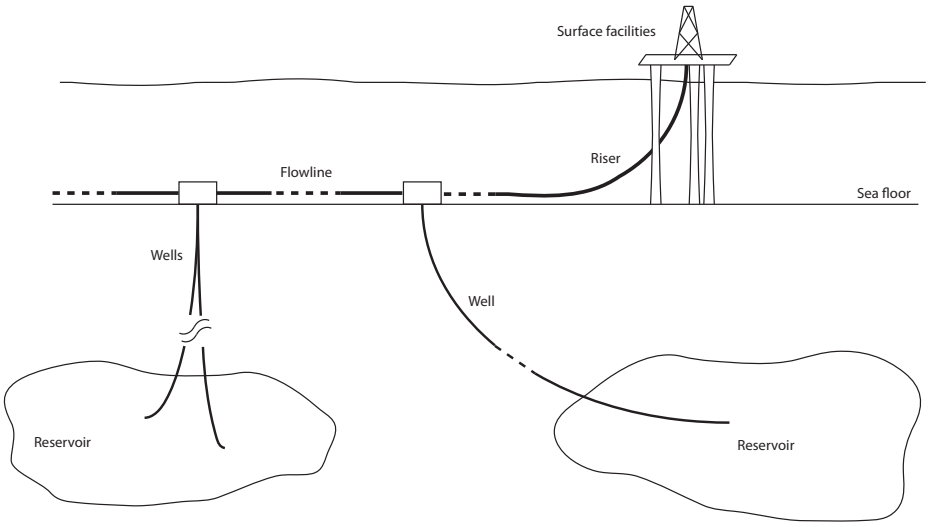

Figure 1.1: Schematic view of an offshore field

Wells As mentioned above, wells are long pipes connecting the reservoirs to the wellhead. The wellhead can be located at the seabed, for offshore fields, or on land for onshore fields. The length of a well ranges from several hundred meters to several thousands. Some wells are purely vertical, whereas some feature a long (several thousand meters) horizontal section followed by a vertically inclined one. Finally, some vertical wells are activated by gas-lift. For these, a casing is built around the well, and filled with gas. The gas is then injected through a one-way valve at the bottom of the well, alleviating the liquid column there. All wells are equipped with a remotely actuated choke valve located at the wellhead, which allows to regulate the outflow. The pressure downstream this valve is usually considered constant, which is a valid assumption only for short periods (typically over several days).

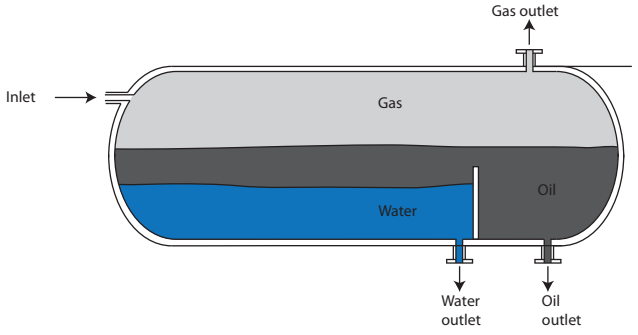

Figure 1.2: Schematic view of a three-phase separator

Flowline risers Risers are the vertically inclined sections of the flowlines. They connect the seabed installations to the surface facilities. The horizontal part of flowlines lies on the seabed and its geometry is subject to possible terrain irregularities. In particular, the riser is, on some flowlines, preceded by a low-point angle which is known to facilitate the occurrence of the slugging phenomenon. Again, the multiphase flow coming out of a flowline can be regulated by means of an actuated choke valve. A separator, where the pressure is kept constant, is usually installed downstream this valve.

1.2 Multiphase slugging flow

In this section, we describe the slugging phenomenon both from a physical and industrial viewpoint. We describe the conditions that favor its occurrence, as well as the consequences on the level of oil production and the downstream processes.

1.2.1 Physical description

Multiphase flow regimes

Consider a mixture of gas and liquid flowing through a pipe. The flow regime corresponds to the geometric repartition of the different phases inside the pipe. Among the many factors influencing the nature of the flow are the geometry of the pipe, the pressure and temperature conditions inside it, the density, viscosity and composition of the fluids, and their relative and absolute velocities. Thus, a given system can experience different flow regimes over time if these conditions change. Figure 1.3 pictures the most common two-phase (gas-liquid) flow regimes. Of course, this list is not comprehensive and many intermediate situations can occur. A common tool to describe the

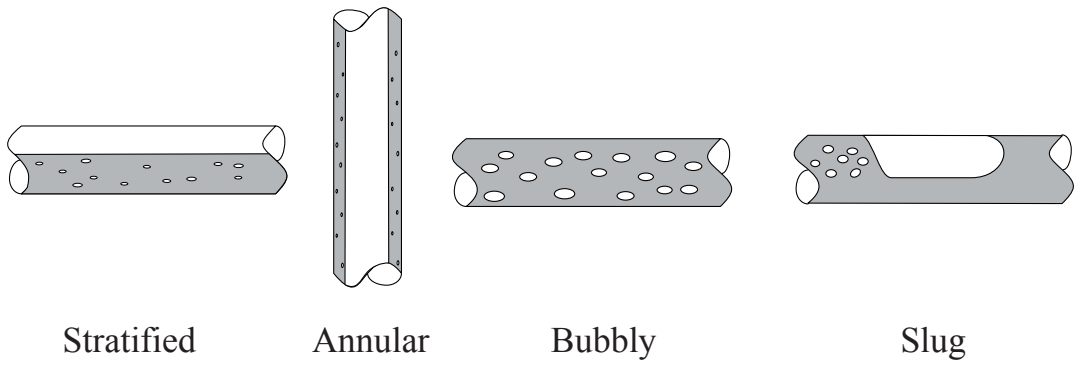

Figure 1.3: Most common gas-liquid flow regimes

behaviors of systems subject to gas-liquid flow are the flow pattern (or flow regimes) maps, such as the one pictured on Figure 1.4. They are constructed by varying the flow

rates of each phase over a wide range and monitoring the resulting flow regime. Unfortunately, these maps lack generality, as the shape of the resulting regions depends highly on other parameters listed above (density of the fluids, temperature, pressure, etc.). For this reason, other systems of coordinates are considered to draw these maps, such as the superficial velocities of each phase, or more complicated dimensionless parameters. We now focus on the slug flow regime and its occurrences in the oil industry.

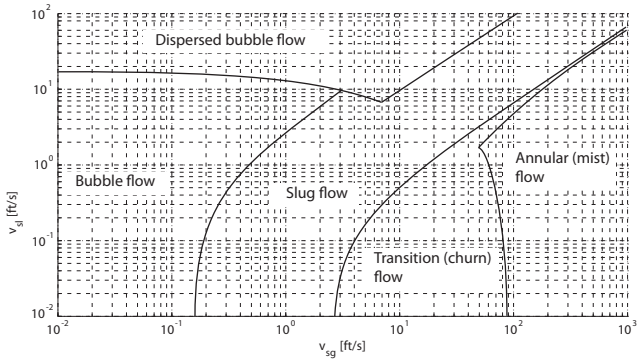

Figure 1.4: Example of a two-phase flow pattern map proposed in [36]

Slug flow

Geometric description Slug flow is an inhomogeneous gas-liquid flow regime. As opposed to the annular or bubbly flows, the spatial distribution of the gas and liquid phases is not invariant by translation along the pipe axis. More precisely, it is characterized by the formation of elongated bubbles of gas flowing through the pipe, periodically separated by "slugs" of liquid. The relative and absolute sizes of the slugs and elongated bubbles may significantly vary from one system to another.

Slug flow in the oil industry Oil wells and flowlines are prone to the slug flow regime since they convey gas-liquid mixtures[1]. Its occurrences can be classified in four categories depending on the size of the slugs, and the causes at their birth

- *Hydrodynamic slugging* occurs in almost every system subject to gas-liquid flow, and features short slugs. Experimental studies [44] report that the minimum length for a slug unit (liquid slug + elongated bubble) to exist is around 32 times the pipe diameter. Shorter slugs naturally disappear. Even though the mechanisms at the birth of these short slugs are poorly understood, hydrodynamic

[1]Even though the flow is, rigorously, three-phase (oil, water and gas), oil and water are often considered as one lumped liquid phase. This is the choice we make here, and from now on, the flow will be considered two-phase (gas-liquid).

slugging is not detrimental to the oil recovery process, and is usually considered inevitable. Thus, we will discard hydrodynamic slugging from our future studies.

- *Terrain-induced slugging* arises on flowlines when the terrain features crests and dips, such as the one flowline schematically depicted on Figure 1.5. A particular case of terrain-induced slugging is the *severe slugging*. It corresponds to the existence of a low-point angle at the base of the riser (rising section of the flowline). In the case of severe slugging, there is only one slug in the riser at a time, and its length can reach that of the whole riser. The severe slugging phenomenon has attracted most of the attention in the literature since the late 1970s [7, 27, 28, 46, 52, 54, 55].

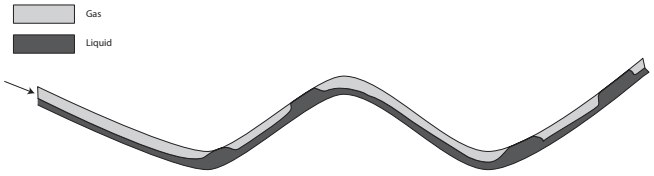

Figure 1.5: Schematic view of a flowline subject to terrain slugging. The accumulation of liquid at the low points blocks the flow of gas at these locations, which causes a build up of pressure. When the pressure is high enough, the liquid is pushed downstream, before another slug is formed.

- *Casing-heading* is a phenomenon arising on gas-lifted wells. On these, an annulus filled with gas is built around the well. The gas is injected through a one-way valve at the bottom of the well. This process may result in the formation of large slugs which hurt the oil recovery process. The casing-heading phenomenon is also well reported in the literature [29, 31, 32, 48].

- *Well instability* designates the occurrence of slugging on wells which are not activated by gas-lift. The mechanisms of this regime, which generally features shorter slugs than the severe slugging, with several slugs simultaneously present in the riser, are not entirely understood.

Figure 1.6 summarizes this description by schematically picturing the family of systems we will focus on in the following chapters. Each of these corresponds to a specific occurrence of slugging described above. The classification is by no mean comprehensive and there are as many existing configurations as there are oil fields. Yet, the restriction to these three classes allows to cover a large variety of systems that share common important features. In particular, the period of the slugging oscillations ranges, for all these systems, from around 30 minutes to a few hours. Besides, we will use the term "slugging" to designate either the severe slugging, casing-heading or well instability phenomenon.

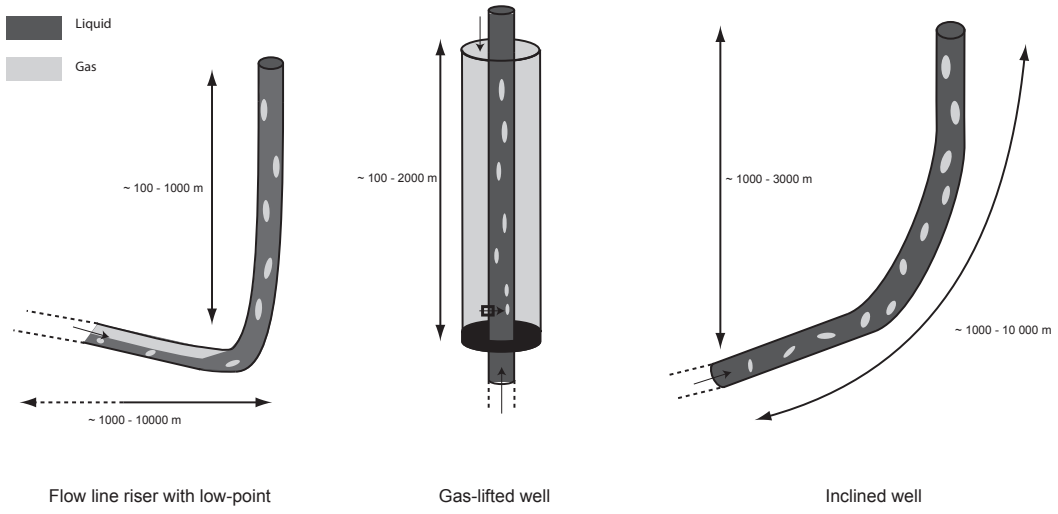

Figure 1.6: Family of systems of interest

1.2.2 Industrial consequences

Slugging is, in all the situations described above, an undesirable phenomenon, because it causes, directly or indirectly, the oil production to decrease. To understand the mechanisms leading to these production losses, consider the bifurcation diagram pictured on Figure 1.7. It plots the open-loop oil production as a function of the outlet valve opening. When the opening is fixed at a large value, the slugging phenomenon causes the production to oscillate: short periods of high production alternate with long periods of low production. The black lines represent the magnitude of these oscillations, while the blue dotted line represents their average (over time). This average is lower than the "nominal" equilibrium production (the red line) for the same opening, which is a direct cause for production losses. The nominal production corresponds to an unstable equilibrium and can e.g. be reached by feedback control.

Besides, the oscillations of production are concomitant with large oscillations of the pressure everywhere inside the pipe. These variations cause wear-and-tear on the facilities and complicate the separation process. To avoid these costly consequences, slugging is typically handled by "choking" the pipe down, i.e. reducing the opening of the outlet valve. Indeed, slugging systems feature a Hopf bifurcation [58]: the occurrence of slugging, for large openings of the outlet valve, is caused by unstable eigenvalues of the system. Conversely, for openings smaller than a certain critical point, referred to as the *bifurcation point*, the equilibrium is stable, and the flow is steady (typically bubbly or annular). Thus, sufficiently choking the pipe allows to suppress the slugging phenomenon. Unfortunately, smaller valve openings correspond to lower levels of production, as indicated Figure 1.7. Although indirect, this is the main cause for production losses associated with slugging.

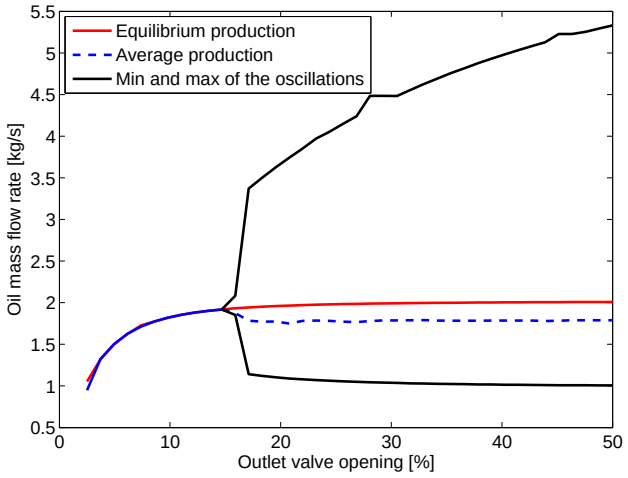

Figure 1.7: Bifurcation diagram of a test well. The diagram was obtained by simulations on a simplified model.

1.3 Modelling

To gain insight into the mechanisms of slugging, we now propose a new model for two-phase flow, under the form of a system of 3 nonlinear coupled transport equations. The model is able to reproduce the pressure and flow rates oscillations which characterize slugging. First, we detail the state-of-the-art on PDE multiphase flow modelling.

OLGA and drift-flux models OLGA is a commercial multiphase flow simulator based on a nonlinear two-fluid PDE model [5]. It is able to reproduce the slugging behavior of numerous systems, including wells subject to casing-heading and most flowline risers experiencing severe slugging. Unfortunately, it rarely manages to reproduce the well instability. Also, its "black box" nature makes it simulation-oriented and does not provide insight into the possible control solutions. It is however a standard simulation tool for multiphase flow in general, more specifically for the slugging phenomenon, and is often used for comparative studies.

Another commercial simulator, TACITE, was developed in the 1990s [21]. It is based on a *drift-flux* (as opposed to two-fluid) PDE model, which means that a single momentum equation is written for both the gas and the liquid. In this formulation, the velocities of the two phases are generally related by an empirical relation called the *slip relation*. Drift-flux models were introduced by Zuber (see e.g. [61]), and continue to attract attention [4, 24, 38]. We follow this approach and now propose a drift-flux model for slugging.

Our model We will now describe a simple drift-flux model able to reproduce the slugging phenomenon. First, we write the classical drift-flux equations and detail the modelling assumptions, in particular the choice of a slip relation. Then, we formulate

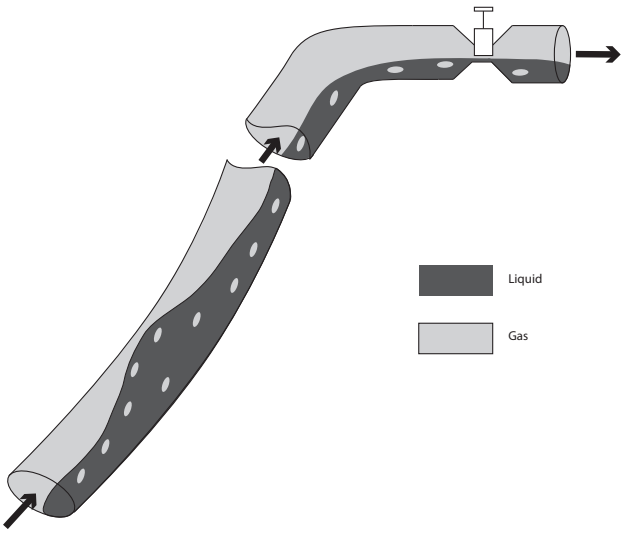

Figure 1.8: Inclined pipe transporting liquid and gas

the problem as a nonlinear hyperbolic system of conservation laws. This allows us to prove well-posedness of the mixed initial-boundary value problem. This also allows to extend a recent result by Bastin et al. [3] and study the stability of the linearized equations around an equilibrium profile. Finally, to reduce the computational time of the simulations for the nonlinear equations, we perform a model simplification, based on the relative magnitude of the characteristic speeds of the system. The numerical simulations show the relevancy of the approach since the model reproduces important features of the slugging phenomenon.

1.3.1 Model equations

We consider the multiphase flow of gas and liquid through an inclined circular pipe as depicted in Figure 1.8. The gas and liquid flow from the reservoir into the pipe, and pass through a remotely controlled valve before being separated in the downstream facilities or entering a manifold. Following the classical drift-flux approach ([9, 18, 20]), the model equations consist of two mass conservation laws, for the gas and the liquid, respectively, and a combined momentum equation. The flow is assumed to be one-dimensional. Thus, the radial and angular variations of all physical quantities are neglected. This yields the following system of PDEs

$$\frac{\partial \alpha_g \rho_g}{\partial t} + \frac{\partial \alpha_g \rho_g v_g}{\partial z} = 0 \tag{1.1}$$

$$\frac{\partial \alpha_l \rho_l}{\partial t} + \frac{\partial \alpha_l \rho_l v_l}{\partial z} = 0 \tag{1.2}$$

$$\frac{\partial \alpha_g \rho_g v_g + \alpha_l \rho_l v_l}{\partial t} + \frac{\partial P + \alpha_g \rho_g v_g^2 + \alpha_l \rho_l v_l^2}{\partial z} = F_g^W + F_l^W - \rho_m g \sin\theta(z) \tag{1.3}$$

where, for $k = G$ or L, α_k denotes the volume fraction of phase k, ρ_k denotes its density, and v_k its velocity. P denotes the pressure, ρ_m is the density of the mixture and F_k^W accounts for the friction of phase k against the pipe walls. $\theta(z)$ is the inclination of the pipe. $t > 0$ is the time variable and $z \in [0, L]$ the space variable, with L being the total length of the pipe. In order to put the system under a conservative form[11], several additional relations are needed. First, the two following physical definitions hold

$$\alpha_g + \alpha_l = 1 \qquad \text{and} \qquad \rho_m = \alpha_g \rho_g + \alpha_l \rho_l \tag{1.4}$$

Then, two empirical relations, given below, allow to "close" the system.

Ideal gas The gas is supposed to follow the ideal gas law, which (locally) reads $P = \rho_g R_g T$, with R_g being the specific gas constant, and T is the temperature. One should notice that the pressure at one location in the pipe is assumed to be equal to the pressure in the gas phase.

Slip relation Following [48], the velocities of gas and liquid are assumed to satisfy the following slip relation

$$v_g - v_l = \frac{v_\infty}{\alpha_l} \tag{1.5}$$

where v_∞ is a *constant* parameter. In most drift-flux models [18, 24], v_∞ depends on the state of the system, following empirical laws depending on the flow regime under consideration (annular, dispersed, stratified, respectively). Yet, in [48], it was shown that the slugging oscillations could be fairly reproduced in a multiphase simulator, even with a constant v_∞. We follow this approach here.

Eventually, the following simplifying assumptions are made

Incompressible liquid The liquid is assumed to be incompressible, which implies that $\rho_l(t, z) = \rho_l = \text{cst}$. This is a classical assumption for the liquid phase.

Neglectible friction The friction against the walls is assumed to be neglectible with respect to gravity ($F_g^W = F_l^W = 0$). This is a reasonable assumption as severe slugging is known to be a gravity-dominated phenomenon [52].

1.3.2 Boundary conditions

The boundary conditions are given at both ends of the pipe. At the bottom, the flow of liquid is assumed to depend linearly on the pressure drop between the pipe and the

reservoir (alternatively, other sources of liquid could be considered as well)

$$\Phi_l(t, z = 0) = \alpha_l(t, z = 0)\rho_l v_l(t, z = 0) = \mathrm{PI}\,[P_r - P(t, z = 0)] \tag{1.6}$$

The constant coefficient PI is called the Productivity Index. The pressure in the reservoir P_r is assumed constant. Also at the bottom end of the pipe, the flow of gas is assumed to be constant

$$\Phi_g(t, 0) = \alpha_g(t, 0)\rho_g(t, 0)v_g(t, 0) = \Phi_g \tag{1.7}$$

Eventually, at the top, the total outflow is assumed to be governed by a multiphasic valve equation of the (general) form

$$\Phi_l(L) + \Phi_g(L) = \alpha_l(L)\rho_l v_l(L) + \alpha_g(L)\rho_g(L)v_g(L) = C_{out}Z\sqrt{\rho_m(L)\,(P(L) - P_s)} \tag{1.8}$$

where P_s is the constant pressure in the separator. The valve (or "choke") opening, Z, is the control input. The choke is remotely actuated. Its opening can be continuously adjusted to control the flow, e.g. stabilizing it using feedback loops. In (1.8), the time variable is omitted for readability.

1.3.3 Formulation as a (well-posed) mixed initial-boundary value hyperbolic problem

As is, the system (1.1)-(1.2)-(1.3) is in implicit form, which is hardly suitable for any mathematical analysis. Thus, we re-formulate the conservation equations as a hyperbolic system of PDE. Consider the following state vector

$$u = \begin{pmatrix} u_1 & u_2 & u_3 \end{pmatrix}^T = \begin{pmatrix} \frac{\alpha_g\rho_g}{\alpha_g\rho_g + \alpha_l\rho_l} & \frac{P}{\mathrm{bar}} & v_g \end{pmatrix}^T$$

where the pressure is divided by 1 bar $= 1 \times 10^5$ Pa to ensure, later, proper numerical conditioning of the solver. Combining equations (1.1)-(1.2)-(1.3), and the static relations (1.4) and (1.5) allows the system to be rewritten in conservative form

$$\frac{\partial H(u)}{\partial t} + \frac{\partial F(u)}{\partial z} = G(z, u)$$

Then, noticing that $\frac{\partial H(u)}{\partial t} = H'(u)\frac{\partial u}{\partial t}$, the system can be rewritten under the quasi-linear form

$$\frac{\partial u}{\partial t} + A(u)\frac{\partial u}{\partial z} = S(z) \tag{1.9}$$

where $A(u) = H'(u)^{-1}F'(u)$ and $S(z) = H'(u)^{-1}G(z, u)$. The expressions of $A(u)$ and S are given in Appendix A. To guarantee that A and all the other functions of u are C^1 functions, we restrict our study to a compact set

$$u \in K \subset \Omega = (0, 1) \times (P_s, P_r) \times (0, +\infty) \subset \mathbb{R}^3 \tag{1.10}$$

For each value of $u \in K$, A has 3 real eigenvalues $(\lambda_1(u), -\lambda_2(u), \lambda_3(u))$, as well as a set of linearly independent left eigenvectors $l(u) = \begin{pmatrix} l_1(u) \\ l_2(u) \\ l_3(u) \end{pmatrix}$. Again, the expressions of the λ_i and l_i are given in Appendix A. This guarantees that system (1.9) is hyperbolic, in the sense of the definition given in [42]. One should notice that u_1 is a Riemann invariant for the system, as it is the case in the model of [48]. Moreover, all the numerical applications that we have performed so far have shown that the following inequalities hold

$$\forall u \in K, \forall i = 1, 2, 3, \qquad \lambda_i(u) > 0 \tag{1.11}$$

$$\forall u \in K \qquad \lambda_1(u) > \lambda_3(u) \tag{1.12}$$

some of which are difficult to prove by mathematical analysis given the complexity of the expressions of the λ_i. This ensures that the system is strictly hyperbolic, see again [42]. In order to establish the well-posedness of the mixed initial-boundary value problem, the boundary conditions (1.6)-(1.7)-(1.8) must be rewritten. This is done in Appendix A where well-posedness is established using a theorem from [42]. We now linearize the model around the equilibrium and investigate the stability of the equilibrium through the construction of a strict control Lyapunov function.

1.3.4 Sufficient conditions for stability

Canonical form A linearization of the system about an equilibrium profile $(\bar{u}_1, \bar{u}_2, \bar{u}_3)$ yields

$$\frac{\partial \delta u}{\partial t} + A(\bar{u}(z))\frac{\partial \delta u}{\partial z} + \tilde{S}(z)\delta u = 0 \tag{1.13}$$

with

$$\tilde{S}(z) = \begin{pmatrix} \dfrac{\partial A}{\partial u_1}(\bar{u})\bar{u}'(z) & \dfrac{\partial A}{\partial u_2}(\bar{u})\bar{u}'(z) & \dfrac{\partial A}{\partial u_3}(\bar{u})\bar{u}'(z) \end{pmatrix}$$

In (1.13), $A(\bar{u}(z))$ is diagonalizable. We have

$$L(z)A(\bar{u}(z)) = \Lambda(\bar{u}(z))L(z)$$

with $L(z) = \begin{pmatrix} l_1(\bar{u}(z)) \\ l_2(\bar{u}(z)) \\ l_3(\bar{u}(z)) \end{pmatrix}$ and $\Lambda(z) = \begin{pmatrix} \lambda_1(\bar{u}(z)) & 0 & 0 \\ 0 & -\lambda_2(\bar{u}(z)) & 0 \\ 0 & 0 & \lambda_3(\bar{u}(z)) \end{pmatrix}$. Thus, conisdering the change of variables

$$\chi = L(z)\delta u$$

and left-multiplying (1.13) by $L(z)$ yields

$$\frac{\partial \chi}{\partial t} + \Lambda(z)\frac{\partial \chi}{\partial z} = -\Sigma(z)\chi \tag{1.14}$$

with

$$\Sigma(z) = L(z)\left(\tilde{S}(z)L^{-1}(z) + A(\bar{u}(z)(L^{-1})'(z)\right)$$

The expression of $\Sigma(z)$ is too complicated to be written in details. However, one should notice that the third line of Σ is only filled with 0. Indeed, the original state variable u_1 is a Riemann invariant. This structure is preserved by the preceding transformation, and $\chi_3 = u_1$ is also a Riemann invariant for (1.14)[2]. This property will be of great importance when investigating the stability of the equilibrium in Section 1.3.4. As a result, we will write

$$\Sigma = \begin{pmatrix} \sigma_{1,1} & \sigma_{1,2} & \sigma_{1,3} \\ \sigma_{2,1} & \sigma_{2,2} & \sigma_{2,3} \\ 0 & 0 & 0 \end{pmatrix}$$

Finally, following [3], we define the following expressions

$$\varphi_1(z) = \exp\left(\int_0^z \frac{\sigma_{1,1}(s)}{\lambda_1(s)}ds\right), \qquad \varphi_2(z) = \exp\left(-\int_0^z \frac{\sigma_{2,2}(s)}{\lambda_2(s)}ds\right), \qquad \varphi(z) = \frac{\varphi_1(z)}{\varphi_2(z)}$$

and make the following change of variables

$$y_1(t,z) = \varphi_1(z)\chi_1(t,z), \qquad y_2(t,z) = \varphi_2(z)\chi_2(t,z), \qquad y_3(t,z) = \chi_3(t,z)$$

This yields the following system

$$\begin{pmatrix} y_1 \\ y_2 \\ y_3 \end{pmatrix}_t + \begin{pmatrix} \lambda_1(z) & 0 & 0 \\ 0 & -\lambda_2(z) & 0 \\ 0 & 0 & \lambda_3(z) \end{pmatrix}\begin{pmatrix} y_1 \\ y_2 \\ y_3 \end{pmatrix}_z + \begin{pmatrix} 0 & \varphi(z)\sigma_{1,2}(z) & \varphi_1(z)\sigma_{1,3}(z) \\ \varphi^{-1}(z)\sigma_{2,1}(z) & 0 & \varphi_2(z)\sigma_{2,3}(z) \\ 0 & 0 & 0 \end{pmatrix}\begin{pmatrix} y_1 \\ y_2 \\ y_3 \end{pmatrix} = 0 \tag{1.15}$$

Boundary conditions The boundary conditions are given by the following equations relating the state variables at the boundaries. Denoting $u_i(0) = u_i(t,0)$, we have, at the left-hand side

$$h_l(u_1(0), u_2(0), u_3(0)) = \begin{pmatrix} \rho_l u_1(0)u_2(0)u_3(0) - \Phi_g\left[\rho_l R_g T u_1(0) + (1-u_1(0))u_2(0)\right] \\ \Phi_g - u_1(0)\left[\Phi_g + \rho_l v_\infty + PI(p_r - u_2(0))\right] \end{pmatrix} = \begin{pmatrix} 0 \\ 0 \end{pmatrix}$$

[2]This can be verified by computing explicitly Σ or, simply, by linearizing the following equation, verified by u_1: $\frac{\partial u_1}{\partial t}(t,z) + \lambda_3(t,z)\frac{\partial u_1}{\partial z}(t,z) = 0$.

and, at the right-hand side,

$$h_r(u_1(L), u_2(L), u_3(L), Z) = \frac{\rho_l u_2(L) u_3(L)}{\rho_l R_g T u_1(L) + (1 - u_1(L)) u_2(L)} - v_\infty \rho_l - C_{out} Z \sqrt{\frac{\rho_l u_2(L)(u_2 - p_s)}{\rho_l R_g T u_1(L) + (1 - u_1(L)) u_2(L)}} = 0$$

The linearized equations now read

$$\frac{\partial h_l}{\partial u}(\bar{u}(0))\delta u(t, 0) = 0$$
$$\frac{\partial h_r}{\partial u}(\bar{u}(L))\delta u(t, L) = 0$$

Thus,

$$\frac{\partial h_l}{\partial u}(\bar{u}(0))L^{-1}(\bar{u}(0))\begin{pmatrix} \varphi_1^{-1}(0) & 0 & 0 \\ 0 & \varphi_2^{-1}(0) & 0 \\ 0 & 0 & 1 \end{pmatrix} y(t, 0) = 0$$
$$\frac{\partial h_r}{\partial u}(\bar{u}(L))L^{-1}(\bar{u}(L))\begin{pmatrix} \varphi_1^{-1}(L) & 0 & 0 \\ 0 & \varphi_2^{-1}(L) & 0 \\ 0 & 0 & 1 \end{pmatrix} y(t, L) = 0$$

Eventually, the boundary conditions can be expressed as follows

$$\begin{cases} \begin{pmatrix} y_1(0) \\ y_3(0) \end{pmatrix} = \begin{pmatrix} k_1 \\ k_3 \end{pmatrix} y_2(0) \\ y_2(L) = \begin{pmatrix} k_2 & k_2' \end{pmatrix} \begin{pmatrix} y_1(L) \\ y_3(L) \end{pmatrix} \end{cases} \tag{1.16}$$

Stability of the equilibrium: construction of a strict control Lyapunov function We now investigate the stability of the linearized system (1.15) with boundary conditions (1.16). We are able to apply a result for 2×2 systems from [3], by exploiting the cascade structure of the equations. In particular, the impact of the source terms on stability are handled by using the fact that y_3 is a Riemann invariant. We define the following candidate control Lyapunov function

$$V(t) = \int_0^L \left(q_1(z) y_1(t, z)^2 + q_2(z) y_2(t, z)^2 + q_3(z) y_3(t, z)^2 \right) dz \tag{1.17}$$

where q_1, q_2 and $q_3 \in C^1([0, L], (0, +\infty))$ are yet to be defined. Differentiating V and integrating by parts, one obtains

$$\dot{V}(t) = -B(t) - \int_0^L I(t)$$

with

$$B(t) = \left[\lambda_1 q_1 y_1^2 - \lambda_2 q_2 y_2^2 + \lambda_3 q_3 y_3^2\right]_0^L$$

$$I(t) = \begin{pmatrix} y_1 & y_2 & y_3 \end{pmatrix} \begin{pmatrix} -(\lambda_1 q_1)_z & 2\varphi\sigma_{1,2} q_1 & 2\varphi_1\sigma_{1,3} q_1 \\ 2\varphi^{-1}\sigma_{2,1} q_2 & (\lambda_2 q_2)_z & 2\varphi_2\sigma_{2,3} q_2 \\ 0 & 0 & -(\lambda_3 q_3)_z \end{pmatrix} \begin{pmatrix} y_1 \\ y_2 \\ y_3 \end{pmatrix} dz$$

$$= \begin{pmatrix} y_1 & y_2 & y_3 \end{pmatrix} \underbrace{\begin{pmatrix} -(\lambda_1 q_1)_z & \varphi\sigma_{1,2} q_1 + \varphi^{-1}\sigma_{2,1} q_2 & \varphi_1\sigma_{1,3} q_1 \\ \varphi\sigma_{1,2} q_1 + \varphi^{-1}\sigma_{2,1} q_2 & (\lambda_2 q_2)_z & \varphi_2\sigma_{2,3} q_2 \\ \varphi_1\sigma_{1,3} q_1 & \varphi_2\sigma_{2,3} q_2 & -(\lambda_3 q_3)_z \end{pmatrix}}_{Q} \begin{pmatrix} y_1 \\ y_2 \\ y_3 \end{pmatrix} dz$$

We now show that there exist functions q_1, q_2 and q_3 such that I is a strictly positive definite quadratic form with respect to (y_1, y_2, y_3) almost everywhere in $[0, L]$. A necessary and sufficient condition is that the principal minors of Q are strictly positive a.e. in $[0, L]$. Consider now the following functions

$$f(z) := \lambda_1(z) q_1(z), \qquad \forall z \in [0, L]$$
$$g(z) := \lambda_2(z) q_2(z), \qquad \forall z \in [0, L]$$

and

$$a(z) := \frac{\varphi(z)\sigma_{1,2}(z)}{\lambda_1(z)}, \qquad b(z) := \frac{\varphi^{-1}(z)\sigma_{2,1}(z)}{\lambda_2(z)}, \qquad \forall z \in [0, L]$$

With the same notations, Proposition 1 in [3] states that, if the maximal solution of the Cauchy problem

$$\eta'(z) = \left|a(z) + b(z)\eta^2(z)\right|, \eta(0) = 0 \tag{1.18}$$

is defined on $[0, L]$, then there exist q_1 and q_2 such that

$$-(\lambda_1 q_1)_z > 0 \qquad \text{a.e. in } [0, L]$$
$$(\lambda_2 q_2)_z > 0 \qquad \text{a.e. in } [0, L]$$
$$-(\lambda_1 q_1)_z (\lambda_2 q_2)_z > (\varphi\sigma_{1,2} q_1 + \varphi^{-1}\sigma_{2,1} q_2)^2 \qquad \text{a.e. in } [0, L]$$

This ensures that the two first principal minors of Q are strictly positive. In particular, $\det(P) = \begin{vmatrix} -(\lambda_1 q_1)_z & \varphi\sigma_{1,2} q_1 + \varphi^{-1}\sigma_{2,1} q_2 \\ \varphi\sigma_{1,2} q_1 + \varphi^{-1}\sigma_{2,1} q_2 & (\lambda_2 q_2)_z \end{vmatrix} > 0$. The last principal minor of Q reads

$$-(\lambda_3 q_3)_z \det(P) - \varphi_2\sigma_{2,3} q_2 \begin{vmatrix} -(\lambda_1 q_1)_z & \varphi_1\sigma_{1,3} q_1 \\ \varphi\sigma_{1,2} q_1 + \varphi^{-1}\sigma_{2,1} q_2 & \varphi_2\sigma_{2,3} q_2 \end{vmatrix} +$$
$$\varphi_1\sigma_{1,3} q_1 \begin{vmatrix} \varphi\sigma_{1,2} q_1 + \varphi^{-1}\sigma_{2,1} q_2 & \varphi_1\sigma_{1,3} q_1 \\ (\lambda_2 q_2)_z & \varphi_2\sigma_{2,3} q_2 \end{vmatrix}$$

Thus, it suffices to chose q_3 such that

$$q_3(z) > 0 \quad \text{and} \quad (\lambda_3 q_3)_z < \alpha(z), \quad \forall z \in [0, L]$$

with

$$\alpha(z) = \frac{-\varphi_2\sigma_{2,3}q_2 \begin{vmatrix} -(\lambda_1 q_1)_z & \varphi_1\sigma_{1,3}q_1 \\ \varphi\sigma_{1,2}q_1 + \varphi^{-1}\sigma_{2,1}q_2 & \varphi_2\sigma_{2,3}q_2 \end{vmatrix} + \varphi_1\sigma_{1,3}q_1 \begin{vmatrix} \varphi\sigma_{1,2}q_1 + \varphi^{-1}\sigma_{2,1}q_2 & \varphi_1\sigma_{1,3}q_1 \\ (\lambda_2 q_2)_z & \varphi_2\sigma_{2,3}q_2 \end{vmatrix}}{\det(P)}$$

to ensure that I is a strictly positive definite quadratic form with respect to (y_1, y_2, y_3) almost everywhere in $[0, L]$. One can e.g. choose

$$q_3(z) = \frac{\|\alpha\|_\infty}{\lambda_3(z)}(2L - z)$$

where $\|\alpha\|_\infty = \max_{z\in[0,L]} \alpha(z)$. We now investigate sufficient conditions on the coefficients of the boundary equations for B to be negative definite. Indeed, B can be written

$$B = \begin{pmatrix} y_1(L) & y_3(L) \end{pmatrix} \begin{pmatrix} \lambda_1(L)q_1(L) - \lambda_2(L)q_2(L)k_2^2 & k_2k_2' \\ k_2k_2' & \lambda_3(L)q_3(L) - \lambda_2(L)q_2(L)k_2'^2 \end{pmatrix} \begin{pmatrix} y_1(L) \\ y_3(L) \end{pmatrix} + (\lambda_2(0)q_2(0) - \lambda_1(0)q_1(0)k_1^2 - \lambda_3(0)q_3(0)k_3^2)y_2(0)^2$$

Thus, a sufficient condition is that k_1, k_2, k_2' and k_3 verify

$$\begin{cases} \lambda_1(0)q_1(0)k_1^2 + \lambda_3(0)q_3(0)k_3^2 < \lambda_2(0)q_2(0) \\ k_2^2 < \dfrac{\lambda_1(L)q_1(L)}{\lambda_2(L)q_2(L)} \\ k_2'^2 < \dfrac{\lambda_3(L)q_3(L)}{\lambda_2(L)q_2(L)} \\ \left[\lambda_2(L)q_2(L) - 1\right]^2 (k_2k_2')^2 \\ - \lambda_2(L)q_2(L)\left[\lambda_1(L)q_1(L)k_2'^2 + \lambda_3(L)q_3(L)k_2^2\right] + \lambda_1(L)q_1(L)\lambda_3(L)q_3(L) > 0 \end{cases} \tag{1.19}$$

Conclusion Under assumptions (1.19), if the maximal solution of (1.18) is defined on $[0, L]$, then V as defined by (1.17) is a control Lyapunov function for system (1.15) with boundary conditions (1.16).

Because of the state transormations from the phsyical equations, these conditions are difficult to interpret. Also, they are conservative, as most conditions derived from Lyapunov analysis. However, the following remark can be made. The condition that the maximal solution of the Cauchy problem (1.18) should not explode in final time is more likely to be verified by shorter wells. This is consistent with, e.g., the Bøe criterion [7], which is a sufficient condition for the occurence of severe slugging. The criterion takes the form of a lower bound on the inlet superficial velocity of liquid, which is inversely proportional to the length of the riser.

1.3.5 Numerical solving of the equations

In this section, we illustrate the capabilities of the proposed model with numerical simulations. The main result is that the model is able to reproduce the oscillations corresponding to the slugging behavior of a well. As is, the proposed numerical scheme does not allow to perform simulations when the geometry of the system presents an angle (i.e. $\theta(z^*) < 0$ at a certain location z^* in the pipe). Thus, the model can only be used, for the moment, to study expansion-driven instabilities in vertical wells, rather than severe slugging. First, we proceed to a model simplification.

A system with two time scales

The numerical computation of the eigenvalues of matrix $A(u)$ in (1.9) in several test cases have shown us that the following comparison holds

$$\forall u \in K, \quad \lambda_1(u), \lambda_2(u) \gg \lambda_3(u) \tag{1.20}$$

Typical values are $\lambda_{1,2} \approx 300$ m.s^{-1} and $\lambda_3 \approx 1$ m.s^{-1}. This suggests that the system has two time scales: a slow transport phenomenon (corresponding to λ_3) coupled with fast transport dynamics with opposite signs (λ_1 and$-\lambda_2$). The large pressure oscillations of the slugging phenomenon, which can have a period of 30 minutes to a few hours, correspond to the slow transport phenomenon. To focus on the slow dynamics, we proceed to a model reduction analog to Tikhonov's theorem [57]. First, we consider system (1.9) and left-multiply it by each of the eigenvectors $l_i(u)$, $i = 1, 2, 3$. This yields[3]

$$\begin{cases} l_1(u)\left[\dfrac{\partial u}{\partial t} + \lambda_1(u)\dfrac{\partial u}{\partial z} - S(z)\right] = 0 \\ l_2(u)\left[\dfrac{\partial u}{\partial t} + \lambda_2(u)\dfrac{\partial u}{\partial z} - S(z)\right] = 0 \\ l_3(u)\left[\dfrac{\partial u}{\partial t} + \lambda_3(u)\dfrac{\partial u}{\partial z}\right] = 0 \end{cases} \tag{Σ}$$

We now consider the following class of systems, parametrized by a small parameter ϵ

$$\begin{cases} l_1(u)\left[\dfrac{\partial u}{\partial t} + \lambda_1(u,\epsilon)\dfrac{\partial u}{\partial z} - S(z,\epsilon)\right] = 0 \\ l_2(u)\left[\dfrac{\partial u}{\partial t} + \lambda_2(u,\epsilon)\dfrac{\partial u}{\partial z} - S(z,\epsilon)\right] = 0 \\ l_3(u)\left[\dfrac{\partial u}{\partial t} + \lambda_3(u,\epsilon)\dfrac{\partial u}{\partial z}\right] = 0 \end{cases} \tag{Σ_ϵ}$$

[3]Notice that the source terms do not appear in the last equation since, for all (t, z), $l_3(u(t,z))S(z) = \begin{pmatrix} 1 & 0 & 0 \end{pmatrix}\begin{pmatrix} 0 \\ 0 \\ -g\sin\theta(z) \end{pmatrix} = 0$

where

$$\lambda_1(u,\epsilon) = \frac{\lambda_1^*(u)}{\epsilon} \qquad S(z,\epsilon) = \frac{S^*(z)}{\epsilon}$$
$$\lambda_2(u,\epsilon) = \frac{\lambda_2^*(u)}{\epsilon}$$
$$\lambda_3(u,\epsilon) = \lambda_3^*(u)$$

System (Σ) correspond to (Σ_ϵ) for a particular choice of ϵ. Now, multiplying the first two equations of System (Σ_ϵ) by ϵ yields

$$\begin{cases} l_1(u)\left[\epsilon\dfrac{\partial u}{\partial t} + \lambda_1^*(u)\dfrac{\partial u}{\partial z} - S^*(z)\right] = 0 \\ l_2(u)\left[\epsilon\dfrac{\partial u}{\partial t} + \lambda_2^*(u)\dfrac{\partial u}{\partial z} - S^*(z)\right] = 0 \\ l_3(u)\left[\dfrac{\partial u}{\partial t} + \lambda_3^*(u)\dfrac{\partial u}{\partial z}\right] = 0 \end{cases}$$

Finally, taking the limit as ϵ goes to zero yields the following system

$$\begin{cases} l_1(u)\left[\lambda_1^*(u)\dfrac{\partial u}{\partial z} - S^*(z)\right] = 0 \\ l_2(u)\left[\lambda_2^*(u)\dfrac{\partial u}{\partial z} - S^*(z)\right] = 0 \\ l_3(u)\left[\dfrac{\partial u}{\partial t} + \lambda_3^*(u)\dfrac{\partial u}{\partial z}\right] = 0 \end{cases} \qquad (\Sigma_0)$$

System (Σ_0) is an approximation of system (Σ) where the fast dynamics are considered instantaneous with respect to the slow transport phenomenon[4]. Up to our knowledge, there is no result that guarantee that the solutions of (Σ_0) are "close" to the solutions of (Σ). Yet, numerical simulations show that it is the case and that the approximation is valid. We now present a numerical solver for system (Σ_0).

A numerical scheme for system (Σ_0)

We now present a numerical scheme that allows us to compute the solutions of system (Σ_0). The computation involves a Euler finite differences scheme for the discretization in time. At each time step, a centered finite differences scheme for the space discretization leads to the formation of a $3P \times 3(P+1)$ linear system of equations. This system is coupled with 3 nonlinear equations relating the state components

[4] In the sense of [30] who exposes a series expansion of solution of PDE, the solution of (Σ_0) corresponds to the first term in the series expansion of the solution of (Σ_ϵ)

at the boundary. The total $3(P+1)\times 3(P+1)$ system is solved using Newton's algorithm. We now detail this method. Consider a time-space grid

$$\{t \in \{0, \Delta t, ..., n\Delta t, ...\},\ z \in \{0, \Delta z, ..., p\Delta z, ...L = P\Delta z\}\}$$

with

$$\forall u \in K \qquad \frac{\Delta z}{\Delta t} \ll \lambda_1(u), \lambda_2(u) \qquad \frac{\Delta z}{\Delta t} > \lambda_3(u) \tag{1.21}$$

Let u be a solution of system (Σ_0). To compute its discrete time derivative, we chose a simpler Euler scheme. For the computation of the space derivatives, we chose an *implicit centered scheme*. This yields

$$\begin{aligned}\frac{\partial u}{\partial t}(t,z) &= \frac{u(n,p) - u(n-1,p)}{\Delta t}\\ \frac{\partial u}{\partial z}(t,z) &= \frac{u(n,p+1) - u(n,p-1)}{2\Delta z}\end{aligned}$$

with the concise notations $u(n,p) = u(n\Delta t, p\Delta z)$. According to the considered scheme, the discretized equations corresponding to system (Σ_0) read, for $p = 1, ..., P-1$

$$\begin{cases} l_1(n-1,p)\left[\lambda_1^*(n-1,p)\dfrac{u(n,p+1)-u(n,p-1)}{2\Delta z} - S^*(p)\right] = 0\\ l_2(n-1,p)\left[\lambda_2^*(n-1,p)\dfrac{u(n,p+1)-u(n,p-1)}{2\Delta z} - S^*(p)\right] = 0\\ l_3(n-1,p)\left[\dfrac{u(n,p)-u(n-1,p)}{\Delta t} + \lambda_3^*(n-1,p)\dfrac{u(n,p+1)-u(n,p-1)}{2\Delta z}\right] = 0 \end{cases}$$

where the solution at time $(n-1)\Delta t$, $u(n-1,p)$ is known for all p. In the equations above, one notes, for sake of conciseness, $l(n,p) = l(u(n\Delta t, p\Delta z))$ and $\lambda(n,p) = \lambda(u(n\Delta t, p\Delta z))$. The system is still under-determined, 6 more equations are required. The first three are given by the discretization of system (Σ_0) at the boundaries

$$\begin{cases} l_1(u(n-1,0))\left[\lambda_1^*(n-1,0)\dfrac{u(n,1)-u(n,0)}{\Delta z} - S^*(1)\right] = 0\\ l_2(u(n-1,P))\left[\lambda_2^*(n-1,P)\dfrac{u(n,P)-u(n,P-1)}{\Delta z} - S^*(P)\right] = 0\\ l_2(u(n-1,P))\left[\dfrac{u(n,P)-u(n-1,P)}{\Delta t} + \lambda_3^*(n-1,P)\dfrac{u(n,P)-u(n,P-1)}{\Delta z}\right] = 0 \end{cases}$$

Denoting

$$U = \begin{pmatrix} u_1(n,0) & \cdots & u_1(n,P) & u_2(n,0) & \cdots & u_2(n,P) & u_3(n,0) & \cdots & u_3(n,P)\end{pmatrix}^T$$

and

$$l_i(n,p) = \begin{pmatrix} l_{i,1}^p & l_{i,2}^p & l_{i,3}^p \end{pmatrix}$$

this yields the following $3P \times 3(P+1)$ linear system

$$MU - V = 0$$

with M being given in Table 1.1

and

$$V = \begin{pmatrix} \frac{\Delta z}{\lambda_1^*(n-1,0)} l_1(u(n-1,0))S^*(0) \\ \frac{\Delta z}{\lambda_1^*(n-1,1)} l_1(u(n-1,1))S^*(1) \\ \vdots \\ \frac{\Delta z}{\lambda_1^*(n-1,P-1)} l_1(u(n-1,P-1))S^*(P-1) \\ \frac{\Delta z}{\lambda_2^*(n-1,1)} l_2(u(n-1,1))S^*(1) \\ \frac{\Delta z}{\lambda_2^*(n-1,2)} l_2(u(n-1,2))S^*(2) \\ \vdots \\ \frac{\Delta z}{\lambda_2^*(n-1,P)} l_2(u(n-1,P))S^*(P) \\ \frac{u_1(n-1,1)}{\Delta t} \\ \frac{u_1(n-1,2)}{\Delta t} \\ \vdots \\ \frac{u_1(n-1,P)}{\Delta t} \end{pmatrix}$$

The last 3 equations are given by the boundary conditions, which consist of two nonlinear equations at the left boundary and one at the right. They read, for the left boundary

$$h_l(u_1(n,0), u_2(n,0), u_3(n,0)) = 0 \tag{1.22}$$

and, for the right

$$h_r(u_1(n,P), u_2(n,P), u_3(n,P), Z) = 0 \tag{1.23}$$

h_l and h_r are defined by (A.5) and (A.6), and Z is the control input. The total $3(P+1) \times 3(P+1)$ system (typically, $P \approx 100$) is solved, at each time step, using Newton's algorithm. The Jacobian can be computed analytically, but it has to be inverted numerically, which tends to slow the computation down.

Algorithm for the reduced implicit centered scheme

Given an initial vector

$$U^0 = (u_1(0,0) \quad ... \quad u_1(0,P) \quad u_2(0,0) \quad ... \quad u_2(0,P) \quad u_3(0,0) \quad ... \quad u_3(0,P))^T \in \mathbb{R}^{3(P+1)}$$

representing the initial state of the system (1.9) and a time step Δt, iterate the following, starting with $n = 1$

(i) from U^{n-1}, compute the eigenvalues $\lambda_i^*(n-1,p)$, $i = 1,2,3$, and the eigenvectors $l_i(n-1,p)$, $i = 1,2,3$, according to the analytical expressions given in Appendix A by (A.1) and (A.2), respectively;

(ii) consider $F^{n-1}(U^n) = 0$ consisting of $M^{n-1}U^n - V^{n-1} = 0$ and (1.22)-(1.23), and the Jacobian $\nabla F^{n-1}(U^n) = \begin{pmatrix} M^{n-1} \\ \frac{\partial h_l}{\partial U}(U^n) \\ \frac{\partial h_l}{\partial U}(U^n) \end{pmatrix}$. Solve $F^{n-1}(U^n) = 0$ by a Newton method;

(iii) increase n and go to step (i)

$$
M = \left(\begin{array}{cccccc|cccccc|cccccc|cccccc}
-l^0_{1,1} & l^0_{1,1} & 0 & \cdots & 0 & & -l^0_{1,2} & l^0_{1,2} & 0 & \cdots & 0 & & -l^0_{1,3} & l^0_{1,3} & 0 & \cdots & 0 & \\
-\frac{l^1_{1,1}}{2} & 0 & \frac{l^1_{1,1}}{2} & \cdots & 0 & & -\frac{l^1_{1,2}}{2} & 0 & \frac{l^1_{1,2}}{2} & \cdots & 0 & & -\frac{l^1_{1,3}}{2} & 0 & \frac{l^1_{1,3}}{2} & \cdots & 0 & \\
\vdots & \ddots & \ddots & \ddots & 0 & & \vdots & \ddots & \ddots & \ddots & 0 & & \vdots & \ddots & \ddots & \ddots & 0 & \\
0 & \cdots & -\frac{l^{P-1}_{1,1}}{2} & 0 & \frac{l^{P-1}_{1,1}}{2} & & 0 & \cdots & -\frac{l^{P-1}_{1,2}}{2} & 0 & \frac{l^{P-1}_{1,2}}{2} & & 0 & \cdots & -\frac{l^{P-1}_{1,3}}{2} & 0 & \frac{l^{P-1}_{1,3}}{2} \\
\hline
-\frac{l^1_{2,1}}{2} & 0 & \frac{l^1_{2,1}}{2} & \cdots & 0 & & -\frac{l^1_{2,2}}{2} & 0 & \frac{l^1_{2,2}}{2} & \cdots & 0 & & -\frac{l^1_{2,3}}{2} & 0 & \frac{l^1_{2,3}}{2} & \cdots & 0 \\
0 & \ddots & \ddots & \ddots & \vdots & & 0 & \ddots & \ddots & \ddots & \vdots & & 0 & \ddots & \ddots & \ddots & \vdots \\
\vdots & \ddots & -\frac{l^{P-1}_{2,1}}{2} & 0 & \frac{l^{P-1}_{2,1}}{2} & & \vdots & \ddots & -\frac{l^{P-1}_{2,2}}{2} & 0 & \frac{l^{P-1}_{2,2}}{2} & & \vdots & \ddots & -\frac{l^{P-1}_{2,3}}{2} & 0 & \frac{l^{P-1}_{2,3}}{2} \\
0 & \cdots & \cdots & -l^P_{2,1} & l^P_{2,1} & & 0 & \cdots & \cdots & -l^P_{2,2} & l^P_{2,2} & & 0 & \cdots & \cdots & -l^P_{2,3} & l^P_{2,3} \\
\hline
-\frac{\lambda_3(n,1)}{2\Delta z} & \frac{1}{\Delta t} & \frac{\lambda_3(n,1)}{2\Delta z} & \cdots & 0 & & & & & & & & & & & & \\
0 & \ddots & \ddots & \ddots & 0 & & & & & & & & & & & & \\
\vdots & \ddots & -\frac{\lambda_3(n,P-1)}{2\Delta z} & \frac{1}{\Delta t} & \frac{\lambda_3(n,P-1)}{2\Delta z} & & & & & \mathbf{0} & & & & & & \mathbf{0} & \\
0 & \cdots & \cdots & -\frac{\lambda_3(n,P)}{\Delta z} & \frac{\Delta z+\lambda_3(n,P)\Delta t}{\Delta t\Delta z} & & & & & & & & & & & & \\
\end{array}\right)
$$

Table 1.1: Matrix corresponding to the discretized equations.

Description	Symbol	Value
Ideal gas constant	R	8.314
Gravity constant	g	9.81 m.s^{-2}
Molecular mass of the gas	M	$2.29 \times 10^{-}2$ kg.mol^{-1}
Length of the riser	L	2450 m
Inclination of the riser	θ	$\pi/2$ rad
Temperature	T	369 J.K^{-1}.mol^{-1}
Density of the liquid	ρ_l	781 kg.m^{-3}
Slip velocity	v_∞	0.01 m.s^{-1}
Outlet valve constant	C_{out}	0.1754 [-]
Productivity Index	PI	1.1×10^{-3} s.m^{-1}
Surface inflow rate of gas	Φ_g	43.86 kg.s^{-1}.m^{-2}
Separator pressure	P_s	20 bar
Reservoir pressure	P_r	150 bar
Time step	Δt	10 s
Space step	Δz	62.8205 m

Table 1.2: List of the parameters of the PDE model

Numerical simulations

The aforedescribed algorithm has been used to compute the solution of system (Σ_0) with parameters corresponding to a 2450 meter-long vertical well. Table 1.2 gives a list of the parameters used for the computation. Figure 1.9 pictures the result of a simulation of the model over 16 hours, during which the opening of the outlet valve was changed. The simulation starts at a 95% valve opening, and the solution is initialized at the corresponding equilibrium profile. The pressure starts oscillating with an increasing magnitude, which indicates that the operating point is unstable. After approximately 6,5 hours, the opening of the outlet valve is reduced to 55%. The magnitude of the oscillations settles around 10 bar. Finally, the opening is reduced to 25%: the oscillations vanish and the pressure settles at its equilibrium value. This indicates that the bifurcation point of the model lies between 25% and 55% outlet valve opening. To illustrate the mechanism of the oscillations, snapshots of the liquid mass hold-up profiles over one slugging cycle are pictured on Figure 4. The relevance of the model reduction of Section 1.3.5 appears when comparing the computation times for such a simulation with the computation times of the numerical solver presented in [16][5]. Indeed, when considering the fast dynamics instantaneous, the minimal time step required to satisfy the CFL conditions is 300 times larger, which accelerates the computation by the same factor. This 16 hours simulation took approximately 40 seconds on a Dual Core 2.8 GHz processor running a Matlab implementation of the algorithm.

[5]This solver, based on the method of characteristics, did not take advantage of the separation of the time scales of the system

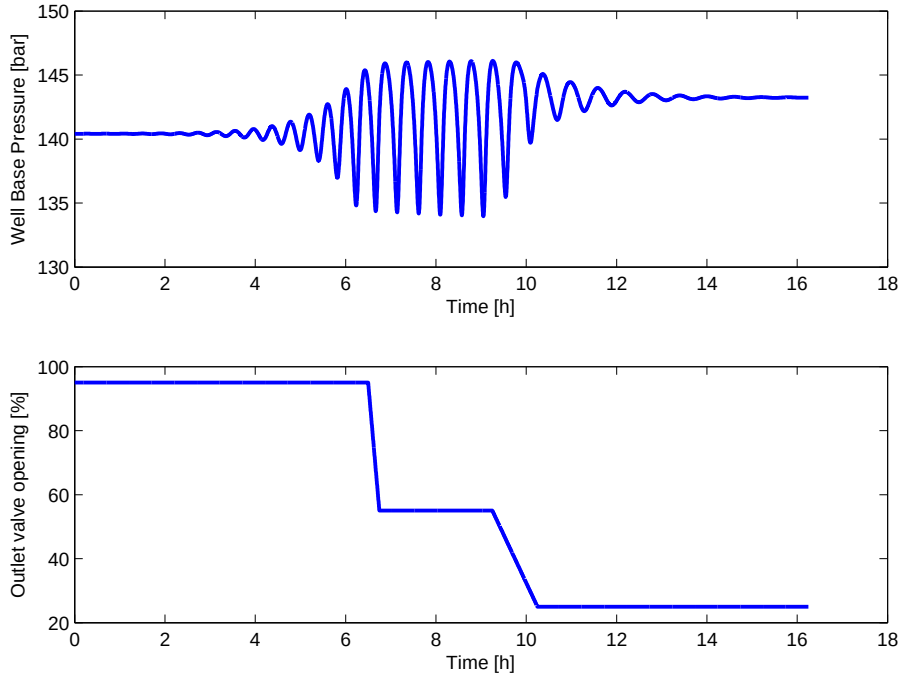

Figure 1.9: Evolution of the Well Base Pressure as the outlet valve opening is stepped down.

However, some improvements could be made to the numerical scheme: the solver has difficulties computing the solution when it approaches the boundaries of the open domain Ω defined by (1.10). Indeed, near these critical points, the considered functions are not C^1, which makes Newton's algorithm fail to converge. A more advanced solving method should be considered.

1.4 State-of-the-art control solutions

As mentioned in Section 1.2.2, slugging is typically handled by reducing the opening of the outlet valve, until an open-loop stable operating point is reached. In order to operate around open-loop *unstable* operating points (which correspond to higher production levels), several stabilization techniques have been considered since the 1930s (see [6, 13, 17, 23, 46, 56]). Recently, active control of the outlet valve has been identified as a very promising and cost-effective solution [25]. If used with a well-chosen information signal, it allows to counteract the pressure and flow rate oscillations concomitant with the occurrence of slugging, and thus to stabilize the flow. Classically, pressure measurements are used in feedback loops to actuate the valve. Most of the state-of-the-art strategies are single-variable (PI) controllers using only the bottom pressure sensor (i.e. the sensor located at the base of the well or flowline riser), when it is available (see e.g. [12, 13, 23, 26] for successful implementations of such

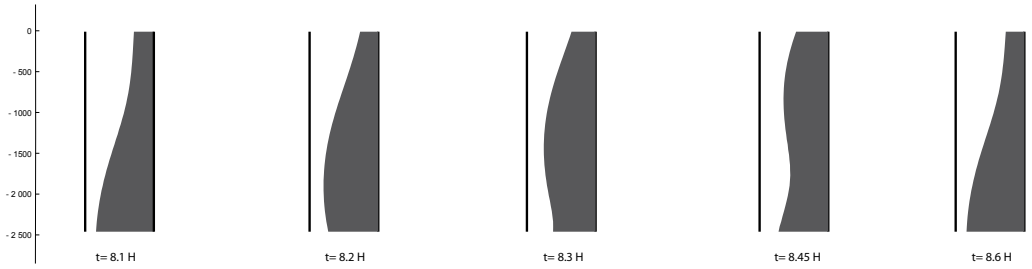

(a) Liquid mass hold-up profiles

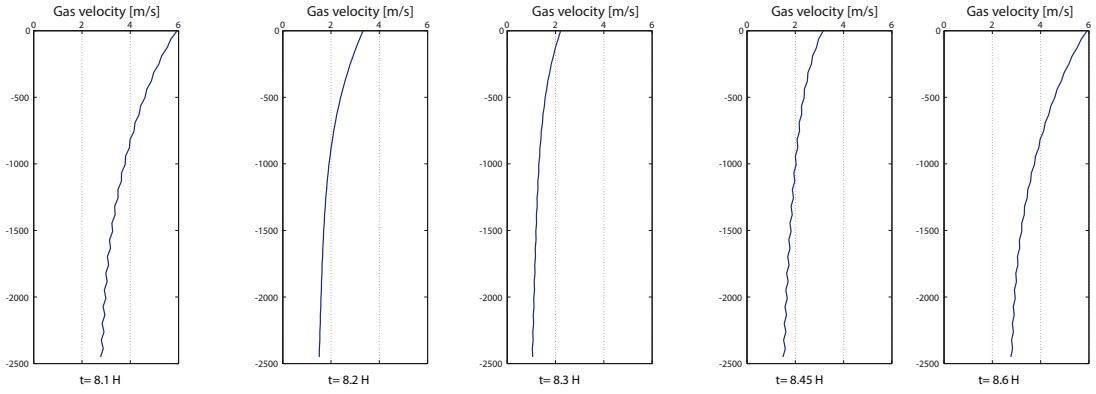

(b) Gas velocity profiles

Figure 1.10: Liquid mass hold-up and gas velocity profiles at different time instants. At t = 8.1 h, a slug is formed at the bottom of the pipe. It is then transported upwards and expelled over the next .5 hours, while another slug is formed. The velocity of the flow is inhomogeneous in space and time: the slugging cycle comprises phases of acceleration and deceleration, as pictured on Figure (b).

controllers). As will be discussed further, such simple controllers are not always well suited to deal with the complex dynamics involved in slugging. Since they cannot incorporate anticipation terms[6], PI controllers have difficulties handling oscillations over wide ranges of operating points. Moreover, the use of sensors located at the bottom of the pipes can be troublesome, since maintenance is very difficult at these locations.

To compensate for these shortcomings, recent efforts have focused on model-based control solutions. Simplified models, based on nonlinear Ordinary Differential Equations (ODE), such as [52] or [32] manage to capture the main features of the slugging phenomenon. In particular, there are able to reproduce the pressure and flow rate oscillations observed on slugging systems. Besides, their relative simplicity[7] allows for mathematical analysis and it is possible to derive control laws and estimators from them. For example, [1, 19, 47, 48] propose state estimators based on the Jansen model [32] that allow to reconstruct a possibly missing bottom pressure measurement from only topside sensors on a gas-lifted well. The estimate is then used in a PI feedback loop in simulations. Although, as pointed out by Skogestad, the performances of such a method are limited [51], we will show that it can be successfully extended to the stabilization of other slugging systems. Another use of simplified models is found in [52] and [48], where the efficiency of several control strategies are analytically compared using ODE-based models. Finally, [35] and [59] propose to derive nonlinear control laws from a simple model derived from the Van der Pol oscillator.

Another way to improve existing controllers is to use additional sensors in cascade structures. Siversten et al. have performed experiments both on small-scale [50] and medium-scale [49] facilities using various combinations of density, flow, and pressure measurements to suppress slugging. The results are very promising, in particular, it is shown that the flow may be stabilized with the sole use of topside sensors.

[6] In particular, derivative terms are usually discarded due to noise level on the sensor

[7] compared e.g. to PDE-based models such as the one presented in Section 1.3

Chapter 2

A model for control

Un modèle pour le contrôle

Le modèle proposé au chapitre précédent ne fournit malheureusement que peu de renseignements sur les possibles solutions de stabilisation du phénomène de slugging. C'est le cas de la grande majorité des modèles d'EDP, dont l'analyse mathématique est encore peu aisée. Dans la lignée des contributions de Jansen et al. [32], Imsland [31], Sinègre [48] et Storkaas [52], nous proposons dans ce chapitre un modèle de dimension finie, conçu dans le but d'élaborer des lois contrôle. Ce modèle s'obtient en écrivant la loi de conservation de la masse pour des volumes aggrégés de gaz et de liquide, plutôt que pour des tranches infinitésimales du tuyau (comme c'est le cas pour les modèles d'EDP). Malgré cette simplification du caractère distribué du problème, le modèle est capable de reproduire les oscillations de pression et de débit qui caractérisent le slugging. Une propriété intéressante est que les paramètres peuvent (et doivent) être calibrés, selon une procédure détaillée dans ce chapitre, afin d'ajuster le comportement du modèle et le faire correspondre à celui du système considéré. Ainsi, l'amplitude ou la forme des oscillations du modèle peuvent être modifiées afin qu'elles soient proches de celles de données mesurées. Enfin, le modèle peut être utilisé pour estimer des variables non mesurées au moyen d'un observateur, ou élaborer des lois de contrôle avancées, comme celles exposées au Chapitre 3. Le chapitre est organisé comme suit. Dans la Section 2.1, nous détaillons les équations du modèle et discutons les principales hypothèses de modélisation. Dans la section 2.2, nous procédons à une analyse des propriétés dynamiques du modèle. En particulier, après la construction d'un ensemble compact invariant dans lequel l'existence et l'unicité des solutions sont garanties, nous prouvons l'existence d'une orbite périodique pour un système de dimension 2 approchant le modèle. Enfin, nous présentons en Section 2.3 la procédure de calibration mentionnée ci-dessus.

As highlighted in Chapter 1, existing PDE models give little insight into possible control solutions to the slugging problem. Following the works of Jansen et al. [32],

Imsland [31], Sinègre [48] and Storkaas [52], we propose a finite-dimensional model obtained by writing the mass conservation laws for lumped volumes of gas and liquid (rather than for infinitesimal sections of the pipe). Despite this simplification of the spatial dependence of the state variables, the model is able to reproduce the pressure and flow rate oscillations that characterize the slugging phenomenon. Importantly, the parameters of the model can (and must) be chosen, following a proposed tuning procedure, to match the behavior of a given system. Using *a priori* information on a considered well or flowline riser, the procedure allows to calibrate the model so that, e.g., the shape of the simulated pressure oscillations is close to actual measured data. As will appear in Chapter 3, the model can be used to estimate state information by means of an observer, or to elaborate advanced control laws. The chapter is organized as follows. In Section 2.1, we present the model equations and discuss modeling assumptions. In Section 2.2, we proceed to a dynamical systems analysis of the model. After constructing a compact set where the solutions of the model are properly defined (i.e., where their existence and uniqueness is guaranteed), we prove, for a second-order approximate model, the existence of a periodic orbit corresponding to the slugging cycle. Finally, in Section 2.3, we present the procedure used to calibrate the parameters of the model.

2.1 Detailed model description

In this section, we present our model originally proposed in [14]. We recall its origins and discuss modeling assumptions.

2.1.1 Origins of the model

The model has been largely inspired by the contributions of [32] and [52]. These models are used to reproduce the slugging phenomenon in gas-lifted wells and flowline risers with low-points, respectively. Both have in common that the very nature of the system induces a separation of it into three volumes, not necessarily spatially distinct. In [32], the casing (filled only with gas to be injected into the well) is separated from the tubing (containing one volume of gas, and one of liquid) by the gas injection valve. In the Storkaas model [52], the separation is suggested by the existence of a low-point angle in the geometry of the pipe. The oil, accumulating at the bottom of the riser, acts at this location as a valve for the gas, the opening of which is determined by the height of liquid. In both cases, the gas, accumulating upstream the separating valve, cause a build-up of pressure, which is the culprit of the instability.

2.1.2 Model description

Consider now the pipe depicted in Figure 2.1. It is subjected to constant inflows of gas and liquid, and the outflow can be controlled thanks to a choke valve. In order to

preserve the structure of the Jansen and Storkaas models, which have proved efficient in reproducing the slugging phenomenon for their specific applications, we propose the following new idea: even when the geometry does not suggest such a separation, an irregularity in the pipe may cause the gas to stop flowing steadily. This irregularity is modeled by a 'virtual valve' [14]. Upstream this virtual valve, gas accumulates and forms a large elongated bubble, where a build-up of pressure occurs, eventually generating instability. The part of the pipe located downstream the virtual valve will be referred to as the *riser*. We now detail the other modeling assumptions.

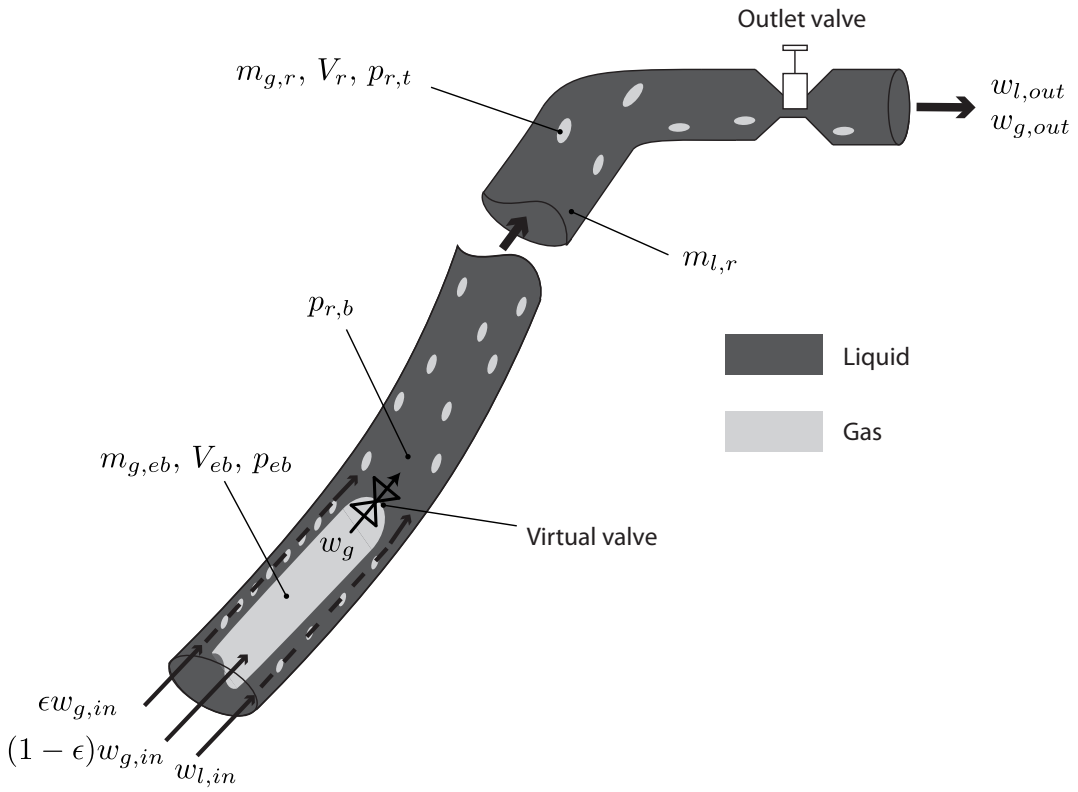

Figure 2.1: Schematic view of the considered transport pipe.

Mass balance equations The state variables are the mass of gas in the elongated bubble $m_{g,eb}$, the mass of gas in the rest of the riser $m_{g,r}$ and the mass of liquid in the riser $m_{l,r}$. Mass conservation read

$$\dot{m}_{g,eb}(t) = (1-\epsilon)w_{g,in} - w_g(t) \tag{2.1}$$

$$\dot{m}_{g,r}(t) = \epsilon w_{g,in} + w_g(t) - w_{g,out}(t) \tag{2.2}$$

$$\dot{m}_{l,r}(t) = w_{l,in} - w_{l,out}(t) \tag{2.3}$$

where $w_{g,in}$ and $w_{g,out}$ (resp. $w_{l,in}$ and $w_{l,out}$) are the mass flow rates of gas (resp. liquid) entering (*in*) the riser and coming out (*out*) of the riser ; and w_g is the mass flow rate of gas through the virtual downhole choke. Note that, in this model, a fraction of the gas flow (determined by $\epsilon \in (0, 1)$) goes directly to the upper part of the riser (along with the liquid), whereas the remaining accumulates in the bottom part of volume V_{eb}, causing a build-up of pressure.

Description of mass flows As mentioned above, the inflow rates of gas and liquid are assumed constant. This is an important assumption because it prevents the model from reproducing the production decrease due to the occurence of slugging. Indeed, with constant inflows, the equilibrium outflow is constant and independent from the operating point, and therefore the equilbrium level of production is the same for all values of the valve opening (whether they correspond to stable or unstable points). Also, in order to satisfy the mass conservation law, the average production over one slugging cycle must be equal to the inflow during the same period. Thus, the phenomenon described by Figure 1.7 cannot be reproduced by this model. Pressure-dependent inflows can be considered, but make the mathematical analysis much more difficult and complicate the calibration of the model. For the gas flow through the virtual valve, we assume a linear relation

$$w_g = C_g \max(0, (p_{eb} - p_{r,b})) \tag{2.4}$$

where p_{eb} is the pressure in the elongated bubble, and $p_{r,b}$ the pressure in the riser downstream the valve. C_g is assumed constant, which means that the virtual valve is either fully closed or fully opened. The $\max(0, \cdot)$ function indicates that no back-flow is admitted through the valve. The total flow through the outlet valve is given by a classical valve equation

$$w_{out} = C_{out} u \sqrt{\rho_m (p_{r,t} - p_s)} \tag{2.5}$$

The density of the mixture ρ_m is assumed constant, equal to the density liquid ρ_l. This error will be corrected by tuning the parameter C_{out}, as indicated in Section 2.3.4. On the other hand, p_s is the (constant) separator pressure/manifold pressure, whereas $p_{r,t}$ is the pressure at the top of the riser, upstream the production valve. u is the opening of the choke, which is the actuator of the system, and C_{out} is the choke constant. The flow rates of gas and liquid are computed from the respective mass fractions

$$\begin{aligned} w_{l,out} &= \frac{m_{l,r}}{m_{l,r} + m_{g,r}} \approx w_{out} \\ w_{g,out} &= \frac{m_{g,r}}{m_{l,r} + m_{g,r}} \approx \frac{m_{g,r}}{m_{l,r}} w_{out} \end{aligned}$$

We assume no change in slip through the valve.

Closure relations on the pressures The pressures in the riser are determined by the ideal gas law. The volume of the elongated bubble V_{eb} is assumed constant, whereas the gas downstream the virtual valve is compressible. Its volume is determined by the amount of liquid in this part of the riser: $V_{g,r} = V_r - \frac{m_{l,r}}{\rho_l}$, where V_r is the volume of the riser. The pressure balance over the riser is assumed to be stationary, consistently with existing models [48, 52]

$$
\begin{aligned}
p_{eb} &= \frac{m_{g,eb} RT}{M V_{eb}} \\
p_{r,t} &= \frac{m_{g,r} RT}{M(V_r - \frac{m_{l,r} + m_{l,still}}{\rho_l})} \\
p_{r,b} &= p_{r,t} + (m_{l,r} + m_{l,still}) \frac{g \sin\theta}{A}
\end{aligned}
$$

θ is the mean inclination of the pipe, and A the cross-section area. One should note that the effect of the mass of gas on the gravity pressure drop is neglected, compared to that of the mass of liquid. $m_{l,still}$ is a constant parameter used for tuning purposes. It represents the minimum mass of liquid present in the riser at all times. Indeed, apart from the case of severe slugging (where $m_{l,still}$ may be 0), the riser is never filled only with gas, and only a part of the liquid is concerned by the dynamics (2.1)-(2.2)-(2.3).

2.1.3 Sustained oscillations of the proposed model

The proposed model (2.1)-(2.2)-(2.3) has the ability to reproduce the oscillations observed on real slugging systems. To illustrate this point, Figure 2.2 shows the variations of the pressures and flow rates simulated with this model. The system under consideration is a 7200-meter long well located in the North Sea. To match the behavior of the well, the parameters need to be calibrated. A tuning procedure is described in Section 2.3. Before focusing on the analytical properties of the proposed model, we now qualitatively analyze the oscillations of the system. Three phases, depicted in Figure 2.3 can be identified. The oscillations are created by the accumulation of gas in volume V_{eb}, which can only be emptied through the virtual valve if the pressure p_{eb} is greater than the bottom-hole pressure $p_{r,bh}$. The three phases are as follows.

Phase 1 The bottom hole pressure is low because the mass of liquid in the riser is small and causes only a small gravity pressure drop. Therefore, the virtual valve is open ($p_{r,bh} < p_{eb}$) and gas flows out from V_{eb} at a high rate, causing the pressure in the elongated bubble (p_{eb}) to decrease rapidly. When p_{eb} is small enough, V_{eb} starts filling again ($w_g < w_{g,in}$) and m_{eb} increases. Yet, $m_{l,r}$ increases more rapidly than $m_{g,eb}$ (due to low output flow rates), and therefore the valve closes ($p_{r,bh} \geq p_{eb}$) at point A in the timeline.

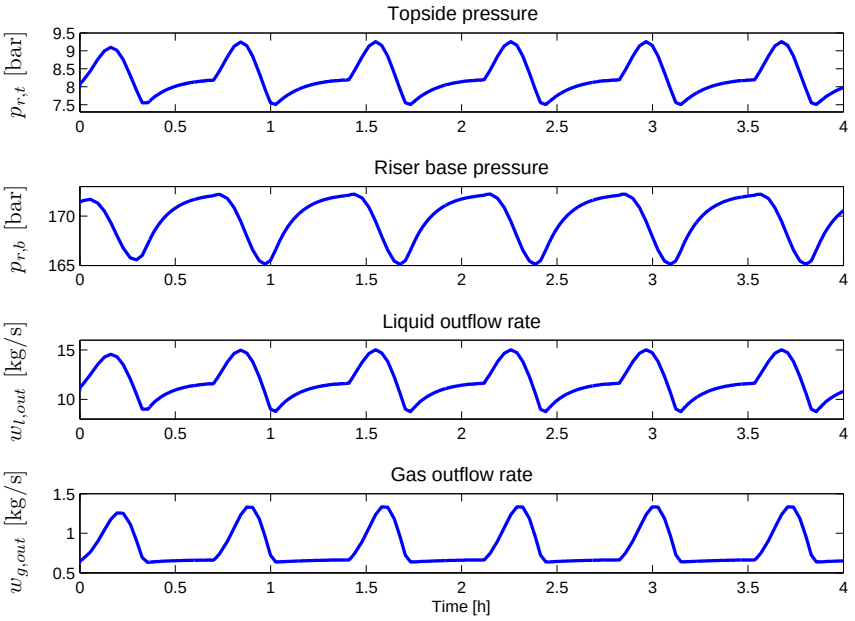

Figure 2.2: Pressure and flow rate oscillations of the reduced model

Phase 2 After a sharp increase, $m_{l,r}$ reaches an asymptotic value, whereas $m_{g,eb}$ increases steadily. Therefore, the virtual valve remains closed until p_{eb} reaches the asymptotic value of $p_{r,bh}$ and the valve opens again at point B in the timeline.

Phase 3 When the valve opens, the riser is filled with liquid (the value of $m_{l,r}$ is high) and the gas entering the upper part of the riser is highly compressed. This increases the pressure at the choke and therefore the outflows get very high: the riser is suddenly emptied of its liquid and gas. It is the blow-out phase. After this blow-out, the masses, the flows and the pressures go back to low values, and, eventually, the cycle repeats when point C in the timeline is reached.

We now focus on a more quantitative approach by investigating the dynamical properties of the model.

2.2 Dynamical analysis

As discussed in Section 2.1.3, the proposed model has the ability to reproduce the pressure and flow rate oscillations corresponding to the slugging phenomenon. From a dynamical systems point of view, this corresponds to the existence of a limit cycle for the system. We prove the existence of such a periodic orbit in Section 2.2.2. First, we construct a positively invariant compact set in which the existence and uniqueness of the solutions to the Cauchy problem are guaranteed.

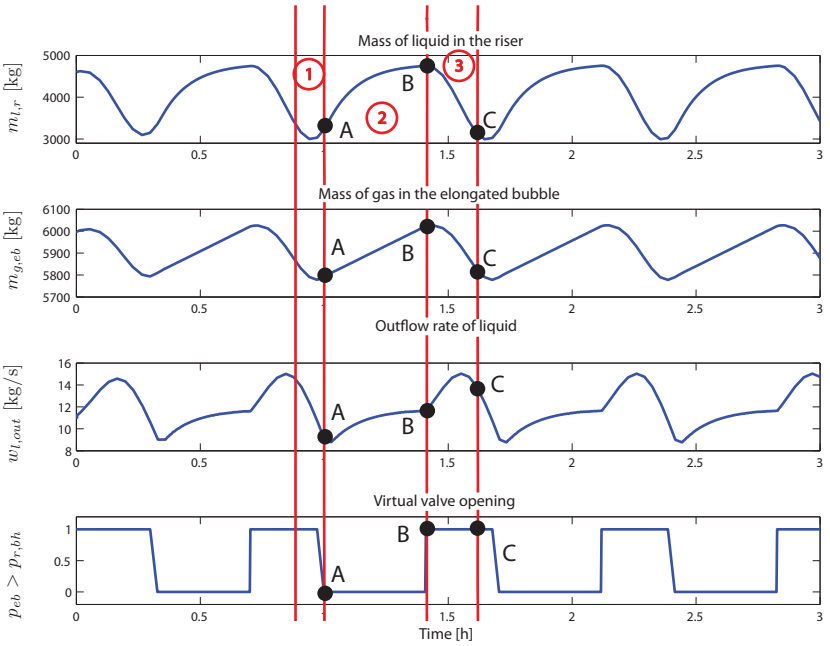

Figure 2.3: The three stages of the oscillations

2.2.1 Existence and uniqueness of solutions: construction of an adequate compact set

In this section, we construct a compact set $K \subset \mathbb{R}^3$, positively invariant for (2.1)-(2.2)-(2.3). Its construction is based both on physical considerations (e.g., the volume of liquid cannot exceed the total volume of the riser) and computational practicality (e.g., the terms inside square roots should not approach zero). The construction aims at yielding the largest, physically sound, set where the right-hand-side of the dynamics equations are smooth functions of the states. A natural approach consists in looking for an invariant compact set under the form of a rectangular domain. It appears that the following representation of the system is particularly suited to such a construction. Consider the set of independent state variables $(\chi_1,\chi_2,\chi_3) = (m_{g,eb}, \frac{m_{g,r}}{m_{l,r}}, m_{l,r})$. With these variables, system (2.1)-(2.2)-(2.3) rewrites

$$\dot{\chi}_1 = (1-\epsilon)w_{g,in} - C_g \max\left[0, a\chi_1 - b\frac{\chi_2\chi_3}{m_l^\Delta - \chi_3} - c(\chi_3 + m_{l,still})\right] \tag{2.6}$$

$$\dot{\chi}_2 = \frac{1}{\chi_3}\left(\epsilon w_{g,in} - C_g \max\left[0, a\chi_1 - b\frac{\chi_2\chi_3}{m_l^\Delta - \chi_3} - c(\chi_3 + m_{l,still})\right] - \chi_2 w_{l,in}\right) \tag{2.7}$$

$$\dot{\chi}_3 = w_{l,in} - C_{out}u\sqrt{\rho_l\left(b\frac{\chi_2\chi_3}{m_l^\Delta - \chi_3} - p_s\right)} \tag{2.8}$$

where

$$a = \frac{RT}{MV_{eb}}, \qquad b = \frac{\rho_l RT}{M}, \qquad c = \frac{g\sin\theta}{A}, \qquad m_l^\Delta = \rho_l V_r - m_{l,still} \tag{2.9}$$

We first consider a rectangular domain K', which is positively invariant for (2.6)-(2.7)-(2.8), defined by $K' = [\chi_1^-, \chi_1^+] \times [\chi_2^-, \chi_2^+] \times [\chi_3^-, \chi_3^+]$ with

$$\begin{aligned}
\chi_1^- &= c\frac{m_{3,still}}{a}, & \chi_1^+ &= \frac{1}{C_g a}\left[-\epsilon w_{g,in} + \frac{\bar{p}_{r,t}}{b}\frac{1-\mu}{\mu}w_{l,in}\right] + \frac{\bar{p}_{r,t}}{a} + c\frac{\mu m_l^\Delta + m_{3,still}}{a} \\
\chi_2^- &= \frac{\bar{p}_{r,t}}{b}\frac{\eta}{1-\eta}, & \chi_2^+ &= \frac{\bar{p}_{r,t}}{b}\frac{1-\mu}{\mu} \\
\chi_3^- &= \mu m_l^\Delta, & \chi_3^+ &= (1-\eta)m_l^\Delta
\end{aligned}$$

where $\bar{p}_{r,t} = p_s + \frac{w_{l,in}^2}{\rho_l C_{out}^2 u^2}$ is the equilibrium topside pressure corresponding to a given operating point $u \in (0, 1)$. The two parameters $0 < \eta < 1$ and $0 < \mu < 1$ are chosen such that[1]

$$\eta < \frac{b\epsilon GLR}{\bar{p}_{r,t} + b\epsilon GLR}, \quad \eta + \mu < 1 \tag{2.10}$$

and

$$\eta\mu w_{g,in} - \frac{w_{l,in}}{b}\bar{p}_{r,t}(1-\mu)\eta - C_g\bar{p}_{r,t}(1-\mu-\eta) + C_g\frac{g\sin\theta}{A}m_l^\Delta(1-\mu-\eta)\eta\mu \le 0 \tag{2.11}$$

where $GLR = \frac{w_{g,in}}{w_{l,in}}$ is the equilibrium gas-liquid mass ratio. The boundaries of K' are constructed to ensure that the vector field defined by the right-hand-side of (2.6)-(2.7)-(2.8) points inside K' at the boundaries. For example, we have

$$\begin{aligned}
\dot{\chi}_3(\chi_1, \chi_2, \chi_3^-) &= w_{l,in} - C_{out}u\sqrt{\rho_l\left(b\frac{\chi_2\chi_3^-}{m_l^\Delta - \chi_3^-} - p_s\right)} \\
&\ge w_{l,in} - C_{out}u\sqrt{\rho_l\left(b\chi_2^+\frac{\mu}{1-\mu} - p_s\right)} && \text{by definition of } \chi_3^- \\
&\ge w_{l,in} - C_{out}u\sqrt{\rho_l(\bar{p}_{r,t} - p_s)} && \text{by definition of } \chi_2^+ \\
&\ge 0 && \text{by definition of } \bar{p}_{r,t}
\end{aligned}$$

Similarly, the following inequalities are verified for all $(\chi_1, \chi_2, \chi_3) \in K'$

$$\begin{aligned}
\dot{\chi}_1(\chi_1^-, \chi_2, \chi_3) &\ge 0, & \dot{\chi}_1(\chi_1^+, \chi_2, \chi_3) &\le 0 \\
\dot{\chi}_2(\chi_1, \chi_2^-, \chi_3) &\ge 0, & \dot{\chi}_2(\chi_1, \chi_2^+, \chi_3) &\le 0 \\
\dot{\chi}_3(\chi_1, \chi_2, \chi_3^-) &\ge 0, & \dot{\chi}_3(\chi_1, \chi_2, \chi_3^+) &\le 0
\end{aligned}$$

[1] Inequalities (2.10) and (2.11) are verified for $\eta = \mu = 0$. Even though the two parameters must be strictly positive, this guarantees, by continuity, that they hold for sufficiently small values of η and μ.

This proves that K' is positively invariant. To ensure that the right-hand side of (2.6)-(2.7)-(2.8) is a smooth function of the states, we have yet to guarantee that the expression inside the square root in Equation (2.8) remains strictly positive. Thus, we construct K as the intersection of the rectangular set K' with a domain where this condition is always fulfilled. We consider the following family of domains, indexed by $\sigma > 0$

$$\mathcal{D}_\sigma = \left\{ (\chi_1, \chi_2, \chi_3) \in \mathbb{R}^3 \ / \ b\frac{\chi_2\chi_3}{m_l^\Delta - \chi_3} - p_s \geq \sigma \right\}$$

We now show that there exists a certain σ^* such that $K \cap D_{\sigma^*}$ is positively invariant. First, we notice that the flow points inside $K' \cap \mathcal{D}_0$. Indeed, for any $\chi \in K' \cap \partial\mathcal{D}_0 = K' \cap \left\{ b\frac{\chi_2\chi_3}{m_l^\Delta - \chi_3} = p_s \right\}$, we have

$$\begin{aligned}
\frac{d}{dt}\left(b\frac{\chi_2\chi_3}{m_l^\Delta - \chi_3} \right) =& \frac{b}{m_l^\Delta - \chi_3}\left[\epsilon w_{g,in} + C_g \max(0, a\chi_1 - b\frac{\chi_2\chi_3}{m_l^\Delta - \chi_3} - c(\chi_3 + m_{l,still})) \right. \\
& \left. + w_{l,in}\frac{\chi_2\chi_3}{m_l^\Delta - \chi_3} - m_l^\Delta \frac{\chi_2}{m_l^\Delta - \chi_3} u C_{out} \sqrt{\rho_l \left(b\frac{\chi_2\chi_3}{m_l^\Delta - \chi_3} - p_s \right)} \right] \qquad (2.12) \\
=& \frac{b}{m_l^\Delta - \chi_3}\left[\epsilon w_{g,in} + C_g \max(0, a\chi_1 - p_s - c(\chi_3 + m_{l,still})) + \frac{p_s}{b} \right] \\
>& \delta \qquad (2.13)
\end{aligned}$$

for some $\delta > 0$. Then, we denote $f : \mathbb{R}^3 \to \mathbb{R}$ the function at the right-hand side of (2.12). f is continuous on the the compact set K', therefore it is uniformly continuous on K'. Thus, there exists γ such that

$$\forall (x, y) \in K'^2 \qquad \|x - y\| < \gamma \Rightarrow |f(x) - f(y)| < \frac{\delta}{2} \qquad (2.14)$$

where δ is defined by (2.13). We now pick

$$K = K' \cap \mathcal{D}_{\sigma^*} \qquad \text{where} \qquad \sigma^* = \frac{\gamma}{2}\frac{\chi_3^-}{m_l^\Delta - \chi_3^-}$$

K is positively invariant. Indeed, we have, for any $(\chi_1^*, \chi_2^*, \chi_3^*)^T \in K' \cap \partial\mathcal{D}_{\sigma^*} = K' \cap \left\{ b\frac{\chi_2^*\chi_3^*}{m_l^\Delta - \chi_3^*} = p_s + \sigma^* \right\}$

$$\begin{aligned}
\left\| (\chi_1^*, \chi_2^*, \chi_3^*)^T - \left(\chi_1^*, p_s\frac{m_l^\Delta - \chi_3^*}{b\chi_3^*}, \chi_3^* \right)^T \right\| &= \left\| \left(0, \sigma^*\frac{m_l^\Delta - \chi_3^*}{\chi_3^*}, 0 \right)^T \right\| \\
&\leq \sigma^*\frac{m_l^\Delta - \chi_3^-}{\chi_3^-} < \gamma
\end{aligned}$$

where γ is defined by (2.14). This implies $|f(\chi_1^*,\chi_2^*,\chi_3^*) - f(\chi_1^*, p_s,\chi_3^*)| < \frac{\delta}{2}$. Since $(\chi_1^*, p_s\frac{m_l^\Delta-\chi_3^*}{b\chi_3^*},\chi_3^*) \in K' \cap \partial\mathcal{D}_0$, then $f(\chi_1^*, p_s\frac{m_l^\Delta-\chi_3^*}{b\chi_3^*},\chi_3^*) > \delta$. Finally, this yields

$$f(\chi_1^*,\chi_2^*,\chi_3^*) > \frac{\delta}{2}$$

which shows that K is positively invariant. Besides, K is the intersection of two compact sets, thus it is a compact set. Finally, the right-hand-side of (2.6)-(2.7)-(2.8) is a C^1 function of the states on the compact set K, therefore it is globally Lipschitz on K. This ensures then existence and uniqueness of the trajectories starting in K in the sense of Proposition 2.2.1.

Proposition 2.2.1 *For all $t_0 \in \mathbb{R}$ and $\chi_0 \in K$ there is a unique solution χ to* (2.6)-(2.7)-(2.8) *verifying $\chi(t_0) = \chi_0$. This solution is defined for all $t \geq t_0$.*

Proof This is a direct application of [37, Theorem 3.3, p.94].

We now investigate the existence of a periodic orbit for the model, corresponding to the slugging phenomenon.

2.2.2 Existence of a limit cycle

The slugging phenomenon is characterized by periodic oscillations of the pressure and flow rates inside the pipe. In [48], it is shown, using the Poincaré-Bendixson criterion (see e.g. [37, Lemma 2.1]), that these correspond to the existence of a limit cycle for a reduced second-order model. The reduced model is obtained, there, by assuming that the mass of liquid is proportional to the mass of gas in the riser. We follow a similar approach by considering an affine relation between these two state variables. For this reason, we consider the same set of variables $(x_1, x_2, x_3) = (m_{g,eb}, m_{g,r}, m_{l,r})$ initially used to derive Equations (2.1)-(2.2)-(2.3). With the notations given by (2.9), the model reads

$$\dot{x}_1 = (1-\epsilon)w_{g,in} - C_g \max\left[0, ax_1 - \frac{bx_2}{m_l^\Delta - x_3} - c(x_3 + m_{l,still})\right] \tag{2.15}$$

$$\dot{x}_2 = \epsilon w_{g,in} + C_g \max\left[0, ax_1 - \frac{bx_2}{m_l^\Delta - x_3} - c(x_3 + m_{l,still})\right] - \frac{x_2}{x_3}C_{out}u\sqrt{\rho_l\left(\frac{bx_2}{m_l^\Delta - x_3} - p_s\right)} \tag{2.16}$$

$$\dot{x}_3 = w_{l,in} - C_{out}u\sqrt{\rho_l\left(\frac{bx_2}{m_l^\Delta - x_3} - p_s\right)} \tag{2.17}$$

This representation is equivalent to the representation of Section 2.2.1 since the application $\varphi : (\chi_1,\chi_2,\chi_3) \in \mathbb{R}^3 \mapsto (x_1, x_2, x_3) = (\chi_1,\chi_2\chi_3,\chi_3) \in \mathbb{R}^3$ is a C^1-diffeomorphism on K. Moreover, $\varphi(K)$ is a compact invariant set for (2.15)-(2.16)-(2.17). We now

study a model close to (2.15)-(2.16)-(2.17) by making the following approximation: for a given value of the control input (outlet valve opening) $\bar{u} \in (0, 1)$, we assume that the following linear relation is always satisfied

$$x_3 = m_l^\Delta - \frac{b}{\bar{p}_{r,t}} x_2 \tag{2.18}$$

One should notice that (2.18) is equivalent to assuming that the topside pressure ($p_{r,t} = \frac{bx_2}{m_l^\Delta - x_3}$) is always equal to its equilibrium value $\bar{p}_{r,t}$. Under this assumption, Equations (2.15)-(2.16) rewrite

$$\begin{aligned}
\dot{x}_1 =& (1-\epsilon) w_{g,in} - C_g \max\left[0, a x_1 - \bar{p}_{r,t} - c(m_l^\Delta - \frac{b}{\bar{p}_{r,t}} x_2 + m_{l,still})\right] \\
\dot{x}_2 =& \epsilon w_{g,in} + C_g \max\left[0, a x_1 - \bar{p}_{r,t} - c(m_l^\Delta - \frac{b}{\bar{p}_{r,t}} x_2 + m_{l,still})\right] - \frac{x_2}{m_l^\Delta - \frac{b}{\bar{p}_{r,t}} x_2} w_{l,in}
\end{aligned}$$

Noting

$$\alpha = C_g a, \quad \beta = C_g \frac{bc}{\bar{p}_{r,t}}, \quad \gamma = C_g \left(\bar{p}_{r,t} + c m_l^\Delta + c m_{l,still}\right), \quad \delta = w_{l,in} \frac{\bar{p}_{r,t}}{b}, \quad \nu = m_l^\Delta \frac{\bar{p}_{r,t}}{b}$$

yields

$$\dot{x}_1 = (1-\epsilon) w_{g,in} - \max(0, \alpha x_1 + \beta x_2 - \gamma) \tag{2.19}$$

$$\dot{x}_2 = \epsilon w_{g,in} + \max(0, \alpha x_1 + \beta x_2 - \gamma) - \delta \frac{x_2}{\nu - x_2} \tag{2.20}$$

We also consider the following compact set

$$D = [x_1^-, x_1^+] \times [x_2^-, x_2^+] = [\chi_1^-, \chi_1^+] \times [\chi_2^- \chi_3^+, \chi_2^+ \chi_3^-] = [\chi_1^-, \chi_1^+] \times [\eta\nu, (1-\mu)\nu]$$

We now state the main result of this section.

Theorem 2.2.1 *Under the assumption* $\alpha - \beta + \frac{(w_{g,in}+\delta)^2}{\eta\delta} > 0$*, system* (2.19)-(2.20) *has a periodic orbit lying in D. Conversely, if* $\alpha - \beta + \frac{(w_{g,in}+\delta)^2}{\eta\delta} < 0$*, the system has only one (locally) asymptotically stable stationary point.*

Proof The proof relies on the fact that D is positively invariant for (2.19)-(2.20). This is a direct consequence of the positive invariance of K for (2.6)-(2.7)-(2.8). Indeed, we have, e.g.

$$\begin{aligned}
\dot{x}_2(x_1, x_2^-) &= \epsilon w_{g,in} + \max(0, \alpha x_1 + \beta x_2 - \gamma) - \delta \frac{x_2^-}{\nu - x_2^-} \\
&\geq \epsilon w_{g,in} - w_{l,in} \frac{\bar{p}_{r,t}}{b} \frac{\eta}{1-\eta} \\
&> 0 \quad \text{by definition of } \eta
\end{aligned}$$

Similarly, the other bounds of D were chosen such that the computations are the same as in the proof of invariance of K in Section 2.2.1. Besides, system (2.19)-(2.20) has a single equilibrium given by

$$\bar{x}_1 = \frac{(1-\epsilon)w_{g,in} + \gamma - \beta\bar{x}_2}{\alpha}, \qquad \bar{x}_2 = \frac{w_{g,in}}{w_{g,in}+\delta}\nu$$

The Jacobian matrix around this equilibrium reads

$$J = \begin{pmatrix} -\alpha & -\beta \\ \alpha & \beta - \frac{(w_{g,in}+\delta)^2}{\eta\delta} \end{pmatrix}$$

Its determinant is $\det(J) = \alpha\frac{(w_{g,in}+\delta)^2}{\eta\delta} > 0$, so the eigenvalues of J have the same sign. Therefore, the equilibrium is asymptotically stable if

$$\text{tr}\,(J) = -\alpha + \beta - \frac{(w_{g,in}+\delta)^2}{\eta\delta} < 0$$

and unstable if $\text{tr}\,(J) > 0$. If the equilibrium point is unstable, the Poincaré-Bendixson theorem can be applied. This shows the existence of a periodic orbit lying in D for the nonlinear system (2.19)-(2.20). If $\text{tr}\,(J) < 0$, the equilibrium point is also asymptotically stable for the nonlinear system (see e.g. [37], Theorem 4.7).

We now go back to studying the dynamics of the full model (2.1)-(2.2)-(2.3), and present a tuning procedure that can be used to match the behavior of real systems.

2.3 Parameter tuning

In this section, we describe how to choose the parameters in model (2.1)-(2.2)-(2.3) to match the behavior of a given system, following a procedure initially proposed in [15]. These parameters are: L, θ, A, g, ρ_l, R, T, M, p_s, $w_{g,in}$, $w_{l,in}$, C_{out}, $m_{l,still}$, V_{eb} and ϵ. The procedure requires *a priori* information on the system. First, the geometry of the pipe is required to set the values of L, A, and θ. The equilibrium values of the topside pressure $\bar{y}_{r,t}(\bar{u})$ and downhole pressure $\bar{y}_{r,b}(\bar{u})$ at one operating point $\bar{u}$ are also required. These values can be measured, when corresponding sensors are available, or otherwise estimated by an advanced multiphase flow simulator (such as OLGA™). They determine the correct values of the choke constant C_{out} and the still mass of liquid $m_{l,still}$. Also, the value of the production choke opening that causes oscillations to appear on the real system u^* is needed. The analytic study of the bifurcation point of the model then determines the volume V_{eb} of the elongated bubble. Eventually, the magnitude of the pressure oscillations determines the fraction of gas ϵ that is not trapped in the elongated bubble.

2.3.1 Length of the riser

The riser is defined, in the model, as the part of the pipe downstream the virtual valve. The location of this valve is unknown *a priori*. In some cases, the geometry suggests a natural location, where an irregularity in the flow is likely to occur. It usually takes the form of an angle, when the well has a near-horizontal part followed by an inclined one. Once again, in the case of a low-point angle (when the near-horizontal part is declining), this assumption is consistent with the works of Storkaas [52]. When nothing in the geometry suggests the existence of an irregularity, other considerations, such as the location of the sensors can determine the most suited location for the virtual valve. The geometry of the real well, considered for sake of illustration in this section, and depicted on figure 2.7, clearly indicates that the virtual valve must be placed at the end of the near-horizontal section. This location coincides with that of the downhole pressure sensor.

2.3.2 Straightforward parameters

Numerous parameters in the model can be directly inferred from the geometry of the system, or the nature of the liquid-gas mixture. For example, the inclination parameter θ is the mean inclination of the pipe, and the cross-section area A is known. Similarly, the separator pressure and the temperature inside the pipe are measured and almost constant in practice. As a result, values for θ, A, g, ρ_l, R, T, M and p_s can be obtained from the geometry of the well under consideration and PVT data sheets for the fluid characteristics.

2.3.3 Inflow rates

Next, values must be given to the inflow rates of liquid ($w_{l,in}$) and gas($w_{g,in}$). The difficulty is that they are scarcely measured. Besides, they are not constant: the assumption that they are is a simplification, which is formulated to ease the computations. In the model, the values of the time-average outflow rates are used. They are commonly measured by Multiphase Flow Meters (MPM). At steady-state, the inflow and outflow rates must be constant and equal. Even though the average values of the outflow rates do not match their equilibrium values[2], they lie in the same range. This reveals accurate enough. When no flow meter can be used, an alternative solution is to use a commercial multiphase flow simulator like OLGA™ to compute the steady-state values of the inflow rates from the system characteristics.

2.3.4 Valve constants

As previously mentioned, the model contains two valve equations (2.4)-(2.5): one for the virtual valve, and one for the outlet valve. The constant for the outlet valve is

[2] which is precisely the reason why it is desired to stabilize the flow

usually provided by its manufacturer. Yet, equation (2.5) assumes that the density of the mixture is constant. Therefore, the equilibrium value of the topside pressure cannot perfectly fit the system for all values of the valve opening. For our model, it is given by $\bar{p}_{r,t} = p_s + \frac{w_{l,in}^2}{\rho_l C_{out}^2 u^2}$. To give a value to C_{out}, we choose to match it with the one of the real system $\bar{y}_{r,t}(\bar{u})$ for *one* value of the valve opening $\bar{u}$. To measure the equilibrium topside pressure $y_{r,t}(\bar{u})$, $\bar{u}$ has to lie in the stable region $\bar{u} < u^*$. On the other hand, the chosen equilibrium of the model should be as close as possible to the real one in the *unstable* region, where the flow must be stabilized. As a result, $\bar{u}$ is taken as close as possible to the bifurcation point, but strictly in the stable region. The value of C_{out} must be chosen so that

$$C_{out} = \frac{w_{l,in}}{\bar{u}\sqrt{\bar{y}_{r,t} - p_s}}$$

The second valve constant appearing in (2.4) is that of the virtual valve. Because it is difficult to mathematically study its impact on the dynamics, a rough estimate has to be picked manually at this stage of the tuning procedure. It may then be adjusted afterwards, once the parameters have been chosen, to slightly reshape the simulated oscillations. A typical value for this parameter is $C_g = 10^{-4}$ kg.s.m^{-1}.

2.3.5 Still mass of liquid

As mentioned in Section 2.1.2, the parameter $m_{l,still}$ represents the (minimum) mass of liquid present in the riser at all times. Its value is chosen using the equilibrium value of the bottom hole pressure for one operating point $\bar{u}$, given by

$$\bar{p}_{r,b}(\bar{u}) = \bar{p}_{r,t}(\bar{u}) + (\bar{m}_{l,r}(\bar{u}) + m_{l,still})\frac{g\sin\theta}{A} \tag{2.21}$$

$$= \bar{p}_{r,t}(\bar{u}) + \left(\frac{\bar{p}_{r,t}(\bar{u})}{\bar{p}_{r,t}(\bar{u}) + bGLR}(\rho_l LA - m_{l,still}) + m_{l,still}\right)\frac{g\sin\theta}{A} \tag{2.22}$$

$$= \bar{p}_{r,t}(\bar{u}) + \frac{\bar{p}_{r,t}(\bar{u})LA\rho_l + bGLRm_{l,still}}{\bar{p}_{r,t}(\bar{u}) + bGLR}\frac{g\sin\theta}{A} \tag{2.23}$$

where $GLR = \frac{w_{g,in}}{w_{l,in}}$ is the equilibrium gas-liquid mass ratio, and $b = \frac{\rho_l RT}{M}$. All the parameters except $m_{l,still}$ in this equation are known. Therefore, knowing (or, once again, estimating it with OLGA™) the value of the steady-state bottom hole pressure $\bar{y}_{r,b}(\bar{u})$ of the system for one operating point $\bar{u}$, one should set the parameter $m_{l,still}$ to

$$m_{l,still} = \frac{\bar{y}_{r,b} - \bar{y}_{r,t}}{g/A\sin\theta}\left(1 + \frac{\bar{y}_{r,t}}{bGLR}\right) - \frac{\bar{y}_{r,t}}{bGLR}V_r\rho_l$$

The value of $m_{l,still}$ highly depends on the system under consideration: it can be 0, e.g. for short flowline risers, and can reach $\frac{1}{2}V_r\rho_l$, which corresponds to at least half the riser being permanently filled with liquid.

2.3.6 Elongated bubble

A value for the volume of the elongated bubble V_{eb} has yet to be determined. This parameter is used to set the position of the bifurcation point of the model to that of the real system, which we note u^*. More specifically, the bifurcation point is characterized by the emergence of two purely imaginary eigenvalues. To find the best value for V_{eb}, one could write Routh's criterion for the Jacobian matrix $J(u^*)$ (expressions for the Jacobian matrix coefficients are reported in Appendix B), and solve the obtained equation with respect to V_{eb}. Unfortunately, the criterion does not take the form of an analytically tractable expression, and V_{eb} must be determined with a numerical solver (e.g. Newton's method). One can achieve this by solving the following problem

$$\Re\{\lambda(u^*, V_{eb})\} = 0 \tag{2.24}$$

with respect to V_{eb}, where λ is one of the two complex conjugate eigenvalues of the system (the third eigenvalue being always real). Figure 2.4 represents the variation, for $u = u^*$, of the real part of λ as V_{eb} increases. The corresponding locus of the

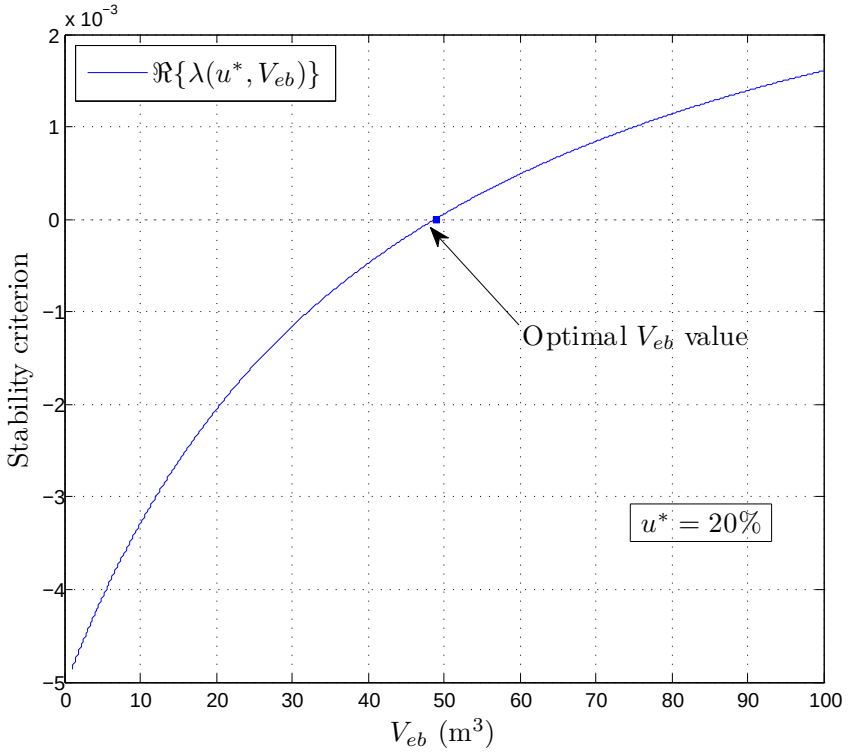

Figure 2.4: Value of $\Re\{\lambda(u^*, V_{eb})\}$ as V_{eb} increases. When the eigenvalues cross the imaginary axis, the criterion is exactly 0. The corresponding value of V_{eb} should be used in the model.

eigenvalues (parametrized by V_{eb}) are plotted in Figure 2.5.

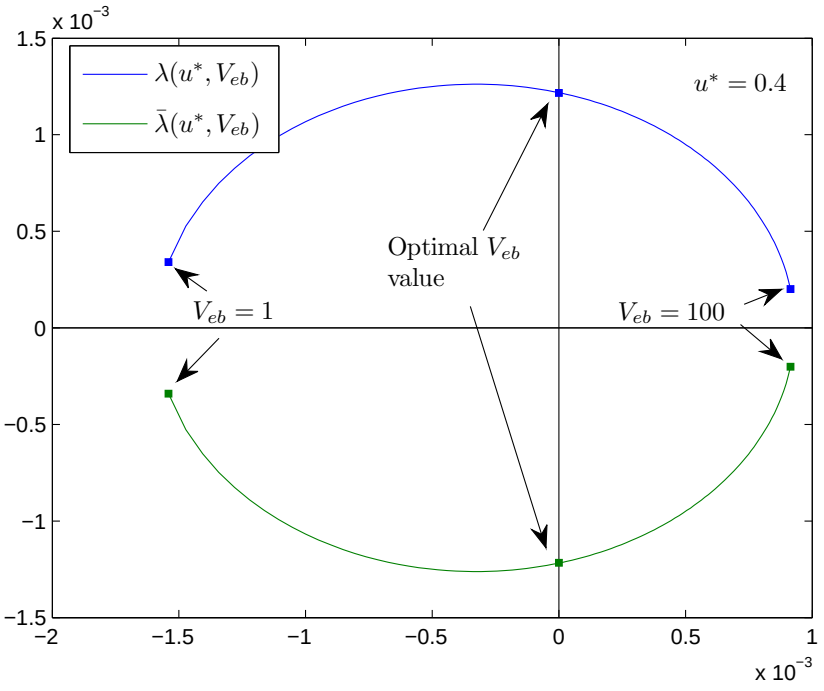

Figure 2.5: Locus of the eigenvalues $\lambda(u^*)$ and $\bar{\lambda}(u^*)$ when V_{eb} varies. For low values of V_{eb}, the eigenvalues are in the LHP. As the parameter increases, the eigenvalues cross the imaginary axis, which corresponds to the criterion plotted in Figure 2.4 being 0.

2.3.7 Split inflow of gas

Eventually, one must choose a value for ϵ, which determines the fraction of the amount of gas that accumulates into the elongated bubble. ϵ directly impacts on the magnitude of the pressure oscillations. In particular, it can be mathematically proven[3] that when the virtual valve is closed, i.e. when $p_{eb} < p_{r,b}$, the mass of liquid $m_{l,r}$ converges asymptotically to $\underline{m}_{l,r} = \frac{\bar{p}_{r,t}}{\bar{p}_{r,t}+\epsilon bGLR}(\rho_l LA - m_{l,still})$, and the topside pressure converges to $\bar{p}_{r,t}$. Yet, these values are only approached because the virtual valve does not remain closed in the observed oscillations. Therefore, the pressure at the base of the riser $p_{r,b}$ converges to a "pseudo-equilibrium"

$$\underline{p}_{r,b} = \bar{p}_{r,t} + (\underline{m}_{l,r} + m_{l,still})\frac{g\sin\theta}{A}$$

When the virtual valve opens again, the mass of liquid soon drops. This point is illustrated in Figure 2.6. Therefore, $\underline{p}_{r,b}$ is a good approximation of the maximum riser base pressure over the cycle. When a measure of the bottom hole pressure is available, ϵ can be chosen to match the peak of the oscillations of $p_{r,b}$ with that of the system $\bar{y}_{r,b}^{max}$

[3] thanks to an analytic integration of (2.1)-(2.2) and its asymptotics.

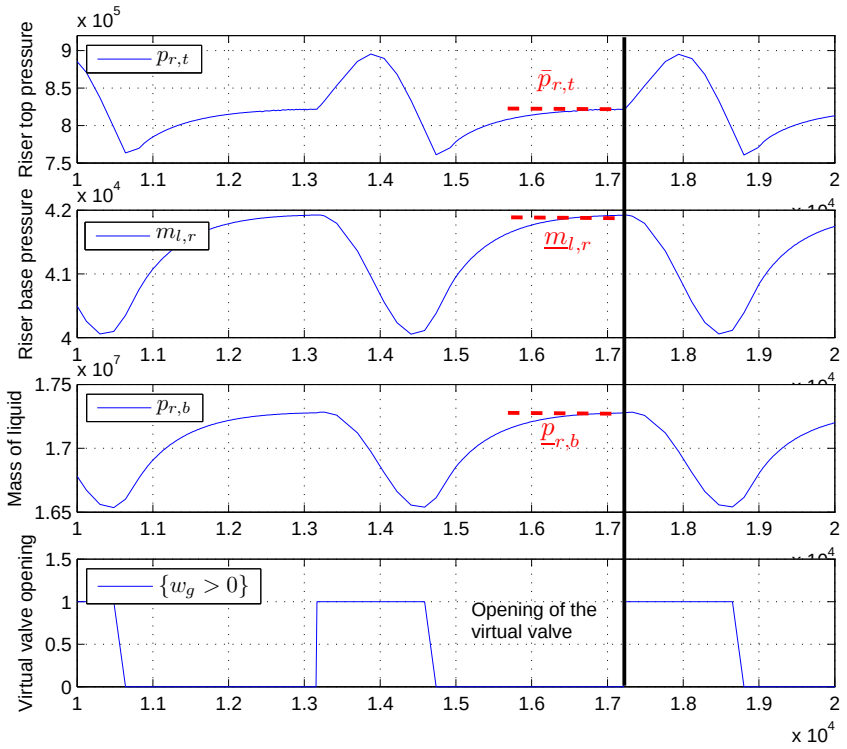

Figure 2.6: Convergence to a pseudo-equilibrium depending on ϵ

by setting

$$\epsilon = \frac{\bar{y}_{r,t}}{bGLR} \frac{\rho_l V_r - (y_{r,b}^{max} - \bar{y}_{r,t}) \frac{A}{g \sin\theta}}{(y_{r,b}^{max} - \bar{y}_{r,t}) \frac{A}{g \sin\theta} - m_{l,still}}$$

Otherwise, when no measure of the downhole pressure is available, ϵ has to be tuned manually, with a trial-and-error approach to match the magnitude of the topside pressure oscillations. As indicated by the expression of $\underline{m}_{l,r}$, the magnitude of the oscillations is a decreasing function of ϵ.

2.3.8 Summary and simulations

Table 2.1 gives a summary of the tuning procedure, along with the corresponding values for a case study. These values, reproduced courtesy of Statoil, correspond to an actual 7731 m-long well in the North Sea, schematically depicted on Figure 2.7. As mentioned in Section 2.3.1, the location of the virtual valve coincides with that of the downhole pressure sensor, at the end of the near-horizontal section. This assumption is validated by the resultant value of volume $V_{eb} = 48$ m^3. Indeed, the total volume of the pipe is, in the model, $LA + V_{eb} = 140.8$ m^3, which is very close to the actual total volume of the well $V = 140.4$ m^3. One should notice that nothing, in the computation

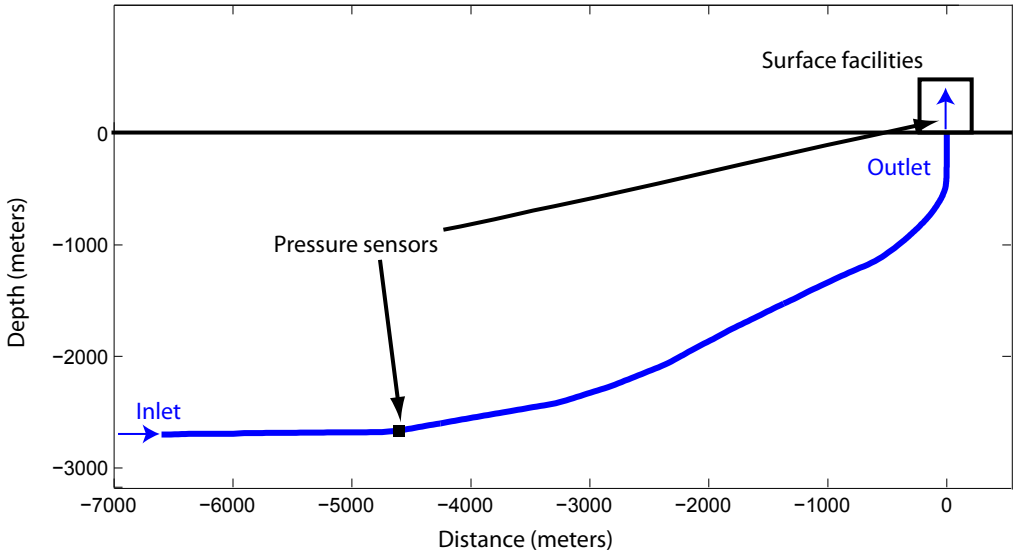

Figure 2.7: Schematic view of the considered well

of V_{eb}, guarantees this equality *a priori*. In general, it would be possible to obtain a total volume $LA + V_{eb}$ greater or smaller than the total well volume. A greater volume would correspond to an elongated bubble originating upstream the well (in the case of a reservoir, e.g.). A smaller value implies that the gas pocket occupies only a part of the volume of the well-section upstream the riser. This is also a valid assumption. Too large or inconsistent discrepancies should lead to reconsider the candidate value for L at the beginning of the identification process. Figure 2.8 shows a comparison between the model dynamics resulting from the aforedescribed tuning procedure and actual well measurements. Because the length L coincides with the depth of the sensor, the reconstructed downhole pressure and the measurements can be directly compared. Should this length differ from the sensor depth, some compensation would be considered, to provide fair comparisons. The results show the relevance of the model as the magnitude and frequency of the simulated oscillations almost match that of the real system. As will be illustrated in Section 3.1.1, the use of an observer taking into account measurements in real-time allows to compensate for the magnitude and frequency offset. In the next chapter, we describe how the model gives insight into the control design.

	Variable	Information used	Value
R	-	$R = 8.314$ J.K^{-1}mol^{-1}	
g	-	$g = 9.81$ m.s^{-2}	
T	Topside temperature sensor	$T = 363$ K	
L	Geometry of the well	$L = 5200$ m	
A	Geometry of the well	$A = 1.77 \times 10^{-2}$ m^2	
θ	Geometry of the well	$\theta = 0.78$ rad	
ρ_l	PVT data sheet	$\rho_l = 900$ kg.m^{-3}	
M	PVT data sheet	$M = 22 \times 10^{-3}$ kg.mol^{-1}	
p_s	Separator pressure sensor	$p_s = 6.6$ bar	
$w_{l,in}$	Multiphase flow meter	$w_{l,in} = 11.75$ kg.s^{-1}	
$w_{g,in}$	Multiphase flow meter	$w_{g,in} = 0.82$ kg.s^{-1}	
C_{out} C_g	Equilibrium topside pressure - at $\bar{u} = 35\%$: $\bar{y}_{r,t} = 8.23$ bar	$C_{out} = 8.32 \times 10^{-2}$ m $C_g = 1 \times 10^{-4}$ m	
$m_{l,still}$	Equilibrium downhole pressure at $\bar{u} = 35\%$: $\bar{y}_{r,b} = 170$ bar	$m_{l,still} = 3.73 \times 10^4$ kg $\approx \frac{1}{3}\rho_l V_r$	
V_{eb}	Bifurcation point $u^* \approx 20\%$	$V_{eb} = 48$ m^3	
ϵ	Max value of the downhole pressure $\bar{y}_{r,b}^{max} = 176$ bar	$\epsilon = 0.78$	

Table 2.1: Summary of the tuning procedure. The parameters are ordered accordingly.

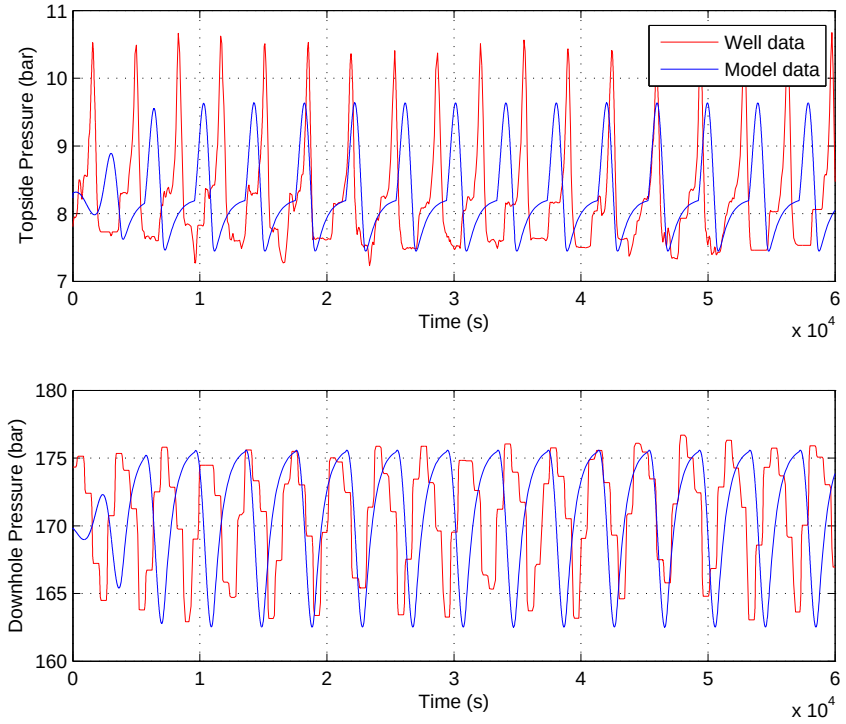

Figure 2.8: Topside and downhole pressure oscillations. Comparison between the model and well dynamics at $u = 35\%$.

Chapter 3

Control solutions

Solutions de contrôle

Dans ce chapitre, nous étudions la suppression du phénomène de slugging sur les puits de pétrole et les risers par actionnement de la vanne de sortie. Plus précisemment, nous proposons des algorithmes de stabilisation pour l'écoulement autour de points de fonctionnement instables en boucle ouverte, en utilisant les mesures provenant de capteurs de pression dans des boucles de rétroaction. Deux scenarios sont considérés, selon qu'un capteur de pression situé en bas du puit ou du riser est disponible ou non, chacun menant à une stratégie de contrôle différente.

Dans le Scenario 1, aucune mesure fiable de la pression à la base du puit (ou du riser) n'est disponible[1]*. Cette situation se présente lorsqu'un capteur, difficilement accessible, tombe en panne, ou simplement lorsqu'aucun capteur n'a été installé à la base du système. A partir d'informations sur l'équilibre du système, que nous exploitons à des fins de calibration du modèle, et d'une mesure de la pression en tête de puit ou de riser, nous proposons un algorithme de type observateur-contrôleur.*

Dans le Scenario 2, où une mesure de la pression de fond est disponible, nous proposons de changer la variable contrôlée de celle traditionnellement choisie dans l'industrie pétrolière. En combinant les mesures de deux capteurs, nous améliorons, au sens détaillé ci-dessous, les performances du simple contrôleur PI.

Du point de vue industriel, le principal objectif de ces lois de contrôle est l'augmentation du niveau moyen de production de pétrole. Toutefois, les effets bénéfiques de la stabilisation sur ce niveau de production ne ressortent pas toujours clairement des expériences à moyenne échelle, telles que considérées dans cette thèse. En effet, pour des raisons pratiques[2]*, les débits moyens sont généralements maintenus artificellement indépendants du point de fonctionnement. Dans ce contexte, un critère retenu pour*

[1] Dans cette situation, la méthode proposée ici est, à notre connaissance, la seule permettant de contrôler efficacement le slugging.

[2] pour éviter, en particulier, l'usure des pompes d'injection.

l'évaluation comparative des performances de chaque contrôleur est l'ouverture maximale de la vanne de sortie autour de laquelle il est possible de stabiliser le système. Plus l'ouverture de vanne est grande, plus la pression d'équilibre correspondante est faible ce qui devrait se traduire, lors du passage à l'échelle, par une augmentation de la production. Un autre critère important, que nous prendrons également en considération, est la robustesse aux changements de conditions opératoires.

Le chapitre est organisé comme suit. Dans la Section 3.1, nous étudions la stabilisation du slugging sans capteur de pression à la base du puits ou du riser. Nous proposons un observateur permettant d'estimer les variables d'état non mesurées, desquelles se déduit une estimation de la pression de fond. Les limitations inhérentes à cette situation, dûes à la présence de zéros instables dans la fonction de transfert du système, sont discutées. Enfin, une validation expérimentale de cette méthode de contrôle est proposée: les estimations sont utilisées dans une boucle de rétroaction pour stabiliser le slugging sur des installations expérimentales de moyenne échelle (le test-rig Statoil de Porsgrunn). Dans la Section 3.2, nous considérons le cas où la pression de fond est mesurée. Dans ce cas, l'importance d'une variable de contrôle spécifique, la masse de liquide contenue dans le riser, est mise en lumière par l'élaboration d'une loi de contrôle théorique. Cette loi de contrôle nonlinéaire, ainsi que sa preuve de convergence, suggèrent que la masse de liquide est une variable appropriée à la stabilisation de l'écoulement. La pertinence de cette approche est validée par des résultats expérimentaux.

In this chapter, we investigate methods for the suppression of the slugging phenomenon on wells or flowline risers, by automatic actuation of the outlet valve. More precisely, we propose control algorithms that aim at stabilizing the flow around open-loop unstable operating points, using the measurements from pressure sensors in feedback loops. The two following distinct industrial setups are considered, each one leading to a different control strategy

Scenario 1 We will first consider the case where no reliable riser base pressure sensor exists. This situation arises e.g. when a sensor, located where maintenance is difficult, fails, or simply when none was installed in the first place. By using only steady-state information on the inlet conditions to calibrate our model, and a pressure sensor located near the outlet of the pipe, the proposed strategy allows to suppress the pressure and flow rates oscillations associated with slugging. This result is consistent with recent results from the litterature [49, 50] where the flow is stabilized using two sensors in a cascade controller.

Scenario 2 When a reliable upstream pressure measurement is available, we propose an alternative control variable to the state-of-the-art method. Combining the measurements from two sensors, the resulting control law yields improved stabilizing properties, in the sense detailed below.

From an industrial point of view, the main objective of these control laws is to increase the production of oil. However, it is not always possible to see the effect of stabilization on production on experimental setups because, for practical reasons, the flow rate average is usually artificially kept independent of the operating point. Thus, in such context, one criterion used to compare the performances of each controller is the maximum opening of the production valve around which the system can be stabilized. A larger valve opening corresponds, at steady-state, to a lower pressure inside the pipe, which will translate, on real oil fields, into a higher oil production. Another important criterion is the robustness to changes in operating conditions. Both will be the subject of investigations.

The chapter is organized as follows. In Section 3.1, we consider the problem of suppressing slugging without a riser base pressure sensor. We propose an observer algorithm able to dynamically estimate the missing measurements. The limitations inherent to this sensing scenario are discussed, and an experimental validation of the design is provided: the estimates are used in a feedback control algorithm to stabilize an experimental multiphase flow loop subjected to slugging. Then, in Section 3.2, we consider the full-sensing scenario. The importance of a specific control variable, namely the mass of liquid in the riser, is highlighted by the design of a nonlinear control law for model (2.1)-(2.2)-(2.3), for which a Lyapunov-based proof of convergence is provided. Again, experiments on a multiphase flow loop illustrate the relevance of the approach.

3.1 Scenario 1: stabilization using topside sensors only

The pressure at the base of the riser was identified as a key variable for control of the slugging phenomenon [13, 23, 26, 52]. Unfortunately, this measurement is not always available. For wells, e.g., the sensors need to be installed several thousands meters deep into the ground, where maintenance is very difficult to perform. Some wells do not have sensors installed at all at these locations. For these reasons, it is interesting to consider the problem of stabilizing a system using only topside sensors in the feedback loop. We now propose an observer algorithm, designed for system (2.1)-(2.2)-(2.3), that reconstructs the three states of the model using only a topside pressure measurement.

3.1.1 Observer design

The structure of the proposed observer resembles a high-gain one [8]. To highlight this feature, one shall rewrite the model using the measured output as a state variable. Using the following set of state variables $(z_1, z_2, z_3) = (m_{eb}, p_{r,t}, m_{l,r})$, the model rewrites

$$\begin{aligned}
\dot{z}_1 =& f_1(z) \\
=& (1-\epsilon) w_{g,in} - C_g \max\left[0, a z_1 - z_2 - c(z_3 + m_{l,still})\right] && (3.1)\\
\dot{z}_2 =& f_2(z) \\
=& \frac{b}{m_l^\Delta - z_3} \Big[\epsilon w_{g,in} + C_g \max(0, a z_1 - z_2 - c(z_3 + m_{l,still})) \\
& + w_{l,in} \frac{z_2}{b} - \frac{m_l^\Delta}{z_3} \frac{z_2}{b} u C_{out} \sqrt{\rho_l (z_2 - p_s)} \Big] && (3.2)\\
\dot{z}_3 =& f_3(z) \\
=& w_{l,in} - C_{out} u \sqrt{\rho_l (z_2 - p_s)} && (3.3)
\end{aligned}$$

with $p_{r,t} = z_2$ as the measured output. The following observer is now considered

$$\dot{\hat{z}}_1 = f_1(\hat{z}) \tag{3.4}$$
$$\dot{\hat{z}}_2 = f_2(\hat{z}) - k(\hat{z}_2 - z_2) \tag{3.5}$$
$$\dot{\hat{z}}_3 = f_3(\hat{z}) \tag{3.6}$$

Remarks on the convergence of the proposed observer

The convergence of this algorithm is rather difficult to study, mainly because of the abrupt periodic changes in the dynamics caused by the openings and closings of the virtual valve. More precisely, the limit cycle of the system has to be separated into two distinct phases, depending on the argument of the $\max(\cdot, 0)$ functions being positive or negative (which corresponds to an open or closed virtual valve). Across this switch plane (defined by $\{a z_1 - z_2 - c(z_3 + m_{l,still}) = 0\}$) , the right-hand side of the dynamics is continuous, but not C^1. When the observer is not perfectly initialized, it may be in a different zone of the plane-phase that the original system. Thus, there is a total of four combinations to study to establish the convergence of the error dynamics, according to which phase the observer and the original system are in. It is difficult to find a Lyapunov function decreasing for all these phases, although numerical simulations suggest that the observer asymptotically converges to the original system, which would imply the existence of such a function. Yet, it is possible to obtain weaker results for some combinations. In particular, consider the phase when the virtual valve is closed both for the observer and the observed system. This corresponds to $a z_1 - z_2 - c(z_3 + m_{l,still}) < 0$ and $a \hat{z}_1 - \hat{z}_2 - c(\hat{z}_3 + m_{l,still}) < 0$. *During this phase*, the error dynamics can

be written

$$\dot{\tilde{z}}_1 = 0 \tag{3.7}$$
$$\dot{\tilde{z}}_2 = f(\tilde{z}_2, \tilde{z}_3, t)\tilde{z}_2 - k\tilde{z}_2 + g(\tilde{z}_2, \tilde{z}_3, t)\tilde{z}_3 \tag{3.8}$$
$$\dot{\tilde{z}}_3 = -h(\tilde{z}_2, \tilde{z}_3, t)\tilde{z}_2 \tag{3.9}$$

with

$$f(\tilde{z}_2, \tilde{z}_3, t) = \frac{w_{l,in} - uC_{out}\rho_l \frac{m_l^\Delta}{z_3}\left(\sqrt{\tilde{z}_2 + z_2 - p_s} + \frac{z_2}{\sqrt{\tilde{z}_2+z_2-p_s}+\sqrt{z_2-p_s}}\right)}{m_l^\Delta - z_3} \tag{3.10}$$

$$g(\tilde{z}_2, \tilde{z}_3, t) = \frac{b\epsilon w_{g,in} + (\tilde{z}_2 + z_2)w_{l,in} + uC_{out}\rho_l(\tilde{z}_2 + z_2)\sqrt{\tilde{z}_2 + z_2 - p_s} m_l^\Delta \frac{m_l^\Delta - (2z_3+\tilde{z}_3)}{z_3(\tilde{z}_3+z_3)}}{(m_l^\Delta - \tilde{z}_3 - z_3)(m_l^\Delta - z_3)} \tag{3.11}$$

$$h(\tilde{z}_2, \tilde{z}_3, t) = \frac{uC_{out}\rho_l}{\sqrt{\tilde{z}_2 + z_2 - p_s} + \sqrt{z_2 - p_s}} \tag{3.12}$$

Equation (3.7) indicates that the z_1 variable is not observable during this phase. Importantly, this is not a major concern, as the riser base pressure $p_{r,b}$ depends on z_2 and z_3 only. In turn, it can be shown that the observation error is decreasing towards zero for the variables z_2 and z_3 in the following sense. Lemma 3.1.1 proves the asymptotic stability of the origin of (3.8)-(3.9). This shows that the riser base pressure can be effectively estimated in this case. The dynamics under consideration correspond to a switched system. Near the usually observed limit cycle, its convergence could be studied by exploiting the fact that during one part of the cycle, two states of the error dynamics converge to zero while the remaining one is kept constant. Yet, this study is out of the scope of this article. Since the error dynamics of the observer change when the virtual valve reopens for one of the two systems, this does not prove the convergence of the full scheme.

Lemma 3.1.1 *Consider the following system*

$$\dot{\tilde{z}}_2 = f(\tilde{z}_2, \tilde{z}_3, t)\tilde{z}_2 - k\tilde{z}_2 + g(\tilde{z}_2, \tilde{z}_3, t)\tilde{z}_3 \tag{3.13}$$
$$\dot{\tilde{z}}_3 = -h(\tilde{z}_2, \tilde{z}_3, t)\tilde{z}_2 \tag{3.14}$$

with

$$\forall(\tilde{z}_2, \tilde{z}_3, t) \in \mathbb{R}^2 \times \mathbb{R}^+ \qquad |f(\tilde{z}_2, \tilde{z}_3, t)| \leq F \tag{3.15}$$
$$\forall(\tilde{z}_2, \tilde{z}_3, t) \in \mathbb{R}^2 \times \mathbb{R}^+ \qquad 0 < \epsilon \leq g(\tilde{z}_2, \tilde{z}_3, t) < G \tag{3.16}$$
$$\forall(\tilde{z}_2, \tilde{z}_3, t) \in \mathbb{R}^2 \times \mathbb{R}^+ \qquad 0 < \mu \leq h(\tilde{z}_2, \tilde{z}_3, t) < H \tag{3.17}$$

Consider the following candidate Lyapunov function

$$V = \frac{1}{2}\begin{pmatrix} \tilde{z}_2 \\ \tilde{z}_3 \end{pmatrix}^T \begin{pmatrix} \alpha & -\gamma \\ -\gamma & \beta \end{pmatrix} \begin{pmatrix} \tilde{z}_2 \\ \tilde{z}_3 \end{pmatrix} \tag{3.18}$$

with[3]

$$\alpha, \beta, \gamma > 0$$
$$\alpha\beta - \gamma^2 > 0$$
$$\frac{\alpha G - \beta\mu}{\gamma} - F - 4\alpha\epsilon^2 < 0 \tag{3.19}$$
$$\left(\frac{\alpha G - \beta\mu}{\gamma} - F - 4\alpha\epsilon^2\right)^2 > 4\gamma G^2 H + \left(\frac{\alpha G + \beta H}{\gamma} - F\right)^2 \tag{3.20}$$

There exists $k > 0$ *such that the origin of* (3.8)-(3.9) *is uniformly globally asymptotically stable (UGAS).*

The proof of this lemma is given in Appendix C. The validity of Assumptions (3.15)-(3.16)-(3.17) in our case (i.e., with f, g and h defined as (3.10)-(3.11)-(3.12)) relies, for the most part, on the construction of the compact set K in 2.2.1 where they are verified. In particular, the boundedness of f, g, and h, and the strict positivity of h directly follow from this construction. The strict positivity of g can only be verified numerically. In order to prove the convergence of the full observer scheme, possible directions include the patching of Lyapunov functions [33], or the design of a non-smooth Lyapunov function [10]. We now present numerical simulations that validate further the relevance of the design.

Numerical validation of the observer design

The observer was tested on data from the 7731 meter-long well considered in Section2.3.8. The tuning procedure treating the parameters detailed in Table 2.1 was first applied to the model. Conveniently, the data also includes measurements of the bottom pressure used *for comparison only*. Figure 3.1 shows the comparison between the actual topside pressure (used in the observer) and the actual bottom pressure on one hand, and the estimates from the model on the other. Should the bottom sensor fail, the estimates can be used to stabilize a slugging system, as will appear in Section 3.1.3. One should notice that the observer compensates for the magnitude and frequency offsets that existed without the real-time use of the measurements (e.g. on Figure 2.8). However, there exist *a priori* limitations to the efficiency of this technique, that we now review.

3.1.2 RHP zeros

In [53], Storkaas and Skogestad have stressed the difficulty of stabilizing a slugging riser with only a topside pressure measurement, by highlighting the presence of unstable zeros in the transfer function between the measured output (topside pressure) and

[3] One can e.g. pick $\alpha = \sigma^3$, $\beta = 1$, $\gamma = \frac{G}{4\epsilon^2}\sigma$, with $\sigma > 0$ sufficiently large to ensure that these conditions are fulfilled altogether.

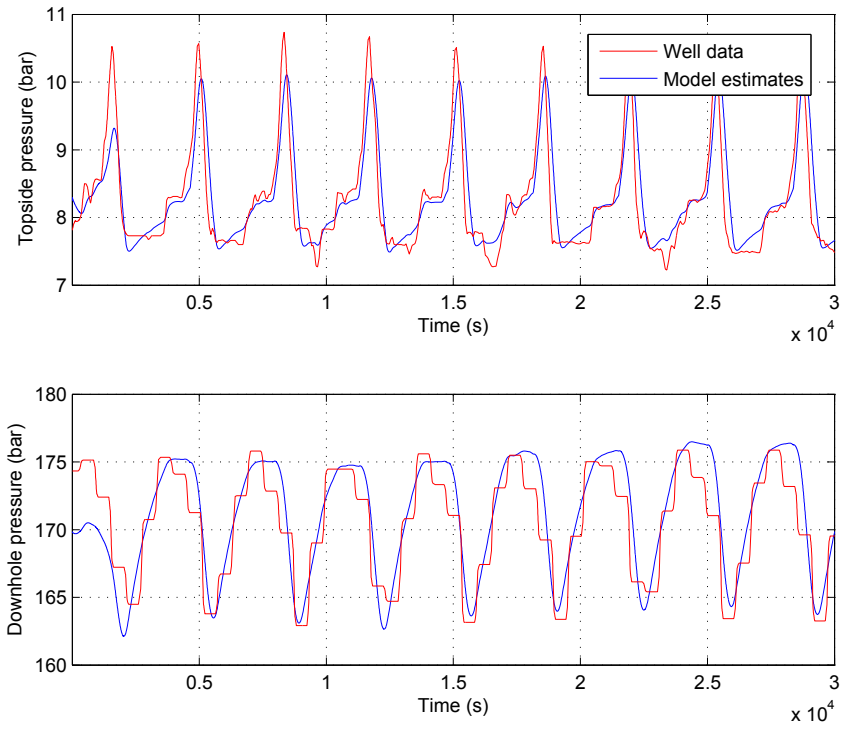

Figure 3.1: Comparison between real measurements and observer estimates. The low sampling of the bottom pressure is only due to database compression.

the control input (the outlet valve opening). Unstable zeros are a well-known limiting factor in the performance-robustness trade-off achievable by a controller [22, 45]. In [53], the statement is illustrated by a case study, where lower bounds on the norm of the sensitivity functions $\|S\|_\infty$ and $\|T\|_\infty$ are computed numerically from a Partial Differential Equations model linearized around two possible equilibria. Skogestad has recently insisted on this point by stating [51]

> *"it will not help to use a state estimator to estimate the bottom pressure from a top pressure measurement. When analyzing the estimated bottom pressure it may seem that it works, because the state estimator (Kalman filter) can be tuned to have fast response, but when we couple everything together there will be a hidden RHP pole-zero cancellation between the controller and the plant. The only option is to change the system, for example, by introducing additional measurements or additional MVs (inputs)."*

Although we fully agree that using an estimator will not suppress the inherent limitations due to unstable poles and zeros, the overall conclusions from Storkaas and Skogestad seem overly conservative. In particular, the following points require discussion

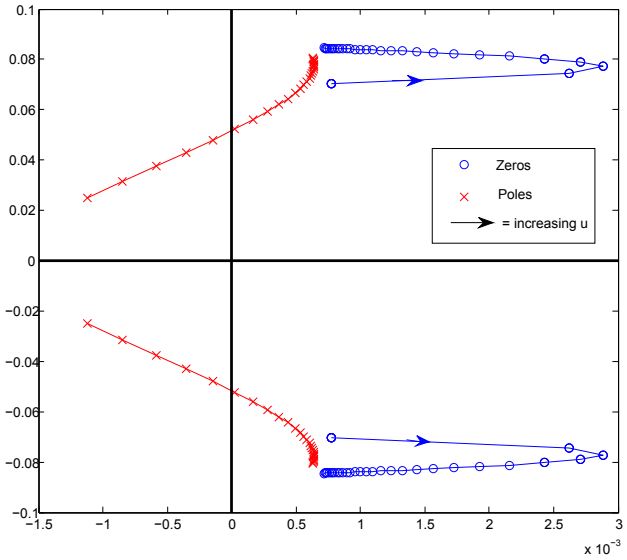

Figure 3.2: Loci of the zeros (in blue) and poles (in red) when u is increased. As expected, the zeros are in the Right Half Plane and get closer to the poles as u gets closer to 1.

- The limitations depend on the considered slugging well or flowline, and for each slugging system, on the considered operating point. Indeed, the plant has an infinite number of equilibria, which can be indexed by the outlet valve opening $u \in [0, 1]$. The limitations depend on the equilibrium around which the system is linearized. This point is illustrated on Figure 3.2, where the positions of the zeros and poles of the system are plotted for various values of the valve opening. The zeros and poles were obtained by linearizing system (2.1)-(2.2)-(2.3) around each $u \in [0, 1]$ (see B for details). As will appear in Section 3.1.3, the limitations may not be too restrictive for a given well or flowline.

- Slugging is a nonlinear phenomenon. This implies that the bottom pressure can be estimated by means of a *nonlinear* observer, as described above. Although this does not remove the limitations due to unstable zeros, the resulting controller may have better stabilizing properties (in particular a larger basin of attraction) than, e.g., a simple PI on the topside pressure.

Despite these remarks, adding a bottom pressure sensor remains (as suggested by [53]) the most efficient solution from a control viewpoint. Yet, when this is not possible, either due to technical or economic reasons, there is still room for a viable solution. This point will be illustrated by the results of Section 3.1.3, where a slugging system is successfully, and robustly (in a sense that will be specified) stabilized using a topside pressure sensor only. It is also illustrated by the experiments of Sivertsen et al. [49, 50] where the flow is stabilized using two topside sensors in a cascade controller.

Parameter	Description	Value
R	Gas constant	8.314 J.K^{-1}.mol^{-1}
T	Temperature	287 K
M	Molecular mass of air	2.9 $\times 10^{-2}$ kg.mol^{-1}
ρ_l	Salty water density	1050 kg.m^{-3}
g	Gravity constant	9.81 m.s^{-2}
θ	Pipe inclination	1.496 rad
D	Pipe diameter	4.6 $\times 10^{-3}$ m
A	Cross-section area	1.8 $\times 10^{-2}$ m^2
p_s	Separator pressure	1 $\times 10^5$ Pa
$w_{l,in}$	Water inflow mass rate	2.0417 kg.s^{-1}
$w_{g,in}$	Air inflow mass rate	4.7 $\times 10^{-3}$ kg.s^{-1}
L	Length of the pipe	15 m
ϵ	Fraction of inflow gas	0.01
C_{out}	Choke constant	6.48 $\times 10^{-5}$ m^2
$m_{l,still}$	Still mass of liquid	32.9 kg
C_g	Virtual valve constant	3.3 $\times 10^{-7}$ m.s
V_{eb}	Volume of the elongated bubble	0.558 m^3

Table 3.1: List of the model parameters used to match the loop slugging oscillations.

3.1.3 Experiments: control with use of estimates

In this section, we present the results of experiments realized on a multiphase flow loop in Porsgrunn, Norway. The experiments validate the approach previously discussed for the first sensing scenario, namely in the absence of a riser base pressure measurement.

Experimental setup The experiments are conducted on a 100 meter-long, 15 meter-high flow loop located in Porsgrunn, Norway, pictured on Figure 3.3. The pipe is filled at constant rates with air and water, playing the role of gas and oil, respectively[4]. Even under these steady inflow conditions, the loop is able to reproduce the slugging behavior. Figure 3.4 shows a schematic view of the geometry of the system, along with a plot of the observed pressure oscillations. We now describe experiments where the slugging is suppressed, with the sole use of topside pressure sensors. For these experiments, the inflow rate of water was set to 7 m^3/h and the inflow rate of air was set to 17 kg/h.

Estimation The parameters of the model are adjusted to match the oscillations, following the procedure described in Section 2.3. Table 3.1 lists the values of all the parameters used. Figure 3.5 shows the resulting estimation from the model, compar-

[4]Low-level controllers ensure that the inflows are kept constant, to avoid wear and tear on the injection pumps

Figure 3.3: Picture of the rising section of the experimental multiphase flow loop MaS-CoT.

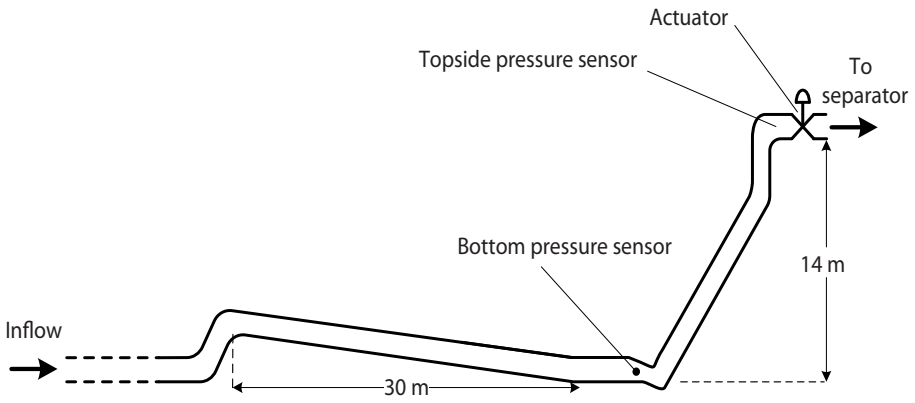

(a) Schematic view of the system

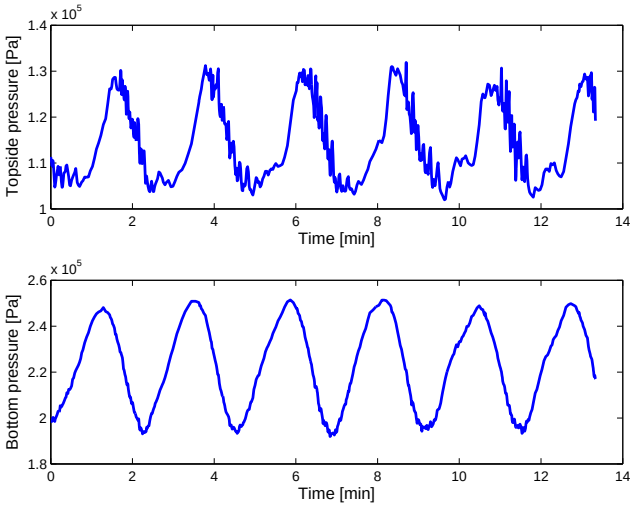

(b) Open-loop oscillations of the topside and bottom pressures

Figure 3.4: Schematic view of the multiphase flow loop and sustained slugging oscillations.

ing the topside and bottom pressure measurements and estimates obtained from (3.4)-(3.5)-(3.6), with an observer gain $k = 1$.

Control experiment The estimates are used in the control scheme represented on Figure 3.6. The controller used is a PI on the bottom pressure, which corresponds to the state-of-the-art method. Figure 3.7 pictures the result of the closed-loop experiment, showing both the estimated bottom pressure (which is used in the feedback loop) and the measured bottom pressure, for comparison. The controller is turned on once the observer has converged, approximately after 11 minutes. The pressure set point was first set to 2.07 bar, which reveals too low for the controller to stabilize. Thus, it was increased to 2.09 bar (event B), where stabilization is achieved (right before

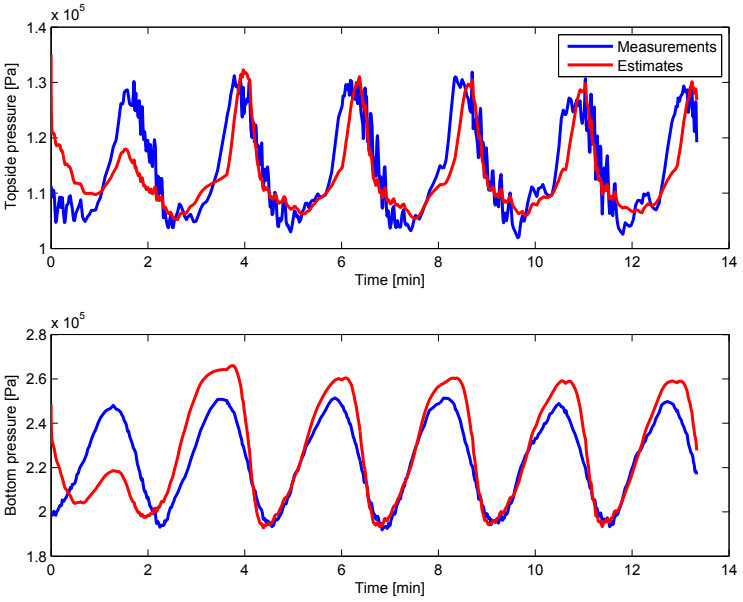

Figure 3.5: Comparison of the estimated and measured pressures. The observer gain of Equation (3.5) is $k = 1$.

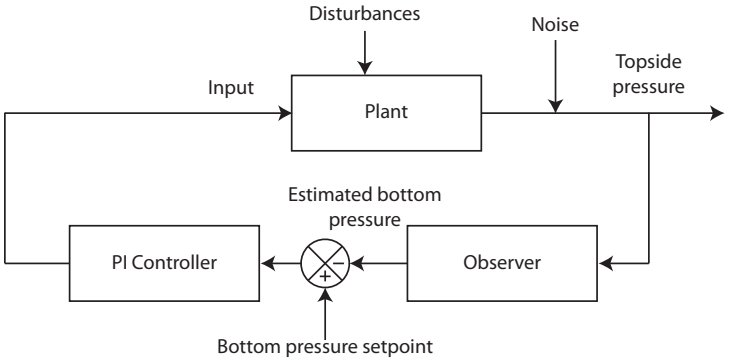

Figure 3.6: Block diagram of the control scheme. The proportional gain of the controller is $K_p = 55$, and the integral time is $T_i = 100s$.

event C). Once the system has converged to its equilibrium (which would be unstable in open-loop), various disturbances are applied (events C,D,E). More precisely, the inflows of gas and liquid are abruptly modified as indicated on Figure 3.7. This not only disturbs the system, but also induces model errors. In the considered case, the controller manages to recover stability (although some steady-state errors cannot be corrected, as expected). Once the controller is turned off (event F), the slugging oscillations start again. The corresponding input actuation is pictured on Figure 3.8. While the controller is on, the choke opening is always higher than the bifurcation point, which means that the system oscillates around open-loop unstable operating points.

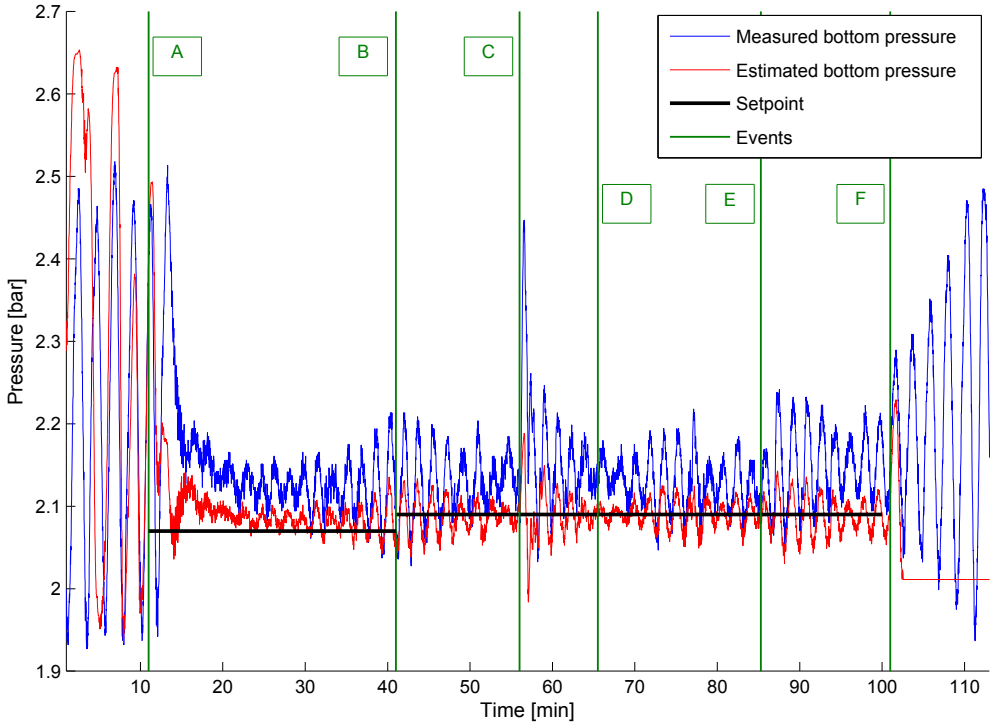

Figure 3.7: Robust stabilization of the plant. The green vertical lines distinguish the following events. A: Controller is turned on, B: Set point is changed from 2.07 bar to 2.09 bar, C: Large variation of the inflow rate of gas, D: Step change (from 7 m^3/h to 6.8 m^3/h) of the liquid inflow rate, E: Step change (from 6.8 m^3/h to 7.2 m^3/h) of the liquid inflow rate, F: Controller is turned off.

These experiments show that this technique allows to stabilize slugging[5].

Remark The success of these experiment is, in part, due to the fact that the limitations due to the unstable zeros (discussed in Section 3.1.2 are not too restrictive for the considered plant. Indeed, the zeros and poles of the system can be computed by linearizing our simplified model (2.1)-(2.2)-(2.3). The corresponding limitations, e.g. on the sensitivity and complementary sensitivity functions, can then be computed, as shown in B. They reveal very mild, which explains that the proposed controller has both relatively good robustness to model errors and disturbance rejection properties. Besides, as pointed out by Sivertsen [49], the models used to compute the limitations may lead to conservative conclusions because of their relative simplicity.

[5]Although the impact on production cannot be seen from these experiments, since the inflows are kept constant.

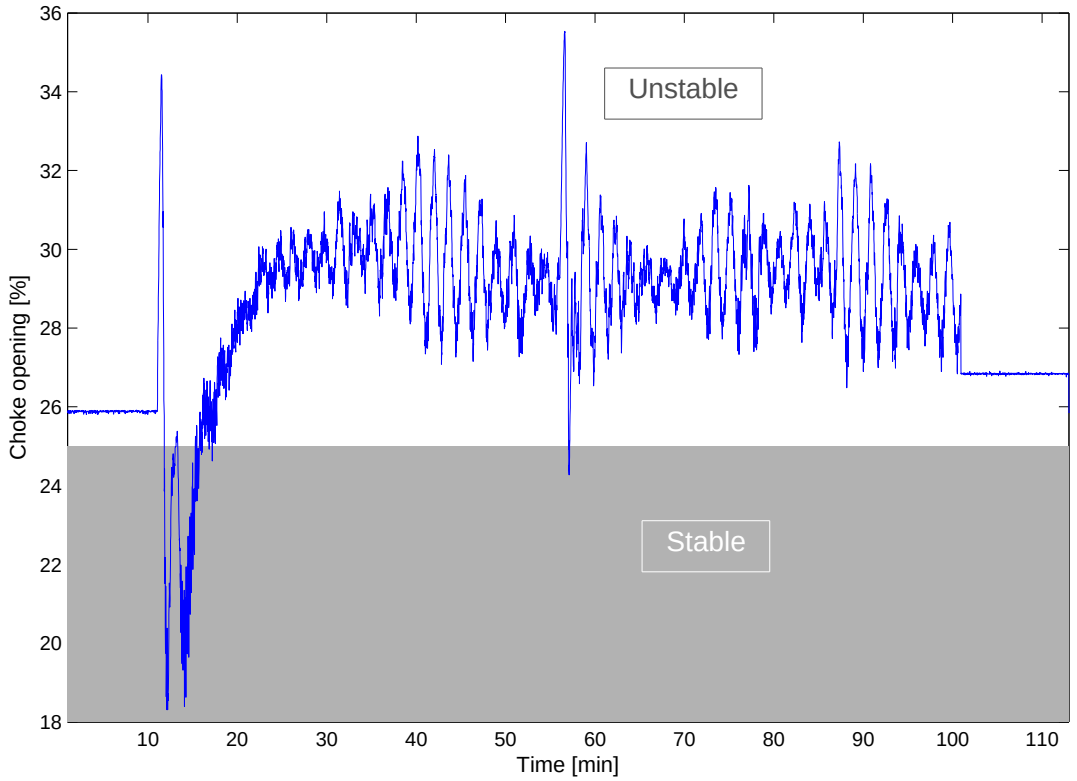

Figure 3.8: Choke actuation during the stabilization. The gray area corresponds to the values of u for which the system is open-loop stable.

3.2 Scenario 2: stabilization with use of riser base sensors

As mentioned in Section 1.4, the state-of-the-art control strategy to counter slugging consists in applying a PI controller to the riser base pressure when a sensor is available. This technique has revealed efficient in numerous implementations reported in the literature [13, 23, 25], and the experiments presented in Section 3.1.3 tend to confirm its potential. However, the study of the model suggests that a natural choice for the controlled variable is the total mass of liquid in the riser, rather than the riser base pressure. This point is illustrated in Section 3.2.1 where a nonlinear control law is designed for model (2.1)-(2.2)-(2.3). The proof of convergence of this control law highlights a particular structure of the model, and the specific role of the mass of liquid. Eventually, experiments conducted on a multiphase flow loop confirm that the proposed controlled variable yields better stabilizing properties than the state-of-the-art method.

3.2.1 A possible stabilizing control law

In this section, we propose a theoretical control law for the model described in Chapter 2. The merits of this law is to stress the role of a particular variable of the system, which zero dynamics are asymptotically stable. This suggests, as illustrated next, an easily implementable controller on this variable, which is the mass of liquid in the riser. The representation of the model used in this section corresponds to that of Section 2.2.1.

Proposition 3.2.1 *Consider system* (2.6)-(2.7)-(2.8)*. The partially linearizing feedback law*

$$u(t) = \frac{w_{l,in} + k(\chi_3(t) - \bar{\chi}_3)}{C_{out}\sqrt{\rho_l(\frac{\chi_2\chi_3}{m_l^{Delta}-\chi_3} - p_s)}} \tag{3.21}$$

with $k > 0$ stabilizes the system around its equilibrium point $(\bar{\chi}_1, \bar{\chi}_2, \bar{\chi}_3, \bar{u})$ which is Locally Asymptotically Stable.

Proof First, we consider the open set $D^+ = \left\{ a\chi_1 - b\frac{\chi_2\chi_3}{m_l^\Delta - \chi_3} - c(\chi_3 + m_{l,still}) > 0 \right\}$ where the expression inside the max functions is strictly positive. We also introduce the error variables $\tilde{\chi}_i = \chi_i - \bar{\chi}_i$. In D^+, the closed-loop system yields the following cascaded error dynamics

$$\dot{\tilde{\chi}}_1 = -C_g a\tilde{\chi}_1 + C_g\frac{\bar{p}_{r,t}}{\bar{\chi}_2}\tilde{\chi}_2 + \tilde{\chi}_3\left[C_g c + b\frac{\tilde{\chi}_2 + \bar{\chi}_2}{(m_l^\Delta - \bar{\chi}_3 - \tilde{\chi}_3)(m_l^\Delta - \bar{\chi}_3)}\right] \tag{3.22}$$

$$\begin{aligned}\dot{\tilde{\chi}}_2 =& \frac{C_g a}{\bar{\chi}_3}\tilde{\chi}_1 - \frac{1}{\bar{\chi}_3}\left(w_{l,in} + \frac{C_g\bar{p}_{r,t}}{\bar{\chi}_2}\right)\tilde{\chi}_2 - \frac{\tilde{\chi}_3}{\bar{\chi}_3(\bar{\chi}_3 + \tilde{\chi}_3)}\left[C_g a\tilde{\chi}_1 - \left(w_{l,in} + \frac{C_g\bar{p}_{r,t}}{\bar{\chi}_2}\right)\tilde{\chi}_2\right] \\ &+ \frac{\tilde{\chi}_3}{(\bar{\chi}_3 + \tilde{\chi}_3)}\left[C_g c + b\frac{\tilde{\chi}_2 + \bar{\chi}_2}{(m_l^\Delta - \bar{\chi}_3 - \tilde{\chi}_3)(m_l^\Delta - \bar{\chi}_3)}\right]\end{aligned} \tag{3.23}$$

$$\dot{\tilde{\chi}}_3 = -k\tilde{\chi}_3 \tag{3.24}$$

We now consider the candidate Lyapunov function $V = \frac{1}{2}\left(\tilde{\chi}_1^2 + \tilde{\chi}_2^2 + \tilde{\chi}_3^2\right)$. In D^+, the time derivative of V is

$$\dot{V} = \begin{pmatrix} \tilde{\chi}_1 \\ \tilde{\chi}_2 \end{pmatrix}^T A \begin{pmatrix} \tilde{\chi}_1 \\ \tilde{\chi}_2 \end{pmatrix} + \begin{pmatrix} \tilde{\chi}_1 \\ \tilde{\chi}_2 \end{pmatrix}^T g(\tilde{\chi}_1, \tilde{\chi}_2, \tilde{\chi}_3)\tilde{\chi}_3 - k\tilde{\chi}_3^2$$

where

$$A = \begin{pmatrix} -C_g a & C_g \frac{\bar{p}_{r,t}}{\bar{\chi}_2} \\ \frac{C_g a}{\bar{\chi}_3} & -\frac{w_{l,in}}{\bar{\chi}_3} - C_g \frac{\bar{p}_{r,t}}{\bar{\chi}_3 \bar{\chi}_2} \end{pmatrix} \quad \text{and} \quad g(\tilde{\chi}_1, \tilde{\chi}_2, \tilde{\chi}_3) = \begin{pmatrix} \left[C_g c + b \frac{\tilde{\chi}_2 + \bar{\chi}_2}{(m_l^\Delta - \tilde{\chi}_3 - \bar{\chi}_3)(m_l^\Delta - \bar{\chi}_3)} \right] \\ \frac{\tilde{\chi}_3}{\tilde{\chi}_3 + \bar{\chi}_3} \left[-\frac{C_g a}{\bar{\chi}_3} \tilde{\chi}_1 + \frac{1}{\bar{\chi}_3} \left(w_{l,in} + \frac{C_g \bar{p}_{r,t}}{\bar{\chi}_2} \right) \tilde{\chi}_2 \right. \\ \left. + C_g c + b \frac{\tilde{\chi}_2 + \bar{\chi}_2}{(m_l^\Delta - \bar{\chi}_3 - \tilde{\chi}_3)(m_l^\Delta - \bar{\chi}_3)} \right] \end{pmatrix}$$

We now use the fact, that g is Lipschitz on the compact set K defined in Section 2.2.1[6].

$$\begin{aligned} \begin{pmatrix} \tilde{\chi}_1 \\ \tilde{\chi}_2 \end{pmatrix}^T g(\tilde{\chi}_1, \tilde{\chi}_2, \tilde{\chi}_3) &\leq \frac{1}{2}(\tilde{\chi}_1^2 + \tilde{\chi}_2^2) + \frac{1}{2}\|g(\tilde{\chi}_1, \tilde{\chi}_2, \tilde{\chi}_3)\|^2 \\ &\leq \frac{1}{2}(\tilde{\chi}_1^2 + \tilde{\chi}_2^2) + \frac{L^2}{2}(\tilde{\chi}_1^2 + \tilde{\chi}_2^2 + \tilde{\chi}_3^2) \end{aligned}$$

$$\begin{aligned} \text{Therefore,} \qquad \dot{V} &\leq -|\lambda_{\min}|(\tilde{\chi}_1^2 + \tilde{\chi}_2^2) + \frac{|\tilde{\chi}_3|}{2}(L^2 + 1)(\tilde{\chi}_1^2 + \tilde{\chi}_2^2) \\ &\quad - \left(k - L^2 \frac{|\tilde{\chi}_3|}{2} \right) \tilde{\chi}_3^2 \end{aligned} \tag{3.25}$$

where $\lambda_{\min}$ is the smallest (in absolute value) eigenvalue of A, which is negative as A is obviously Hurwitz. Let now $c_0 \in \mathbb{R}$ be $c_0 = \sup\{c \in \mathbb{R} \,|\, \{V(x) \leq c\} \subset D^+\}$, and note $\Gamma = \{V(x) \leq c_0\}$ the largest level set of V contained in the region where the max functions are strictly positive. We also consider the set $\Omega = K \cap \Gamma \cap \left\{ |\tilde{\chi}_3| \leq \frac{2|\lambda_{\min}|}{1+L^2} \right\}$. We claim that, provided that $k > \frac{|\lambda_{min}|L^2}{1+L^2}$, Ω is positively invariant and contained in the basin of attraction of $(0,0,0)$. Indeed, inside Ω, we have $\dot{\tilde{\chi}}_3 \leq 0$ and (3.25) shows that we have $\dot{V} \leq 0$. Thus, any trajectory starting in Ω remains in Ω for all future times. As $\dot{V}$ is negative in Ω, this shows, by LaSalle's theorem, that any trajectory starting in Ω converges to $(\tilde{\chi}_1, \tilde{\chi}_2, \tilde{\chi}_3) = (0,0,0)$.

Remarks on the control design Although the proof is quite tedious, the following qualitative analysis provides insight into its mechanisms. The feedback law decouples Equation (3.24) from Equations (3.22) and (3.23), and makes χ_3 (the mass of liquid) converge exponentially to its equilibrium. Consider now system (3.22)-(3.23) with $\tilde{\chi}_3$ as a (vanishing) input. The unforced system (i.e. with $\tilde{\chi}_3 = 0$) simply reads, *inside* D^+

$$\begin{pmatrix} \dot{\tilde{\chi}}_1 \\ \dot{\tilde{\chi}}_2 \end{pmatrix} = A \begin{pmatrix} \tilde{\chi}_1 \\ \tilde{\chi}_2 \end{pmatrix} \tag{3.26}$$

where $A = \begin{pmatrix} -C_g a & C_g \frac{\bar{p}_{r,t}}{\bar{\chi}_2} \\ \frac{C_g a}{\bar{\chi}_3} & -\frac{w_{l,in}}{\bar{\chi}_3} - C_g \frac{\bar{p}_{r,t}}{\bar{\chi}_3 \bar{\chi}_2} \end{pmatrix}$ is Hurwitz. If Equation (3.26) was verified globally (rather than only on D^+), this would make (3.22)-(3.23) be Input-to-State Stable with

[6]The Lipschitzness of g directly follows from the construction of K. In particular, the bounds of the rectangular domain K' are chosen such that g is Lipschitz.

respect to $\tilde{\chi}_3$ (see e.g. [37, Lemma 4.6]). Since $\tilde{\chi}_3$ is converging to 0, this would imply stability of the whole system (again, see [37, Exercise 4.58]). Yet, since the dynamics change when the virtual valve closes (i.e., outside of D^+), an ad-hoc Lyapunov function must be considered, as is done in the proof.

Proposition 3.2.1 suggests that any control law making χ_3 exponentially converge to its equilibrium actually stabilizes the whole system. This result is all the more interesting as, even though the mass of liquid cannot be directly measured, it is closely related to the pressure difference between the bottom and the top of the riser. Indeed, the pressure drop over the riser (ΔP_{riser}) is due to a gravity effect and a friction effect, which is neglectible. Thus, there is an (approximate) affine relation between the mass of liquid and ΔP_{riser}[7]. This idea is related to previous works. The efficiency of controlling directly the pressure drop over the riser, which will be illustrated in Section 3.2.2, has already been investigated in [27], with success. We now investigate this method and compare it with the state-of-the-art control solution.

3.2.2 Results: applying a PI controller on ΔP_{riser}

In this section, we compare the efficiency of different control strategies when measurements are available for both the topside and bottom pressures. In this case, the state-of-the art method consists, as mentioned above, in applying a PI controller to the riser base pressure. The control law (and its proof of convergence) presented in Section 3.2.1 suggests that an alternative control variable is the pressure drop over the riser. To illustrate this point, experiments comparing the performance of a PI controller applied to each of these control variables were conducted.

Experimental setup The experiments were conducted on the multiphase flow loop presented in Section 3.1.3. However, the geometry of the facilities were slightly modified between the two set of experiments, and the inflow rates had to be modified as well to obtain a slugging behavior. Thus, the inflow rates were set to 4 m^3/h for the water, and 26 kg/h for the air.

PI controllers For each control variable (riser base pressure and ΔP_{riser}), the parameters of the PI were tuned by an trial and error iterative method. In particular, for the PI on the riser base pressure, the tuning method described in [23] was applied to find a suitable initial set of parameters. Figures 3.9 and 3.10 correspond to the highest unstable valve opening around which it was possible to stabilize the plant, for each of the considered control variables. Once again, the comparative impact on production cannot be assessed from these experiments. Yet, they clearly show that the pressure drop over the riser is a much better suited control variable than the bottom pressure. Stabilization is achieved almost instantaneously, and around a much larger valve opening (36% versus 27%). As can be seen on Figures 3.9 and 3.10, this yields a lower bottom

[7] For our model, the relation is given by $\Delta P_{riser} = p_{r,b} - p_{r,t} = (m_{l,r} + m_{l,stilll}) \frac{g \sin \theta}{A}$.

pressure (1.83 bar versus 1.95 bar) which should translate, on a real system, into an increase of oil production. No observer was used to perform these experiments.

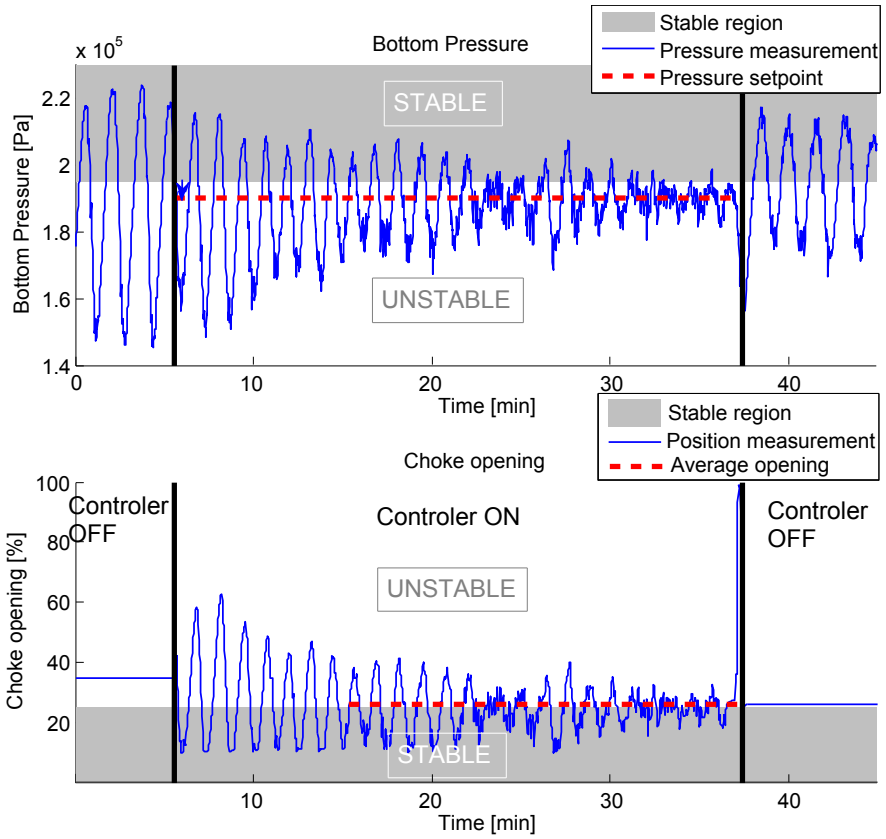

Figure 3.9: Stabilization by the PI on the bottom pressure, corresponding to the highest obtained valve opening (27%).

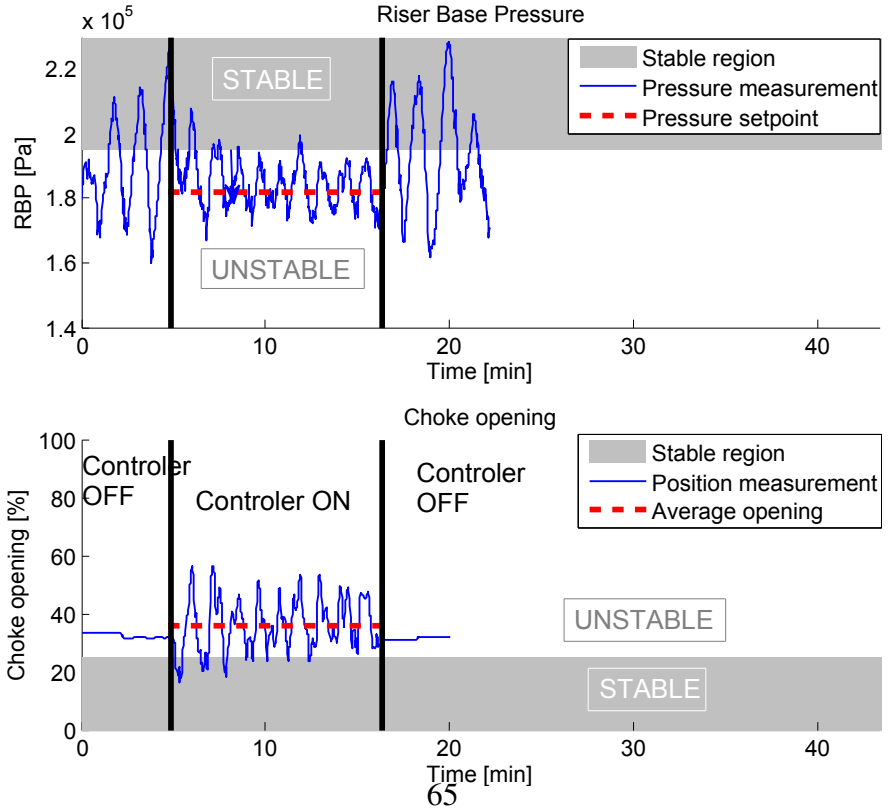

Figure 3.10: Stabilization by the PI on the pressure drop over the riser, corresponding to the highest obtained valve opening (36%).

Chapter 4

Conclusions and perspectives

Conclusions et perspectives

Ce manuscrit est dédié à la supression du slugging sur les systèmes de production de pétrole, par actionnement automatique de la vanne de sortie. Ceci doit permettre d'augmenter le niveau de production et d'améliorer la sécurité sur les installations concernées. L'étude concerne une vaste collection de systèmes, en particulier les puits de pétrole (actionné par gas-lift ou non), ainsi que les risers de flowline. Les solutions proposées tiennent compte des équipements traditionnellement installés sur ces systèmes, en termes d'actionneurs et de capteurs.

Les solutions proposées se basent sur l'étude du slugging, à la fois physique et en tant que système dynamique. En particulier, des lois de commande se déduisent de l'étude d'un modèle de dimension finie, présenté au Chapitre 2. Ce modèle consiste en un système de 3 ODE nonlinéaires couplées, dont les paramètres peuvent être calibrés via une procédure également présentée. La calibration permet au modèle de reproduire le phénomène de slugging et d'ajuster les caractéristiques du cycle limite correspondant (la fréquence et amplitude des oscillations, par exemple), afin qu'elles se rapprochent de celles d'un système donné. Le modèle proposé n'est pas universel: certains systèmes présentent des comportements qui sortent de son domaine de validité, par exemple lorsque l'amplitude des oscillations de la pression de fond est très inférieure à celles de la pression de tête. De plus, le modèle ne permet de décrire que le comportement d'un puits à la fois: l'étude de plusieurs puits interconnectés sort du cadre de ce manuscrit.

Malgré ces limitations, le modèle se révèle un outil puissant pour l'élaboration de lois de contrôle. En particulier, un observateur présenté en Section 3.1.1 permet, à partir de la seule mesure de la pression de tête, l'estimation de tout l'état du modèle. Les états estimés peuvent être ensuite être utilisés dans de simples contrôleurs PI pour supprimer le slugging, comme démontré par les expériences présentées dans le manuscrit. Cette solution de contrôle permet de stabiliser l'écoulement sans utiliser de capteurs de pression de fond, qui ne sont pas toujours présents sur les installations, et pour

lesquels la maintenance s'avère souvent difficile. Toutefois, la calibration du modèle requiert un travail d'ingénierie important, qui pourrait être réduit, dans de futures contributions, par l'étude de contrôleurs adaptatifs (voir par exemple [2, 39], ou [60] pour une application au contrôle du severe slugging). Surtout, les performances et la robustesse de cette méthode présentent des limitations inhérentes à l'utilisation du seul capteur de pression de tête. Nous recommandons une analyse au cas par cas des propriétés de controllabilité linéaire, comme celle de l'Appendice B, de chaque système avant l'implémentation de cette méthode. Si les limitations s'avèrent trop restrictives, il semble que l'installation d'un capteur de pression de fond reste la meilleure solution.

Par ailleurs, le modèle renseigne également sur les propriétés de controllabilité non-linéaire des systèmes soumis au slugging. Nous montrons en particulier, à travers l'élaboration d'une loi de contrôle non-linéaire théorique, que la masse de liquide contenue dans le riser est une variable particulièrement adaptée au contrôle du slugging. Cette information est particulièrement utile lorsqu'une mesure de la pression de fond fiable est disponible, car la relation entre la masse de liquide et la différence de pression entre le bas et le haut du riser est approximativement affine. Nous avons donc testé, lors d'expériences présentées dans ce manuscrit, l'efficacité d'un contrôleur PI appliqué à la différence de pression entre bas et haut du riser, en la comparant à celle d'un contrôleur PI appliqué, comme c'est traditionnellement le cas dans la littérature, à la pression de fond. Le nouveau contrôleur possède de meilleure performances, puisqu'il est capable de stabiliser l'écoulement autour de pression plus basses. Ceci devrait se traduire, lors du passage à l'échelle industrielle, par une augmentation de la production.

L'étude du modèle d'EDP pour le slugging du Chapitre 1 consitue également une contribuion importante de ce mansucrit. Les conditions suffisantes de stabilité données dans la Section 1.3.4 sont un premier pas vers des résultats de stabilisations. Lors de contributions à venir, nous étudierons la possibilité d'appliquer la méthode du backstepping (voir [41]) afin d'élaborer des lois de contrôle stabilisantes. De plus, le modèle pourrait être utilisé pour l'étude du slugging pour une autre classe de systèmes: les très longs pipelines, de l'ordre de plusieurs dizaines, voire centaines de kilomètres. En effet, la formation de slugs sur ces systèmes, par exemple en raisons d'irrégularités du terrain, oblige les industriels à installer des "slugs catchers" en amont des unités de séparations. Ces réservoirs tampons constituent des investissement massifs, et leur installation peut amener à reconsidérer la construction même d'un pipeline. Afin de supprimer ces cots indésirables, des solutions visant à contrôler le débit au moyen de vannes réparties le long du pipeline sont envisagées. Le caractère distribué du problème est, sur ces systèmes plus longs encore que ceux considérés dans ce manuscrit, d'autant plus important, et le modèle du Chapitre 1 pourrait constituer un outil utile à l'élaboration de lois de contrôles.

The problem under consideration in this manuscript is the suppression of slugging

on oil production systems by automatic actuation of the outlet valve, in view of increasing the level of production and the safety of operations. The study concerns a wide range of systems, including (possibly gas-lifted) wells and flowline risers, and takes into account the standard equipments installed on these facilities, in terms of sensors and actuators.

The proposed solutions rely on a physical and dynamical analysis of the phenomenon. In particular, a presented reduced-order model is used to gain insight into the control design. The model consists of a system of three coupled nonlinear ODE, which parameters can be calibrated one-by-one through a presented procedure. This allows the model to match the characteristics of the slugging for most considered systems, including real-scale oil wells. However, the model has failed to reproduce the behavior of some slugging facilities, for which the mechanisms of the slugging seem to differ from the cases considered in this manuscript[1]. Besides, the case of multiple interconnected wells and the effects of pressure variations in a manifold has not been considered in this manuscript.

Despite these shortcomings, the model reveals a handy tool to design control solutions. In particular, a proposed observer algorithm allows to estimate the states of the model from a measurement of the topside pressure only. The fair representativeness of the model is illustrated by the efficiency of this observer to dynamically reconstruct missing measurements. Moreover, the estimates can be used in simple PI feedback loops to stabilize slugging, as illustrated by presented experiments. This control solution does not require the use of a bottom pressure sensor, which are not systematically installed on wells and flowline risers, and for which maintenance is difficult. However, it requires a thorough engineering effort to calibrate the parameters of the model. This constraint could be alleviated, in future works, by the investigation of adaptive controllers (see, e.g. [2, 39], or [60] for an application to control of severe slugging). Most importantly, it is inherently limited in its performances and robustness, and a case-by-case analysis of the linear controllability properties of each considered system, e.g. based on the proposed model[2], is recommended before attempting to apply this control solution. Should the limitations imposed by the sole use of a topside pressure sensor be too restrictive, the installation of a bottom pressure sensor seems to remain the only viable solution to control slugging.

Besides, the model also provides insight the nonlinear controllability properties of slugging systems. In particular, we show, through the design of a theoretical nonlinear feedback law, that the mass of liquid in the riser is a well-suited variable for control of slugging. More precisely, a control law making the mass of liquid exponentially converge to its equilibrium would stabilize the whole system. This reveals particularly useful when reliable measurements of both the bottom and topside pressure exist, since the mass of liquid is approximately an affine function of the pressure difference over the riser. Thus, we experimentally tested the efficiency of applying a PI controller to

[1] In particular, some wells feature large oscillations of the topside pressure, whereas the bottom pressure is nearly steady. The model does not seem to have the potential to account for such a phenomenon.

[2] as is done in Appendix B

the pressure difference over the riser, rather than to the bottom pressure, as is usually reported in the literature. The performances were clearly improved, since the resulting controller managed to stabilize the flow at lower pressure set points than the PI applied to the bottom pressure. This should translate, on large scale systems, into an increase of production. The main limitation of this solution is, of course, that it requires a bottom pressure sensor to be available.

Another contribution of this manuscript lies in the study of the PDE model of Chapter 1. The stability results for the linearized equations constitute a first step towards stabilization results. In particular, future works could investigate the design of backstepping boundary controllers for this 3×3 system of transport equations with varying coefficients following the approach of [40, 41]. Besides, the model could be used to study the occurrence of slugging on long (from tens to hundreds of kilometers) near-horizontal flowlines. Indeed, on these systems, the formation of large slugs, e.g. due to terrain irregularities, forces the construction of large "slug catchers" located upstream the separation facilities. These very large buffer tanks represent colossal investments and sometimes condition the decision on whether to build a flowline or not. To avoid these costly installations, ways to suppress long slugs using valves disposed along the flowline could be investigated. For these systems, the distributed nature of the problem is of even greater importance than in the case of riser slugging, and the PDE model of Chapter 1 could provide insight into possible control solutions.

Bibliography

[1] O.-M. Aamo, G. Eikrem, H. Siahaan, and B. Foss. Observer design for multiphase flow in vertical pipes with gas-lift theory and experiments. *Journal of Process Control*, 15:247–257, 2005.

[2] K. Astrom and B. Wittenmark. *Adaptive control*. Addison-Wesley Longman Publishing Co., Inc. Boston, MA, USA, 1994.

[3] G. Bastin and J.-M. Coron. Further results on boundary feedback stabilization of 2x2 hyperbolic systems over a bounded interval. *Proceedings of IFAC Nolcos 2010, Bologna, Italy*, 2010.

[4] S. Belfroid, R. Pvan Der Linden, G. Alberts, and R. Aasheim R., Schulkes. Severe slugging in oil-well simulations using a drift flux code. pages 357–371, 2010. cited By (since 1996) 0.

[5] K. Bendiksen, D. Maines, R. Moe, and S. Nuland. The dynamic two-fluid model OLGA: Theory and application. *SPE production engineering*, 6(2):171–180, 1991.

[6] E. Blick and L. Boone. Stabilization of naturally flowing oil wells using feedback control. *SPE Paper*, 1986.

[7] A. Bøe. Severe slugging characteristics ; part i:flow regime for severe slugging ; part ii: Point model simulation study. *Presented at Selected Topics in Two-Phase Flow, NTH, Trondheim, Norway*, 1981.

[8] G. Bornard and H. Hammouri. A high gain observer for a class of uniformly observable systems. In *Proceedings of the 30th IEEE Conference on Decision and Control, 1991*, volume vol.2, pages 1494 –1496, dec 1991.

[9] C. E. Brennen. *Fundamentals of multiphase flow*. Cambridge Univ Pr, 2005.

[10] F. Clarke. Nonsmooth analysis in control theory: a survey. *European Journal of Control*, 7(2-3):145–159, 2001.

[11] R. Courant and D. Hilbert. *Methods of Mathematical Physics, Vol. II*. Wiley-Interscience, New York, 1962.

[12] A. Courbot. Prevention of severe slugging in the dunbar 16' multiphase pipeline. *Offshore Technology Conference*, 1996.

[13] M. Dalsmo, E. Halvorsen, and O. Slupphaug. Active feedback control of unstable wells at the brage field. *SPE Annual Technical Conference*, 2002.

[14] F. Di Meglio, G.-O. Kaasa, and N. Petit. A first principle model for multiphase slugging flow in vertical risers. *Conference on Decision and Control*, 2009.

[15] F. Di Meglio, G.-O. Kaasa, N. Petit, and V. Alstad. Reproducing slugging oscillations of a real oil well. *49th IEEE Conference on Decision and Control*, 2010.

[16] F. Di Meglio, G.-O. Kaasa, N. Petit, and V. Alstad. Slugging in multiphase flow as a mixed initial-boundary value problem for a quasilinear hyperbolic system. *2011 American Control Conference (to appear)*, 2011.

[17] F. P. Donohue. Classification of flowing wells with respect to velocity. *Petroleum Transactions, AIME*, 86:226–232, 1930.

[18] E. Duret. *Dynamique et contrôle des écoulements polyphasiques*. PhD thesis, Ecole des Mines de Paris, 2005.

[19] G. O. Eikrem, L. Imsland, and B. Foss. Stabilization of gas-lifted wells based on state estimation. *International Symposium on Advanced Control of Chemical Processes*, 2004.

[20] J. Falcimaigne and S. Decarre. *Multiphase Production*. IFP Publications, 2008.

[21] D. Ferre, V. Bouvier, and C. Pauchon. *TACITE Physical Model Description Manual*. Rapport IFP, 1995.

[22] J. Freudenberg and D. Looze. Right half plane poles and zeros and design tradeoffs in feedback systems. *IEEE Transactions on Automatic Control*, 30(6):555–565, 1985.

[23] J.-M. Godhavn, M. P. Fard, and P. H. Fuchs. New slug control strategies, tuning rules and experimental results. *Journal of Process Control*, 15:547–557, 2005.

[24] A. R. Hasan, C. S. Kabir, and M. Sayarpour. A basic approach to wellbore two-phase flow modeling. *SPE Annual Technical Conference*, 2007.

[25] K. Havre and M. Dalsmo. Active feedback control as the solution to severe slugging. *SPE Annual Technical Conference*, 2001.

[26] K. Havre, K. Stornes, and H. Stray. Taming slug flow in pipelines. *ABB review*, 4:55–63, 2000.

[27] P. E. Hedne and H. Linga. Suppression of terrain slugging with automatic and manual riser choking. *Presented at the ASME Winter Annual Meeting, Dallas, Texas*, 1990.

[28] V. Henriot, A. Courbot, E. Heintze, and L. Moyeux. Simulation of process to control severe slugging: Application to the dunbar pipeline. *SPE Annual Technical Conference*, 1999.

[29] B. Hu. *Characterizing gas-lift instablilities*. PhD thesis, Department of Petroleum Engineering and Applied Geophysics, NTNU, 2004.

[30] A. Il'in. *Partial Differential Equations V*, chapter V. The Boundary Layer, pages 173–210. Springer, 1999.

[31] L. S. Imsland. *Output Feedback and Stabilization and Control of Positive Systems*. PhD thesis, Norwegian University of Science and Technology, Department of Engineering Cybernetics, 2002.

[32] B. Jansen, M. Daslmo, L. Nøkleberg, K. Havre, V. Kristiansen, and P. Lemetayer. Automatic control of unstable gas lifted wells. *SPE annual technical conference*, 1999.

[33] M. Johansson and A. Rantzer. Computation of piecewise quadratic lyapunov functions for hybrid systems. *Automatic Control, IEEE Transactions on*, 43(4):555 –559, Apr. 1998.

[34] G. Kaasa, O. Stamnes, L. Imsland, and O. Aamo. Intelligent Estimation of Downhole Pressure Using Simplified Hydraulic Model. In *IADC/SPE Managed Pressure Drilling and Underbalanced Operations Conference & Exhibition*, 2011.

[35] G.-O. Kaasa, V. Alstad, J. Zhou, and O. M. Aamo. Nonlinear model-based control of unstable wells. *Modeling, Identification and Control*, 28(3):68–77, 2007.

[36] A. Kaya, C. Sarica, and J. Brill. Comprehensive mechanistic modeling of two-phase flow in deviated wells. *SPE Annual Technical Conference and Exhibition*, 1999.

[37] H. K. Khalil. *Nonlinear Systems, 3rd ed.* Upper Saddle River, N.J.: Prentice Hall, 2002.

[38] M. Khasanov, K. Rinat, V. Krasnov, A. Pashali, and S. Guk. A simple mechanistic model for void fraction and pressure gradient prediction in vertical and inclined gas/liquid flow. *SPE Annual Technical Conference*, 2007.

[39] M. Krstic, I. Kanellakopoulos, P. Kokotovic, et al. *Nonlinear and adaptive control design*, volume 222. Wiley New York, 1995.

[40] M. Krstic and A. Smyshlyaev. Backstepping boundary control for first-order hyperbolic pdes and application to systems with actuator and sensor delays. *Systems & Control Letters*, 57(9):750 – 758, 2008.

[41] M. Krstic and A. Smyshlyaev. *Boundary Control of PDEs*. SIAM Advances in Design and Control, 2008.

[42] T. T. Li. *Controllability and Observability for Quasilinear Hyperbolic Systems*, volume 3. Higher Education Press, Beijing, 2009.

[43] W. Lyons and G. J. Plisga. *Standard Handbook of Petroleum & Natural Gas Engineering*. Gulf Professional Publishing, Elsevier, 2005.

[44] Manolis, Mendes-Tatsis, and Hewitt. Average length of slug region, film region, and slug unit in high-pressure gas-liquid slug flow. *International Conference on Multiphase Flow, Lyon*, 1998.

[45] R. H. Middleton. Trade-offs in linear control system design. *Automatica*, 27(2):281–292, 1991.

[46] Z. Schmidt, J. Brill, and H. Beggs. Choking can eliminate severe pipeline slugging. *Oil & Gas Journal*, 12:230–238, 1979.

[47] F. Scibilia, M. Hovd, and R. R. Bitmead. Stabilization of gas-lift oil wells using topside measurements. *Proceedings of the 17th IFAC World Congress*, pages 13907–13912, 2008.

[48] L. Sinègre. *Dynamic study of unstable phenomena stepping in gas-lift activated systems*. PhD thesis, Ecole des Mines de Paris, 2006.

[49] H. Sivertsen, V. Alstad, and S. Skogestad. Medium-scale experiments on stabilizing riser-slug flow. *SPE Projects, Facilities & Construction*, 4(4):156–170, 2009.

[50] H. Sivertsen, E. Storkaas, and S. Skogestad. Small-scale experiments on stabilizing riser slug flow. *Chemical Engineering Research & Design*, 88(2A):213–228, 2010.

[51] S. Skogestad. Feedback: Still the simplest and best solution. *ICEA*, 2009.

[52] E. Storkaas. *Control solutions to avoid slug flow in pipeline-riser systems*. PhD thesis, Norwegian University of Science and Technology, 2005.

[53] E. Storkaas and S. Skogestad. Controllability analysis of two-phase pipeline-riser systems at riser slugging conditions. *Control Engineering Practice*, 15(5):567 – 581, 2007.

[54] Y. Taitel. Stability of severe slugging. *International Journal of Multiphase Flow*, 12(2):203 – 217, 1986.

[55] Y. Taitel, D. Bornea, and A. E. Dukler. Modelling flow pattern transitions for steady upward gas-liquid flow in vertical tubes. *AIChE Journal*, 26, No3:345–354, 1980.

[56] Y. Taitel, S. Vierkandt, O. Shoham, and J. Brill. Severe slugging in a riser system: experiments and modeling. *International Journal of Multiphase Flow*, 16(1):57 – 68, 1990.

[57] A. Tikhonov, A. Vasil'eva, and A. Sveshnikov. *Differential Equations*. Springer-Verlag, Berlin, 1985.

[58] E. Zakarian. Analysis of two-phase flow instablilities in pipe-riser systems. *Proceedings of Pressure Vessels and Piping Conference*, 2000.

[59] J. Zhou, G.-O. Kaasa, and O. Aamo. Nonlinear observer-based control of unstable wells. *Communications, Control and Signal Processing, 2008. ISCCSP 2008. 3rd International Symposium on*, pages 683–688, March 2008.

[60] J. Zhou, G.-O. Kaasa, and O. M. Aamo. Nonlinear adaptive observer control for a riser slugging system in unstable wells. *ACC*, 2008.

[61] N. Zuber. Average volumetric concentration in two-phase flow systems. *J. Heat Transfer*, 87(4):453–468, 1965.

Appendix A

Well-posedness of the drift-flux PDE model

A.1 Analytical expressions

The matrices corresponding to the hyperbolic form of the system read

$$A(u) = \begin{pmatrix} u_3 & 0 & 0 \\ 0 & u_3 & u_2 + \frac{(1-u_1)u_2^2}{\rho_L u_1 R_g T}\text{bar} \\ \frac{\rho_L R_g T u_1 + (1-u_1)u_2\text{bar}}{(1-u_1)^2 u_2{}^2\text{bar}^2}\rho_L R_g T {v_\infty}^2 & \frac{(\rho_L R_g T u_1 + (1-u_1)u_2\text{bar})\left((1-u_1){u_2}^2\text{bar}^2 - \rho_L^2 u_1 R_g T {v_\infty}^2\right)}{\rho_L (1-u_1){u_2}^3\text{bar}^2} & u_3 - 2v_\infty \frac{\rho_L R_g T u_1 + (1-u1)u_2\text{bar}}{u_2\text{bar}} \end{pmatrix}$$

and

$$S(z) = \begin{pmatrix} 0 \\ 0 \\ -g\sin\theta(z) \end{pmatrix}$$

The eigenvalues of $A(u)$ read

$$\begin{pmatrix} \lambda_1 \\ -\lambda_2 \\ \lambda_3 \end{pmatrix} = \begin{pmatrix} u_3 - (1-u_1)v_\infty - \frac{\rho_l R_g T u_1 v_\infty}{u_2} + \frac{\rho_l R_g T u_1 + (1-u_1)u_2}{\rho_l R_g T (1-u_1) u_1 u_2}\sqrt{u_1(1-u_1)R_g T\left[(1-u_1)u_2^2 - \rho_l R_g T u_1^2 \rho_l {v_\infty}^2\right]} \\ u_3 - (1-u_1)v_\infty - \frac{\rho_l R_g T u_1 v_\infty}{u_2} - \frac{\rho_l R_g T u_1 + (1-u_1)u_2}{\rho_l R_g T (1-u_1) u_1 u_2}\sqrt{u_1(1-u_1)R_g T\left[(1-u_1)u_2^2 - \rho_l R_g T u_1^2 \rho_l {v_\infty}^2\right]} \\ u_3 \end{pmatrix} \quad \text{(A.1)}$$

and the left eigenvectors are given by

$$\begin{pmatrix} l_1(u) \\ l_2(u) \\ l_3(u) \end{pmatrix} = \begin{pmatrix} 1 & \frac{(1-u_1)^2 u_2}{\rho_l R_g T \rho_l {v_\infty}^2} - \frac{(1-u_1)u_1}{u_2} & \frac{(1-u_1)u_2\sqrt{u_1(1-u_1)R_g T\left[(1-u_1)u_2^2 - \rho_l R_g T u_1^2 \rho_l {v_\infty}^2\right]}}{\rho_l^2 R_g^2 T^2 {v_\infty}^2 u_1} - \frac{(1-u_1)^2 u_2}{\rho_l R_g T v_\infty} \\ 1 & \frac{(1-u_1)^2 u_2}{\rho_l R_g T \rho_l {v_\infty}^2} - \frac{(1-u_1)u_1}{u_2} & -\frac{(1-u_1)u_2\sqrt{u_1(1-u_1)R_g T\left[(1-u_1)u_2^2 - \rho_l R_g T u_1^2 \rho_l {v_\infty}^2\right]}}{\rho_l^2 R_g^2 T^2 {v_\infty}^2 u_1} - \frac{(1-u_1)^2 u_2}{\rho_l R_g T v_\infty} \\ 1 & 0 & 0 \end{pmatrix} \quad \text{(A.2)}$$

A.2 Well-posedness

To establish the well-posedness of the mixed initial-boundary value problem, the boundary conditions (1.6)-(1.7)-(1.8) must be rewritten to match the hypothesis of, e.g. [42,

Theorem A.2]. More precisely, given a C^1 initial condition

$$\varphi : \quad [0, L] \to K \tag{A.3}$$

there must exist two functions $g_l : \mathbb{R} \to \mathbb{R}^2$ and $g_r : \mathbb{R}^2 \to \mathbb{R}$ such that Equations (1.6)-(1.7)-(1.8) are equivalent to

$$\begin{cases} z = 0 : & \begin{pmatrix} \tilde{v}_1(t,0) & \tilde{v}_3(t,0) \end{pmatrix}^T = g_l(\tilde{v}_2(t,0)) \\ z = L : & \tilde{v}_2(t,L) = g_r(\tilde{v}_1(t,L), \tilde{v}_3(t,L), Z) \end{cases} \tag{A.4}$$

where

$$\tilde{v}(t,z) = l(\varphi(z))u(t,z)$$

and Z is the control input. The existence of such functions only depends on the choice of the initial condition φ. This is due to the fact that the number of equations at each boundary is in accordance with the sign of the eigenvalues (1.11). Indeed, there are two equations at the boundary $z = 0$, which correspond to the two positive eigenvalues, and one equation at $z = L$ corresponding to $\lambda_1 < 0$. Yet, this does not guarantee that the boundary conditions can be inverted compared to the right components of $\tilde{v}$. We now give necessary and sufficient conditions for the existence of g_l and g_r. First, let us rewrite Equations (1.6)-(1.7)-(1.8) in the u variables. We omit the time and space depandance for readability. The left boundary conditions ($z = 0$) read

$$\begin{aligned} &h_l(u_1, u_2, u_3) \\ &= \begin{pmatrix} \rho_l u_1 u_2 u_3 \mathrm{bar} - \Phi_G \left[\rho_l R_g T u_1 + (1 - u_1) u_2 \mathrm{bar}\right] \\ \Phi_G - u_1 \left[\Phi_g + \rho_l v_\infty + PI(p_r - u_2)\right] \end{pmatrix} \qquad = 0 \end{aligned} \tag{A.5}$$

while the right boundary condition reads

$$\begin{aligned} h_r(u_1, u_2, u_3, Z) =& \frac{\rho_l u_2 u_3 \mathrm{bar}}{\rho_l R_g T u_1 + (1 - u_1) u_2 \mathrm{bar}} - v_\infty \rho_l \\ &- C_{out} Z \sqrt{\frac{\rho_l u_2 \mathrm{bar}}{\rho_l R_g T u_1 + (1 - u_1) u_2 \mathrm{bar}} (u_2 - p_s)} \\ =& 0 \end{aligned} \tag{A.6}$$

In the $\tilde{v}$ variables, these can be rewritten

$$z = 0 : \qquad \tilde{h}_l(\tilde{v}_1, \tilde{v}_2, \tilde{v}_3) = h_l(m_1\tilde{v}, m_2\tilde{v}, m_3\tilde{v}) = 0$$

and

$$z = L : \qquad \tilde{h}_r(\tilde{v}_1, \tilde{v}_2, \tilde{v}_3, Z) = h_r(m_1\tilde{v}, m_2\tilde{v}, m_3\tilde{v}, Z) = 0$$

where the m_i are line vectors such that $(m_i)_{i=1,2,3} = l^{-1}$. A necessary and sufficient condition for the functions g_l and g_r to exist is that the following partial Jacobian matrices

$$\begin{pmatrix} \frac{\partial \tilde{h}_l}{\partial \tilde{v}_2}(\tilde{v}_1(0), \tilde{v}_2(0), \tilde{v}_3(0)) & \frac{\partial \tilde{h}_l}{\partial \tilde{v}_3}(\tilde{v}_1(0), \tilde{v}_2(0), \tilde{v}_3(0)) \end{pmatrix}$$

and

$$\begin{pmatrix} \frac{\partial \tilde{h}_r}{\partial \tilde{v}_1}(\tilde{v}_1(L), \tilde{v}_2(L), \tilde{v}_3(L)) \end{pmatrix}$$

are nonsingular. This yields the following necessary and sufficient conditions for the existence of g_l and g_r: the initial condition φ must be such that, for any $u(z) = \begin{pmatrix} u_1(z) & u_2(z) & u_3(z) \end{pmatrix}^T$ verifying Equations (A.5) and (A.6)

$$\det \left| \frac{\partial h_l}{\partial u}(u(0)) \begin{pmatrix} m_{11}(\varphi(0)) & m_{13}(\varphi(0)) \\ m_{21}(\varphi(0)) & m_{23}(\varphi(0)) \\ m_{31}(\varphi(0)) & m_{33}(\varphi(0)) \end{pmatrix} \right| \neq 0$$

and

$$\frac{\partial h_r}{\partial u}(u(L)) \begin{pmatrix} m_{12}(\varphi(L)) \\ m_{22}(\varphi(L)) \\ m_{32}(\varphi(L)) \end{pmatrix} \neq 0 \tag{A.7}$$

If $\varphi(z)$ verifies these conditions, the Implicit Function Theorem guarantees the existence of g_l and g_r. Further, the well-posedness follows, according to Theorem A.2 in [42], given that $\varphi(z)$ also verifies conditions of C^1 compatibility.

More precisely, this theorem guarantees that there exists $\delta > 0$ such that the hyperbolic system (1.9) with initial condition (A.3) and boundary conditions (A.4) admits a unique local C^1 solution $u = u(t, z)$ on the domain

$$\{(t, z) \mid 0 \leq t \leq \delta, \quad 0 \leq z \leq L\}$$

Appendix B

Linear analysis of model (3.1)-(3.2)-(3.3)

In this chapter, we linearize the model described in Section 2 around a family of equilbria indexed by $\bar{u} \in (0, 1)$. Then, we recall the limitations imposed by the presence of unstable zeros in the transfer function of a linear plant. Finally, the linearized model is used to explicitly compute the zeros and poles of the plant for various values of $\bar{u}$, and the associated limitations, for a specific slugging system. To simplify the computations, we chose the representation where the measured output is a state variable, namely (3.1)-(3.2)-(3.3). This choice does not affect the analysis since the equilibrium, zeros and poles are independent of the representation used.

B.1 Equilibrium of (3.1)-(3.2)-(3.3)

First, one should notice that there can be no equilibrium for the whole system when the virtual valve is closed, that is to say when the expression inside the $\max(\cdot, 0)$ functions is negative. Thus, setting the left-hand-side of Equations (3.1)-(3.2)-(3.3) to zero yields the following expressions of the equilibrium

$$\bar{z}_1 = \frac{w_{g,in}}{C_g a} + \frac{\bar{z}_2}{a} + c\frac{\bar{z}_3 + m_{l,still}}{a} \tag{B.1}$$

$$\bar{z}_2 = p_s + \frac{1}{\rho_l}\left(\frac{w_{l,in}}{C_{out}\bar{u}}\right)^2 \tag{B.2}$$

$$\bar{z}_3 = \frac{\bar{z}_2}{\bar{z}_2 + bGLR} m_l^{\Delta} \tag{B.3}$$

B.2 Limitations due to unstable zeros

We now recall the limitations imposed by the presence of unstable zeros in the transfer function of a general linear plant. This section is largely inspired by [22], [45] and

[52]. Consider a process $y = G(s)u + G_d(s)d$, stabilized by the controller $K(s)$ yielding the input to the plant $u = K(s)(r - y - n)$. The closed-loop response is

$$y = \frac{GK}{1+GK}r + \frac{1}{1+GK}G_d d - \frac{GK}{1+GK}n \tag{B.4}$$

We classically denote $S = \frac{1}{1+GK}$ the sensitivity function and $T = \frac{GK}{1+GK}$ the complementary sensitivity function. S is the transfer function from input disturbances to the output, and T from noise to output and reference to input. Let p_i, $i \in \left\{1, ..., N_p\right\}$ be the RHP poles of G and z_j, $j \in \{1, ..., N_z\}$ its RHP zeros. For any given $j \in \{1, ..., N_z\}$, the following integral constraint on $|S|$ [22] hold

$$\int_{-\infty}^{+\infty} \log|S(j\omega)| d\theta_{z_j}(\omega) = \pi \sum_{i=1}^{N_p} \log \frac{|\bar{p}_i + z_j|}{|p_i - z_j|} \tag{B.5}$$

where $\theta_{z_j}(\omega) = \arctan\left[\frac{\omega - \Im(z_j)}{\Re(z_j)}\right]$ is a weighting function. This constraint implies the following design limitations

- Since the right-hand side of Equation (B.5) is strictly positive, attenuating the disturbances ($|S| < 1$) in a frequency range necessarily increases the disturbances ($|S| > 1$) in another frequency range.
- The constraint is all the more restrictive as the zeros are close to the poles.
- Although similar to the Bode-Freudenberg-Looze constraint

$$\int_0^{\infty} \log|S(j\omega)| d\omega = \pi \sum_{i=1}^{N_p} \Re\{p_i\} \tag{B.6}$$

(B.7)

  Equation (B.5) is much more restrictive. The reason for this is that the interval of integration is weighted by the θ_{z_j} functions. Notice, in particular, that $\int_{-\infty}^{+\infty} d\theta_{z_j}(\omega) = \pi$. Thus, as expressed in [22]

  > *it is not possible to trade off a given amount of sensitivity reduction by allowing $|S(j\omega)|$ to exceed one by an arbitrarily small amount over an arbitrarily large frequency range*

  which would be feasible if there were no unstable zeros and only (B.6) applied.

- Finally, the constraint confirms the intuitive notion that RHP zeros and poles which are close to frequency ranges where attenuation is needed will yield a higher cost in other frequency ranges. The weighing functions yield a precise notion of proximity of a zero or a pole.

A similar relation holds for T and design restrictions limit the tracking performances[1] and the noise reduction properties of the controller. Besides, these integral constraints imply lower bounds on the $\|\cdot\|_\infty$-norm of S and T, which are linked to robustness properties. In particular, $\frac{1}{\|S\|_\infty}$ is the modulus margin. The bounds are given by

$$\|S\|_\infty \geq \max_{j\in 1,\dots,N_z} \left\{ \prod_{i=1}^{N_p} \frac{|\bar{p}_i + z_j|}{|p_i - z_j|} \right\} \tag{B.8}$$

$$\|T\|_\infty \geq \max_{j\in 1,\dots,N_p} \left\{ \prod_{j=1}^{N_z} \frac{|\bar{z}_j + p_i|}{|z_j - p_i|} \right\} \tag{B.9}$$

Again, the closer the zeros are to the poles, the higher the peaks in S and T will be.

B.3 Linearized model and RHP zeros

We now describe how to numerically compute the zeros and poles of the linearized model around any equilibrium $(\bar{u}, \bar{z}_1, \bar{z}_2, \bar{z}_3)$. Then, we explicitly compute the input-output transfer function from the outlet valve (actuator input) to the topside pressure (measured output) for the well considered in Section 3.1.3. The linearized equations read

$$\frac{d}{dt}\begin{pmatrix} \delta z_1 \\ \delta z_2 \\ \delta z_3 \end{pmatrix} = A \begin{pmatrix} \delta z_1 \\ \delta z_2 \\ \delta z_3 \end{pmatrix} + B\delta u$$

with

$$A = \begin{pmatrix} -C_g a & C_g & C_g c \\ \frac{b}{m_l^\Delta - \bar{z}_3} C_g a & \frac{b}{m_l^\Delta - \bar{z}_3}\left[-C_g - \frac{\epsilon w_{g,in}}{\bar{z}_2} - \frac{\bar{z}_2 + bGLR}{b}\frac{\rho_l (uC_{out})^2}{2w_{l,in}}\right] & \frac{b}{m_l^\Delta - \bar{z}_3}\left(-C_g c + \frac{m_l^\Delta \bar{z}_2 w_{l,in}}{b\bar{z}_3^2}\right) \\ 0 & -\frac{\rho_l(\bar{u}C_{out})^2}{2w_{l,in}} & 0 \end{pmatrix}$$

and

$$B = \begin{pmatrix} 0 \\ -\frac{(\bar{z}_2 + bGLR)^2}{\bar{z}_2 m_l^\Delta}\frac{w_{l,in}}{\bar{u}} \\ \frac{w_{l,in}}{\bar{u}} \end{pmatrix}$$

The measured output is $\delta y = C\delta x$, with

$$C = \begin{pmatrix} 0 & 1 & 0 \end{pmatrix}$$

[1] although these can be theoretically be recovered by means of an observer, as seen in Appendix D.

The input-output transfer reads $\delta y = C(sI - A)^{-1}B\delta u$. For the case considered in Section 3.1.3, the transfer function of the linearized system around $\bar{u} = 0.3$ reads

$$\delta y = \frac{-83141.0776(s^2 - 0.003662s + 0.006748)}{(s + 2.547)(s^2 - 0.0004408s + 0.003304)}\delta u$$

The zeros of the plant are $z = 0.0018 + 0.0821i$ and $\bar{z}$, and the poles are $(p_1, p_2, p_3) = (-2.547, 0.0002 + 0.0575i, 0.0002 - 0.0575i)$. Thus, it is possible to compute the fundamental limitations associated with these unstable zeros and poles, following the results of Section B.2. Inequations (B.8) and (B.9) yield

$$\|S\|_\infty \geq \max_{j=1,2}\left\{\prod_{i=2}^{3}\frac{|\bar{p}_i + z_j|}{|p_i - z_j|}\right\} = 1.0014$$

$$\|T\|_\infty \geq \max_{i=2,3}\left\{\prod_{j=1}^{2}\frac{|\bar{z}_j + p_i|}{|z_j - p_i|}\right\} = 1.0014$$

The lower bounds are very close to 1, which indicates that the limitations are not very restrictive.

Appendix C

Proof of Lemma 3.1.1

Consider the candidate Lyapunov function defined by (3.18). The derivative of V along the trajectories of (3.13)-(3.14) reads

$$\begin{aligned}
\dot{V} =& \left[\alpha(f(\tilde{z},t)-k)+\gamma h(\tilde{z},t)\right]\tilde{z}_2^2 - \gamma g(\tilde{z},t)\tilde{z}_3^2 \\
&+ \left[\alpha g(\tilde{z},t) - \gamma(f(\tilde{z},t)-k) - \beta h(\tilde{z},t)\right]\tilde{z}_2\tilde{z}_3 \\
=& \left[\alpha(f(\tilde{z},t)-k)+\gamma h(\tilde{z},t) + \frac{(\alpha g(\tilde{z},t) - \gamma f(\tilde{z},t) + \gamma k - \beta h(\tilde{z},t))^2}{4\gamma^2 g(\tilde{z},t)^2}\right]\tilde{z}_2^2 \\
&- \gamma g(\tilde{z},t)\left[\tilde{z}_3 - \frac{\alpha g(\tilde{z},t) - \gamma f(\tilde{z},t) + \gamma k - \beta h(\tilde{z},t)}{2\gamma g(\tilde{z},t)}\tilde{z}_2\right]^2 \\
\leq& \frac{1}{G^2}\left[k^2 + 2\left(\frac{\alpha}{\gamma}G - F - \frac{\beta}{\gamma}\mu - 4\alpha\epsilon^2\right)k + 4\gamma G^2 H + \left(\frac{\alpha G + \beta H}{\gamma} + F\right)^2\right]\tilde{z}_2^2
\end{aligned}$$

Conditions (3.19) and (3.20) ensure that there exists $k > 0$ such that

$$\dot{V} \leq -\xi\tilde{z}_2^2 \tag{C.1}$$

This shows that the origin is uniformly stable (Theorem 4.8 in [37], with $W_1 = W_2 = V$ and $D = K$). We will now conclude using Barbalat's Lemma. Integrating (C.1) between 0 and $T > 0$ yields

$$\eta\int_0^T \tilde{z}_2^2(t)dt < V(0) - V(T) \leq V(0)$$

since V is decreasing. Taking the limit as T goes to infinity yields

$$\int_0^{+\infty} \tilde{z}_2^2(t)dt < +\infty \tag{C.2}$$

Besides V is decreasing and radially unbounded, therefore, $\tilde{z}_2$ and $\tilde{z}_3$ are bounded functions of time. Therefore, $\dot{\tilde{z}}_2$ and $\dot{\tilde{z}}_3$, which are continuous functions of $\tilde{z}_2$ and $\tilde{z}_3$, are

also bounded. Therefore, $\tilde{z}_2$ is uniformly continuous. Thus, (C.2) implies, by Barbalat's lemma

$$\lim_{t\to+\infty} \tilde{z}_2(t) = 0 \tag{C.3}$$

Similarly, $\dot{\tilde{z}}_2$ and $\dot{\tilde{z}}_3$ are bounded functions of time. Therefore, $\ddot{\tilde{z}}_3$ and $\ddot{\tilde{z}}_2$, which are continuous functions of $\dot{\tilde{z}}_2$ and $\dot{\tilde{z}}_3$ (since the right-hand side of (3.8)-(3.9) is C^1) are also bounded. Thus, $\dot{\tilde{z}}_2$ is uniformly continuous. (C.3) implies, again by Barbalat's lemma

$$\lim_{t\to+\infty} \dot{\tilde{z}}_2(t) = 0 \tag{C.4}$$

Taking the limit $t \to +\infty$ in (3.9) and using (C.3) and (C.4) yields

$$\lim_{t\to+\infty} \tilde{z}_3(t) = 0 \tag{C.5}$$

This result being valid for any initial time and initial conditions, the origin is uniformly globally attractive. Since it has been shown that it was uniformly stable, it is UGAS.

Appendix D

Theoretical recovery of the tracking performances by an observer

In this section, we study the control design limitations imposed by unstable zeros in the particular setup where the output of interest (y_c, c as 'controlled') cannot be measured, but is observed using a measured output (y_m), and y_m has unstable zero dynamics (whereas y_c does not). The results presented in Section B.2 state that the disturbance rejection and tracking performances *as far as* y_m *is concerned* are limited. Indeed, when there are unstable zeros in the transfer function from the input to the measured variable, *whatever the controller* $K(s)$ *is* (including an observer-controller), the RHP zeros impose limitations. This point will be confirmed here. Further, we cannot expect the observer-controller structure to reject perturbations on y_c, since it is not measured. However, we shall see that the tracking performances *for the controlled variable* y_c can be recovered thanks to the observer. Thus, we consider the following setting

$$y_c = G_{c0}x_0 + G_c u + D_c d \qquad\qquad y_m = G_{m0}x_0 + G_m u + D_m d$$

where G_m has RHP zeros, but G_c does not. One should notice that we considered the effect of the initial conditions, since the plants may be unstable. We also assume that y_c cannot be measured. It is estimated thanks to the following observer

$$\hat{y}_c = L_0\hat{x}_0 + L(y_m + n) + L_u u \tag{D.1}$$

where n is the noise, and L, L_u, G and G_c on one hand, and L_0, G_{m0} ,and G_{c0} on the other hand verify the following relations

$$L_u + LG_m = G_c \qquad\qquad L_0 + LG_{m0} = G_{c0}$$

Thus

$$\begin{aligned}\hat{y}_c &= L_0\hat{x}_0 + L_u u + LG_m u + LG_{m0}x_0 + LD_m + Ln \\ &= L_0(\hat{x}_0 - x_0) + G_{c0}x_0 + G_c u + LD_m + Ln\end{aligned} \tag{D.2}$$

We consider the following feedback

$$u = K(r_c - \hat{y}_c) \tag{D.3}$$

where r_c is the target value for y_c, and K stabilizes the plant. Substituting (D.2) in the last equation yields

$$u = \frac{K}{1 + G_c K} r_c - \frac{KL_0}{1 + G_c K}(\hat{x}_0 - x_0) - \frac{KG_{c0}}{1 + G_c K} x_0 - \frac{KLD_m}{1 + G_c K} d - \frac{KL}{1 + G_c K} n$$

Thus,

$$y_c = \frac{G_c K}{1 + G_c K} r_c - \frac{G_c KL_0}{1 + G_c K}(\hat{x}_0 - x_0) - \frac{G_{c0}}{1 + G_c K} x_0 + \left(D_c - \frac{KLD_m}{1 + G_c K} \right) d - \frac{G_c KL}{1 + G_c K} n$$

As a result,

- there is no limitation *a priori* on the tracking performances for y_c, since a large K will make the term $\frac{G_c K}{1+G_c K}$ as close to 1 as requested
- as expected, the term $D_c d$ cannot be attenuated, which shows that no rejection of the perturbations on y_c is possible. One should also notice that some of the perturbations coming from y_m affect the dynamics of y_c, through the term $-\frac{KLD_m}{1+G_c K}$, but are attenuated by the filtering properties of the observer, that is, with a small L.
- the effect of the initial conditions of the plant can be attenuated by the term $\frac{G_{c0}}{1+G_c K}$ with a large K, and the effect of the initial condition of the observer can be attenuated thanks to the term $\frac{G_c KL_0}{1+G_c K}$ with a small L_0

Yet, the restrictions due to the unstable zeros are still present, but concern the observer-controller structure. To see this, let us rewrite the feedback (D.3) as a function of y_m, using the observer equation (D.1)

$$u = K(r_c - L_0 \hat{x}_0 - L(y_m + n) - L_u u) \tag{D.4}$$

This yields

$$u = \frac{K}{1 + KL_u}(r_c - Ly_m - Ln) - \frac{KL_0}{1 + KL_u} \hat{x}_0 \tag{D.5}$$

Thus

$$y_m = \frac{G_m \frac{K}{1+KL_u}}{1 + G_m \frac{KL}{1+KL_u}} r_c - \frac{G_m \frac{KL}{1+KL_u}}{1 + G_m \frac{KL}{1+KL_u}} n - \frac{G_m \frac{KL_0}{1+KL_u}}{1 + G_m \frac{KL}{1+KL_u}} \hat{x}_0 \tag{D.6}$$

Therefore, the design restrictions imposed by RHP zeros apply to the observer-controller $K' = \frac{KL}{1+KL_u}$, instead of simply K. In particular, using a large gain K (to ensure a good tracking performance for y_c) does not necessarily destabilize the plant.

Production de pétrole : étude dynamique et contrôle des écoulements à bouchons

Résumé : Le slugging (ou écoulement à bouchons) est un régime d'écoulement polyphasique indésirable apparaissant sur les systèmes de production de pétrole. Dans ce manuscrit, nous étudions la dynamique de ce phénomène intermittent dans le but de le supprimer par actionnement automatique de la vanne de sortie. Nous proposons des solutions de contrôle applicables dans une vaste gamme de situations industrielles. Après une analyse quantitative des propriétés physiques du slugging, nous proposons un modèle à paramètres distribués d'écoulement diphasique (gaz-liquide) reproduisant ce phénomène. Le modèle prend la forme d'un système hyperbolique de lois de conservation, pour lequel nous proposons un schéma de résolution numérique. De plus, nous procédons à une analyse de stabilité via la construction d'une fonction de Lyapunov de contrôle stricte pour le problème aux deux bouts avec condition initiale. Ensuite, nous présentons un modèle de dimension finie capable de reproduire les oscillations de pression et de débit qui caractérisent le slugging. Après une analyse des propriétés dynamiques de ce système, nous décrivons comment calibrer les paramètres du modèle afin que son comportement corresponde à celui d'un système donné. Enfin, nous proposons des lois de contrôle sous la forme de boucles de rétroaction, basées sur l'analyse du modèle réduit, dans deux situations industrielles disctinctes : selon qu'un capteur de pression de fond est disponible ou non. Les performances de ces solutions sont comparées avec les méthodes correspondant à l'état de l'art dans chaque situation. La conclusion de cette étude est qu'il n'est pas systématiquement nécessaire de disposer d'un capteur de pression de fond pour stabiliser l'écoulement. Quand un tel capteur est disponible, la loi de contrôle que nous proposons possède de meilleures propriétés de stabilisation que les méthodes communément utilisées dans l'industrie, ce qui, lors du passage à l'échelle, devrait se traduire par une augmentation de la production de pétrole.

Mots clés : Ecoulements à bouchons,Ecoulements multiphasiques, Pétrole,Gaz,Modélisation, Equations aux Dérivees Partielles,Contrôle,Observateurs,Nonlineaires

Dynamics and control of slugging in oil production

Abstract: Slugging is an undesirable multiphase flow regime occurring on oil production facilities. This manuscript studies the dynamics of this intermittent phenomenon in view of suppressing it by feedback actuation of the outlet valve. We propose control solutions applicable in a broad range of industrial settings. After a quantitative description of the physical characteristics of slugging, we propose a model for two-phase (gas-liquid) flow with distributed parameters reproducing the phenomenon. The model takes the form of a hyperbolic system of transport equations, for which we propose a numerical solving scheme. Besides, we proceed to a stability analysis by constructing a strict Lyapunov function for the mixed initial-boundary value problem. Then, we present a reduced-order model which reproduces the pressure and flow rate oscillations of slugging. After a dynamical analysis of this model, we describe how to calibrate its parameters so that its behavior corresponds to that of a given slugging system. Finally, we propose feedback control laws, based on the analysis of the reduced-order model, in two distinct industrial setups: whether a bottom pressure sensor is available or not. The performances of these solutions are compared with the state-of-the art methods in each situation. The conclusion is that a bottom pressure sensor is not systematically required to stabilize the flow. When one is available, the control law we propose yields better stabilization properties than the solution commonly used in the industry, which should improve the oil recovery process.

Keywords: Slugging,Mutliphase flow,Oil,Gas,Modelling,Partial Differential Equations,Control, Observers,Nonlinear

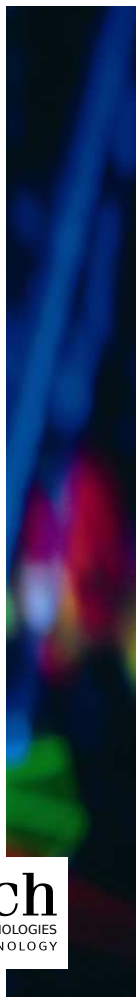

MINES ParisTech

ParisTech
INSTITUT DES SCIENCES ET TECHNOLOGIES
PARIS INSTITUTE OF TECHNOLOGY